UNIVERSITY OF OKLAHOMA

GRADUATE COLLEGE

COMPARATIVE STUDY OF SURFACE PREPARATION AND BOND ANGLE COMBINATIONS FOR BRIDGE REPAIR USING ULTRA-HIGH PERFORMANCE CONCRETE ALTERNATIVE

A THESIS

SUBMITTED TO THE GRADUATE FACULTY

in partial fulfillment of the requirements for the

Degree of

MASTER OF SCIENCE

IN CIVIL ENGINEERING

By

RAINA L. COLEMAN
Norman, Oklahoma
2018

COMPARATIVE STUDY OF SURFACE PREPERATION AND BOND ANGLE COMBINATIONS FOR BRIDGE REPAIR USING ULTRA-HIGH PERFORMANCE CONCRETE ALTERNATIVE

A THESIS APPROVED FOR THE
SCHOOL OF CIVIL ENGINEERING AND ENVIRONMENTAL SCIENCE

BY

Dr. Jeffery S. Volz, PE, SE, Chair

Dr. Royce W. Floyd, PE

Dr. Philip S. Harvey Jr., PE

I would like to dedicate this thesis to my mother, Jenice Jones and my sister, Kalaya Coleman for their unconditional love and support through everything I've ever done.

Acknowledgements

Firstly, I would like to sincerely thank my advisor, Dr. Jeff Volz, for his constant support and confidence in me. I would also like to thank my committee member Dr. Royce Floyd for his patience throughout the process of my research and my committee member Dr. Philip Harvey for his guidance.

To the team of undergraduate and graduate researchers and others that helped me with the research needed to complete this thesis, I am so grateful. Specifically I must credit Mike Schmitz - Fears Structural Engineering Lab Manager, Dr. Jonathan Drury, Trevor Looney, Amy McDaniel, Jacob Choate, Chandler Funderburg, Kayla Buster, Grant Phillips, Stephen Roswurm and Conner Casey. Additionally, thank you to ODOT for funding this project and the Dolese Bros. Co. for donating cement, aggregate, and Glenium.

Lastly, thank you to my friends, family and other loved ones who motivated and supported me throughout this process. I would not be here today without all of them.

Table of Contents

List of Tables

List of Figures

Abstract

Ultra-high performance concrete (UHPC) is a type of concrete with advanced mechanical properties compared to normal strength concrete and that can be used for connections and repairs in bridges. Most UHPC used in the field is proprietary and significantly more costly than normal strength concrete. The Oklahoma Department of Transportation (ODOT) desires a UHPC alternative made with local, non-proprietary materials. In this study, the application of a lab developed UHPC alternative developed by McDaniel (2017) was tested and analyzed. The nature of this study was comparative, so all methods and tests conducted were similar to a previous study performed by Funderburg (2018) with a proprietary UHPC product, the Lafarge product Ductal®.

After reviewing relevant literature, some modification to the UHPC alternative, J3, was required due to the excessive amount of high range water reducer (HRWR) found on the surface of the concrete after mixing. Trial mixes of J3 were made to optimize the amount of HRWR needed in the concrete used for specimens. Next, large scale slab specimens were cast using two panels of ODOT Class AA mix and a UHPC joint connecting the two panels. These slab specimens were tested in flexure, statically and cyclically. Composite modulus of rupture specimens and slant shear specimens were also made and were composed of half normal strength concrete acting as the base concrete and half UHPC. The modulus of rupture specimens were cast at four different interface angles and with three different surface preparations. The modulus of rupture specimens were tested using three point loading and the slant shear specimens were tested in compression. The results of both the large scale and small scale specimens were compared to that of the previous study by Funderburg.

This research study produced promising results in regards to the UHPC alternative. While the J3 mix could benefit from improved workability, all specimens still performed well in the testing stage. The sand blasting surface preparation and 45 degree interface angle performed the best but the wire brushed and 60 degree specimens were also comparable. The slab specimens exceeded the calculated failure load possibly due to the additional strength provided through the UHPC joint. The conclusions made from this study, based on the properties tested, indicate that UHPC mix J3 is a comparable alternative to Ductal® and would be useful for field applications.

1 Introduction

This research study evaluated the use of Ultra-High Performance Concrete (UHPC) in bridge joints in Oklahoma. UHPC is a type of concrete with advanced mechanical properties including high compressive strength, high tensile strength and high durability. While it is more expensive than that of normal strength concrete (NSC), UHPC has a higher durability and therefore lasts longer than NSC. Utilizing UHPC can increase the life span of bridges and other structures while also decreasing the size and number of repairs needed throughout a structure's life span. UHPC is a relatively new material in the industry so further research is necessary to determine which applications it would be the most useful in.

1.1 Purpose of Study

The Oklahoma Department of Transportation (ODOT) is evaluating the use of UHPC for connections and repairs in bridges. A lower cost, alternative UHPC mix design with materials available in Oklahoma is desired. The nature of this study is comparative, so all methods and tests conducted will be similar to a previous study performed by Funderburg (2018). This previous study utilized the Lafarge product Ductal® instead of a local UHPC alternative.

1.2 General Overview

UHPC has recently been introduced in commercial applications. UHPC is composed of various cementitious materials and has a water-to-cementitious materials ratio that is typically less than 0.25. In addition, a high percentage of fiber reinforcement is incorporated into the mixture. The Federal Highway Administration

(FHWA) requires a compressive strength greater than 21.7 ksi to be considered UHPC (Graybeal 2011).

In general, UHPC requires slight modifications to standard concrete procedures. The mixing procedure for UHPC is similar to that of normal strength concrete and a conventional concrete mixer can be used to mix UHPC. However, it must be noted that UHPC requires a higher energy input and prolonged mixing time. A high energy mixer can be used to mitigate this need. Casting procedures can greatly affect the short and long-term properties. UHPC is made up of optimized granular materials and requires a minimal amount of water for hydration. Certain curing procedures should be used to ensure the water will not escape before the concrete hydrates. The addition of heat may often be included in the curing process to decrease the setting time and significantly improve early age properties. Once the UHPC reaches a compressive strength of 14 ksi, the concrete is considered to have reached an acceptable hydration level (Graybeal 2011). As a result of UHPC's advanced properties, many state transportation departments have considered its use.

As previously mentioned, all tests conducted will be similar to that of a previous study where Ductal® was used in all specimens. Ductal® has been used as a baseline for much of the research conducted about UHPC in the industry. Ductal® however is more expensive than typical concrete. Price is one of the largest driving factors for developing and implementing a UHPC alternative mix design for research and construction.

1.3 Previous Implementation

As of the year 2000, UHPC had become commercially available in the United States. While UHPC is a fairly new construction material, in a short amount of time it has made its way into infrastructure applications in North America, Europe and Asia (Graybeal 2013). The most popular applications of UHPC include tee beams, girders, and joints between deck panels. UHPC usage in new construction is a more common application than repair and rehabilitation of older structures. Going forward, some of these previous implementations can be developed to preserve existing infrastructure.

1.4 Research Conducted

This research investigated the bond strength and surface preparation between NSC and UHPC. The bond between the two types of concrete was analyzed through flexural and slant shear testing in small scale specimens. Composite modulus of rupture specimens fabricated from NSC and UHPC were used in flexural testing. Cylinders fabricated from NSC and UHPC were used for slant shear testing. Full scale slab specimens with UHPC joints were loaded statically and cyclically while load, displacement, and strains were monitored. The slab specimens were fabricated from two panels of NSC and one intermediary UHPC joint. The slab specimens were used to mimic replacement of a bridge joint with UHPC. The UHPC alternative, J3, was used for all specimens in this study (McDaniel 2017).

1.5 Goals and Objectives

This study is an addition to a multi-phase project for ODOT (Floyd et al. 2016). The goals of this project include exploring the practicality of the use of a UHPC

alternative and identifying appropriate materials to be used in construction and repair, evaluating best practices, evaluating performance of trial joints and developing specifications regarding UHPC and its use in the state of Oklahoma. The following are objectives for this particular study:

- Determine the best bond angle and surface preparation by flexural testing
- Duplicate small-scale and large-scale testing used in the study of a proprietary UHPC (Funderburg 2018) and compare the results to a non-proprietary UHPC developed from local materials
- Assess the feasibility of the non-proprietary alternative over the proprietary product
- Make recommendations to ODOT as to whether this non-proprietary alternative should be used in future construction and repair

1.6 Outline of Thesis

This thesis is composed of 5 chapters. Chapter 1 gives an overview of this research study and the reason why it is being conducted. Chapter 2 summarizes relevant literature including fiber reinforcement, alternative UHPC mix designs, previous use of UHPC in bridges, slant shear testing, surface preparation, bond angles, and slab joint testing. Chapter 3 explains the approach, methodology, and testing procedures followed to complete the research in this study. It will also detail the type of specimens fabricated, which includes modulus of rupture beams, slant shear cylinders, and slab specimens. Chapter 4 analyzes and explains the data from this research study and

compares it to the results of the previous study (Funderburg 2018). Chapter 5 summarizes the findings and recommends future work to be accomplished.

2 Literature Review

2.1 Overview

This chapter contains a review of the literature related to the implementation of a non-proprietary UHPC alternative mix design in large-scale and small-scale composite specimens. There are multiple factors to consider when casting UHPC. UHPC is comprised of an optimized gradation of dry materials, supplementary cementitious materials, superplasticizers and fiber reinforcement. Because the material is so different than that of NSC, the placement and use of the material has different applications. It is apparent through available research studies that UHPC is a durable material and is successful at extending the life and lowering the maintenance frequency of a structure when used in connections. The UHPC-NSC bond and UHPC as a repair material is still being studied and expanded upon. These subjects will be expanded upon in this chapter.

2.2 Fiber Reinforcement

One of the primary benefits to UHPC is the increased post-cracking tensile strength. UHPC achieves this high post-cracking tensile strength by incorporating fiber reinforcement. Because UHPC requires fiber reinforcement to engage its advanced mechanical properties, certain mixing and casting procedures must be taken into consideration. Graybeal (2011) says that during casting, the use of internal vibration is discouraged because of its ability to rearrange fibers. External vibration is sometimes used when casting NSC to ensure there are no air pockets. Casting procedures can influence the fiber arrangement. Because it is imperative that the fibers in UHPC are

suspended instead of settling (Graybeal 2011), caution must be taken when placing the concrete into forms. If the fibers are not suspended in the concrete, they will not be evenly distributed throughout the specimen. If the fibers are not evenly distributed through the specimen, the full potential of strength may not be utilized. Any changes in the mix design or incorporation of vibration methods must be carefully considered.

Yoo et al. (2015) performed a study that shows steel fibers, both smooth and twisted, can significantly increase the load carrying capacity of a UHPC specimen. The inclusion of fibers at 2% volume increased the load capacity by anywhere from 27% to 54%. The lengthening of said fibers however did not show any noticeable difference in load carrying capacity. In a study performed by Yu et al. (2016), it was determined through dynamic compression testing that the damage resistance of UHPC increased with the addition of fibers and increase in fiber length. Adding fiber reinforcement to UHPC can definitely produce positive results in compressive and tensile strength as well as ductility. The benefits of one type of fiber versus another type in UHPC applications is still unclear.

2.3 Alternative UHPC Mix Designs

As previously discussed, proprietary UHPC products are typically very expensive and deter state departments of transportation from utilizing it. The availability of a non-proprietary UHPC alternative that has the same mechanical properties with a lower cost would be appealing for industry use. A number of mix designs have been lab tested to determine if an alternative with the basic UHPC requirements can be developed. A study was completed by Halit et al. (2008) with

reactive powder concrete, which is an ultra-high strength cement product. This research involved decreasing the amount of cement and silica fume and replacing those with some combination of ground-granulated blast furnace slag (GGBFS) and fly ash. Compressive strengths were tested, and proportions of cementitious materials were adjusted. It was found that proportions of cementitious materials can change while maintaining advanced mechanical properties (Halit et al., 2008). The Yu et al. (2014) study analyzed UHPC by means of optimizing particle packing curves. This study explored workability, air content, porosity, flexural strength and compressive strength. This study showed that by using an optimized packing model, the binder amount can be kept relatively low. In addition, the large amount of unhydyrated cement they found could be mitigated by using some type of filler (Yu et al., 2014).

Because concrete is the most widely used inorganic building material, it can have harsh effects on the environment. The use of ecofriendly construction materials have been considered and studied (Randl et al. 2014). In one study, there was use of fly ash, GGBFS and limestone powder in place of cement for UHPC mix designs (Yu et al. 2015). These various mixes were analyzed and proven successful. This particular study will use a UHPC alternative developed by Amy McDaniel (2017). McDaniel tested a series of 158 alternative mix designs. Various supplementary cementitious materials (SCMs) were used in these mix design combinations. The SCMs considered in this study included Type I and Type III Portland cement, silica fume, VCAS™ and GGBFS. After testing a series of mix designs, four final mix candidates were chosen, and the most promising out of these was selected to do further static, dynamic and bond strength testing. While all the previous studies were to some extent successful in

developing a mix design that could exhibit advanced mechanical properties, field application of the material is the most important consideration.

2.4 Previous Use in Bridges

Since UHPC has been introduced, the material has been utilized several times throughout North America, Europe, Asia and Australia. UHPC is most commonly implemented in prefabricated bridge elements. Prefabricated bridge elements are made off site and transported to the construction site when needed. This method of construction has shortened the construction time, and when UHPC is incorporated, offers increased durability (Graybeal 2013). Prefabricated elements have also been used in field-cast applications, using UHPC to join the precast members that are set in place as seen in Figure 1 (Graybeal 2014). This technique has been used by the departments of transportation in Iowa, Montana, Oregon, Pennsylvania and Massachusetts. Depending on the constructability and field performance, field casting may be a feasible application for Oklahoma bridges.

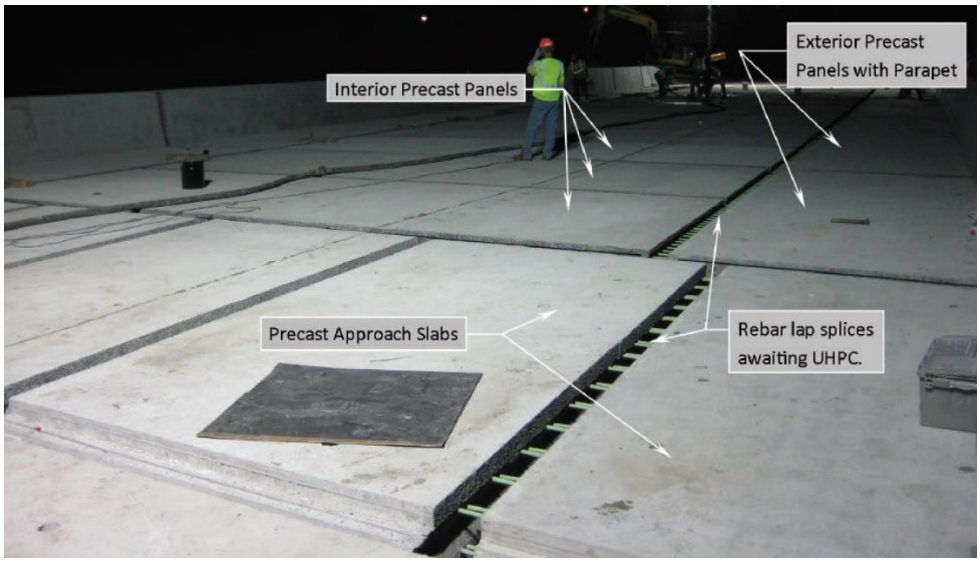

Figure 1: Bridge deck after panel installation and before UHPC placement (Graybeal 2014)

Mi et al. (2018) detailed some prominent uses of UHPC in bridge applications. A bridge in Virginia containing 10 spans was analyzed during this study. One of the spans was constructed using UHPC, and this particular girder span was lighter and thinner than the others. In addition, the rebar layout for this span of the bridge was simplified due to the UHPC's high tensile strength. UHPC has also been implemented in various shapes including u-shaped and pi-shaped bridge girders. The article also mentioned that using UHPC joints between precast elements allowed use of a smaller connection while performing better overall. Because of increasing traffic loads, many researchers are looking to modify and evolve traditional paving techniques with UHPC. All structures in the Mi et al. study (2018) demonstrated exceptional durability and low maintenance costs.

2.5 Previous Slant Shear Tests

Bond strength is an important aspect of bridge repair because the strength of the bond of the concrete determines the longevity of the structure. The American Society for Testing and Materials (ASTM) has specified a way to test the strength of bond but has not specified how to assess the strength between two different concrete types. Slant shear specimens are being used to analyze the bond between two concrete types with a test method developed from variations of ASTM C882-13 (2013) to create a baseline of bond strength. A study by Carbonell Munoz (2014) analyzed bond performance between UHPC and normal concrete. Different interface angles were used in these analyses, but the controlling factor was early age strength. In the Climaco et al. (2001) studies, failure between two concrete types was due to the bond. From these experiments, determining the most effective bond type is the key to prolonged strength.

2.6 Surface Preparation and Bond Angles

Because there is so much deterioration in infrastructure in a short amount of time, state departments of transportation are looking to develop improved repair techniques (Carbonell Munoz 2012). The success of concrete rehabilitation depends on the bond. Perhaps the most critical step in rehabilitation is removal of original concrete and preparation of the surface to prepare for the new concrete. It is important, however, to remove the deteriorated concrete without inflicting additional damage. Any damage throughout this process may affect the long term strength of the structure. Throughout multiple research studies it is agreed upon that the preparation of the surface is one of the main factors influencing bond. It has been found that increasing the roughness of a

substrate surface increases the strength of the bond (Júlio et al. 2004). The experiments that Júlio et al. (2004) performed incorporated surface preparations of steel brushing, partially chipped, sand blasting and as cast, three of which are shown in Figures 2, 3 and 4.

Figure 2: Steel Brushed Surface Preparation (Julio et al. 2004)

Figure 3: Partially Chipped Surface Preparation (Julio et al. 2004)

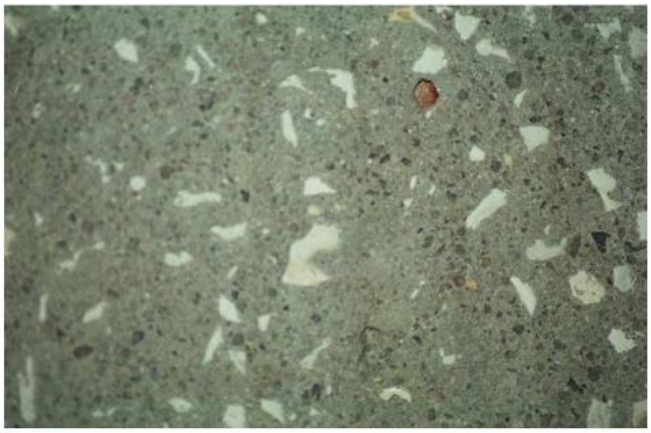

Figure 4: Sand Blasted Surface Preparation (Julio et al. 2004)

In the Julio et al. (2004) study, slant shear and pull off tests reported sand blasting as the most effective surface preparation for bond strength while wire brushing was not as effective in comparison. This supports the idea that a rougher bonding surface will yield a better bond. During the slant shear testing done by Carbonell Munoz (2014), all wire brushed surfaces failed due to bond. While all surface preparations considered in the Julio et al. study satisfied the requirements for ACI 546-06 Guide to Concrete Repair (ACI, 2006), the potential strength of the UHPC was not utilized due to premature failure in the interface. Tayeh et al. (2013) came to the same conclusion as the previous studies through split cylinder testing. Smooth surfaces are typically weaker, and do not reflect real world situations accurately (Climaco et al. 2001).

2.7 UHPC Slab Joint Testing

Testing not only small-scale specimens but large-scale specimens will develop data that can be applied towards field applications. FHWA tested bridge deck components with both transverse and longitudinal joints. These test specimens were fabricated to simulate the connection between precast concrete and UHPC (Graybeal

2010). Testing modes on one slab specimen included cyclic testing of at least 2 million cycles loaded below the cracking strength, then at least 5 million cycles above the cracking strength. If the specimen had not already failed, it was statically loaded to failure. The test setup is shown in Figure 5 and the layout for transverse and longitudinal configurations is shown in Figure 6.

Figure 5: UHPC longitudinal connection cyclic test setup

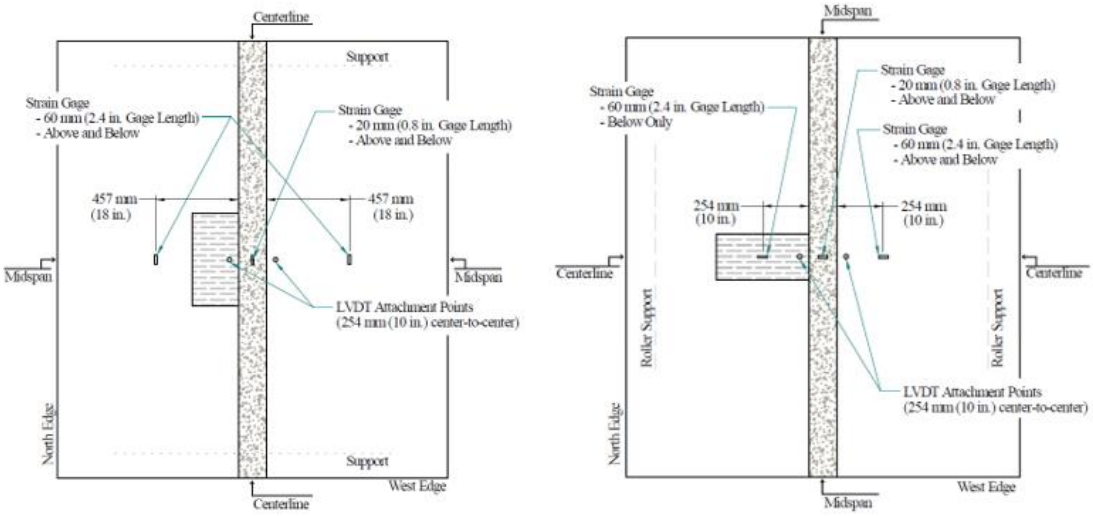

Figure 6: Instrumentation and layout for transverse (left) and longitudinal (right) configurations

The conclusions drawn from this study determined that a UHPC joint connection bonds well to precast concrete which suggests little to no leaks in transverse connections. It is imperative that bridge decks act as monolithic elements due to the possibility of failure otherwise, possibly at the interface. The results in this study

suggest that either transverse or longitudinal orientation would suffice for use in UHPC bonding to normal strength precast concrete.

2.8 Funderburg Study (2018)

In 2018, Chandler Funderburg completed a study involving the evaluation of UHPC as a repair material for bridges in Oklahoma. The purpose of that study was to determine the feasibility of using UHPC instead of NSC because of its advanced mechanical properties. Deteriorated bridge joints are a problem throughout Oklahoma and UHPC could be the solution to long lasting repairs. UHPC requires short steel embedment lengths and therefore may be used in smaller quantities in bridge joints. Funderburg used the proprietary Lafarge product, Ductal®, to fabricate specimens that can evaluate bond strength, flexural capacity and the effects of static and cyclic loading on joint interfaces. She created slant shear specimens, slab specimens and composite modulus of rupture specimens (MOR). The composite MOR specimens were made up of 4 interface configurations (90 degree, 60 degree, 45 degree and shear key) and 3 surface preparations (wire brushed, sand blasted and exposed aggregate). The exposed aggregate surface preparation and 60 degree interface angle performed the best. A majority of her MOR specimens failed in the base concrete showing that the specimens acted monolithically. All 3 slab specimens that were made exceeded the calculated failure load when statically tested. This could be due to the additional strength provided through the UHPC joint. All MOR specimens exceeded the flexural strength of the base concrete and all slab specimens exceeded the estimated capacity.

2.9 McDaniel Study (2017)

In 2017, Amy McDaniel completed a study involving the development of a UHPC alternative mix design that could be used as a repair material for bridges in Oklahoma. Because the Lafarge product Ductal® is approximately 20 times more expensive than typical concrete, a UHPC alternative is desired for use by the ODOT. FHWA defined UHPC as having a compressive strength of 21.7 ksi, a post-cracking tensile strength 0.72 ksi, and high flowability. The goal was for this UHPC alternative to reach the requirements for being considered UHPC. McDaniel developed 158 mix designs iterated from a baseline of other non-proprietary mix designs. Using the concept of particle packing and an optimal combination of supplementary cementitious materials, 9 iterative series, series A through series J, were developed and produced the 3 strongest mixes in compression before heat curing (Table 1). The compressive strengths for the top 3 mix designs, J3, J8 and J13, including fibers and heat curing are shown in Figure 7. The compressive strength results for the final mix design of the UHPC alternative, J3 (Table 2), achieved the FHWA defined post-cracking tensile strength, high flowability and came within 8% of the compressive strength. Although the target compressive strength was not achieved, J3 may still be a practical alternative to be used in field applications.

Table 1: Final Mix Candidate Benefits and Detriments (McDaniel 2017)

		J3	J8	J13
Mortar Flow (in)		10.25 estimated	13 estimated	10
Compression Strength (psi)	1-Day	6011	6083	8360
	7-Day	12131	12516	10093
	28-Day	14837	14031	14772
Benefits:		Very workable texture and mortar flow	Best FA mix, sticky texture likely to suspend fibers well	Best early strength, mortar flow likely to suspend fibers
Detriments:		Low early strength	Low early strength	

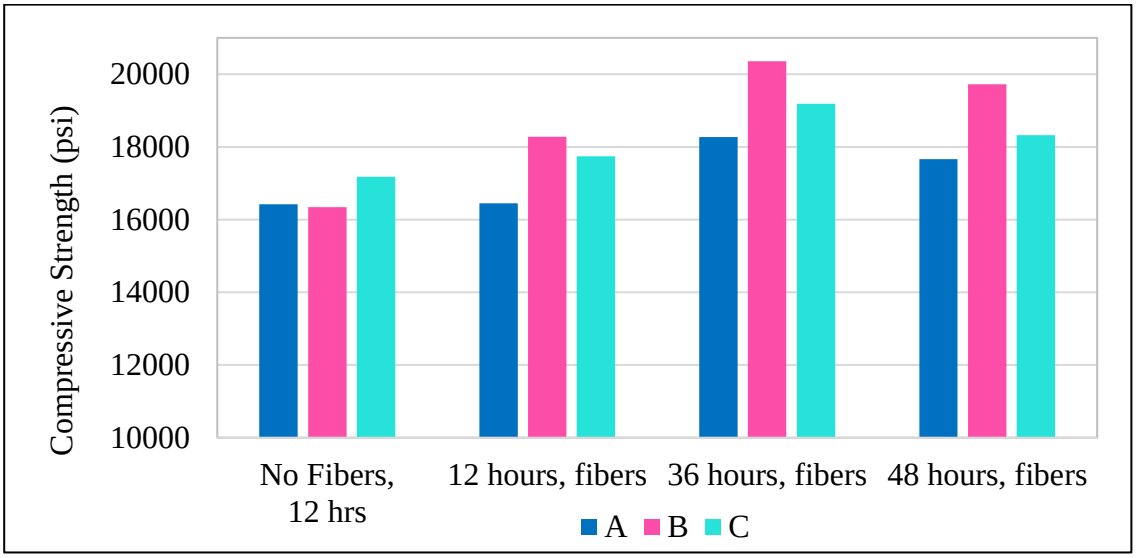

Figure 7: Compressive Strengths for Fiber-Reinforced and Heat Cured. A-J8, B-J3, C-J13 (McDaniel 2017)

Table 2: UHPC alternative mix design, J3 (McDaniel 2017)

Material	Amount per yd^3
Masonry Sand	1965 lb
Type 1 Portland Cement	1180 lb
GGBFS	590 lb
Silica Fume	197 lb
Water	393 lb
HRWR	15.77 fl oz./cwt

3 Approach, Methodology and Testing

This section will outline the approach and methodology for conducting the research in this project. First, there is discussion of the non-proprietary UHPC mix design followed by fabrication of a variety of specimen types to evaluate the performance of this material. These tests include concrete to concrete bond analysis, slant shear and flexural testing.

3.1 UHPC Alternative Mix Design

Because many UHPC mix deigns are proprietary and expensive, a UHPC mix design fabricated from local materials was desired for this study. McDaniel (2017) developed such a mix design, a local alternative UHPC mix named J3 that will be used for all specimens cast in this study. Some initial modifications to J3 were required due to the excessive HRWR found on the surface of the concrete after mixing. Because the HRWR can be adjusted with little effect on the strength of the concrete, 0.1 ft^3 UHPC test batches were conducted and the amount of HRWR was adjusted each time. The only other controlling factor was the mortar flow. An optimized value of HRWR will ensure that the mix is workable and that the fibers are suspended. Table 3 shows the modified McDaniel J3 mix design that was used.

Table 3: UHPC alternative mix design, J3 (McDaniel 2017)

Material	Amount per yd^3
Masonry Sand	1965 lb
Type 1 Portland Cement	1180 lb
GGBFS	590 lb
Silica Fume	197 lb
Water	393 lb
HRWR	15.77 fl oz./cwt

3.2 Casting and Curing of Slab Specimens

3.2.1 Casting

A NSC mix modeled after an ODOT Class AA mix was used for all normal concrete specimens. The specifications for the Class AA mix are shown in Table 4.

Table 4: ODOT Standard Specifications for Concrete Related Bridge Repair (2009)

Concrete Class	Min. Cement Content, lb/yd3	Air Content, %	Water/Cement Ratio, lb/lb	Slump, in.	Min. 28-Day Strength (f'c), psi
AA	564	6.5 ± 1.5	0.25 – 0.44	2 ± 1	4000
A	517	6.0 ± 1.5	0.25 – 0.48	2 ± 1	3000
HDC	825	6.5 ± 1.0	< 0.35	0.5 ± 1	4000
VES I	900	± 1.5	< 0.30	1 – 8	3000
VES III	600	6.0 ± 1.5	< 0.35	1 – 8	3000

Three slab joint specimen were cast and tested to evaluate the performance of UHPC connections. Each slab was fabricated from two normal concrete panels with dimensions of 4 feet wide, 4 feet long, and 8 inches deep and a UHPC joint with dimensions of 1 foot wide, 4 feet long, and 8 inches deep. All reinforcing for the slabs is #5 rebar size. The reinforcing layout for the slabs is shown in Figure 8. The NSC slabs

were designed to have 5 inches of reinforcing steel protruding from one end. This step was done to mimic field work where if a joint is sawn out, reinforcing steel may be exposed. The concrete for the slabs was provided by the Dolese Bros Co.

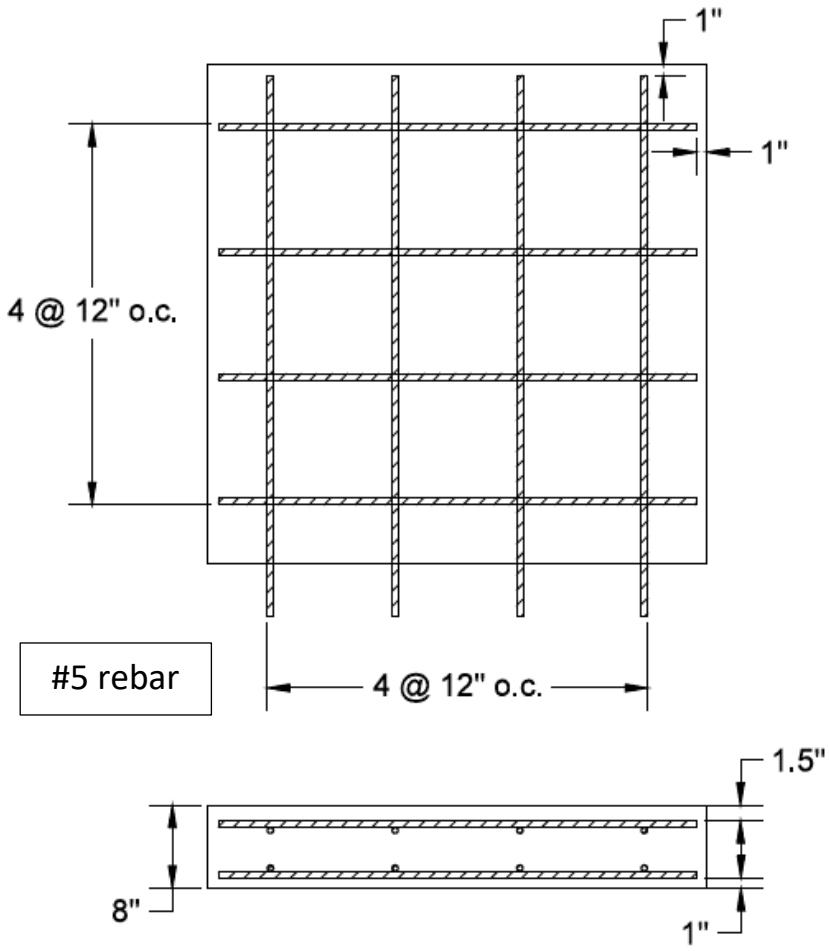

Figure 8: Plan and cross-sectional view of reinforcing bar layout for slab specimens (Funderburg 2017)

Once the concrete was poured into the forms, a broom finish was applied to the top surface of each slab panel. A broom finish is done in the field to promote water drainage perpendicular to traffic flow. Once the concrete was firm to the touch, the

slabs were covered with wet burlap and plastic tarp to retain moisture. Figures 9, 10 and 11 show the panels just prior to casting, after casting, and during curing, respectively.

Figure 9: Rebar layout prior to casting

Figure 10: Panel immediately after casting

Figure 11: Panels curing under wet burlap

3.2.2 Heat Curing

Before the UHPC joint was cast, the normal concrete panels were positioned, and splice bars were tied to the rebar protruding from the panels (Figures 12 and 13). The width of the UHPC joint joining the two normal concrete panels measured 12 inches. The joint form is shown in Figure 13, and the joint after curing is shown in Figure 14. The UHPC joints were heat cured for 36 hours using heat lamps. Thermocouples were used to monitor the temperature throughout the joint. The 36 hour period was determined as the most effective heat curing time from the McDaniel study (2017). Heat lamps were used to maintain a constant internal temperature of approximately 180°F. After 36 hours, the heat lamps were removed and the joints cured in normal conditions until 28 days.

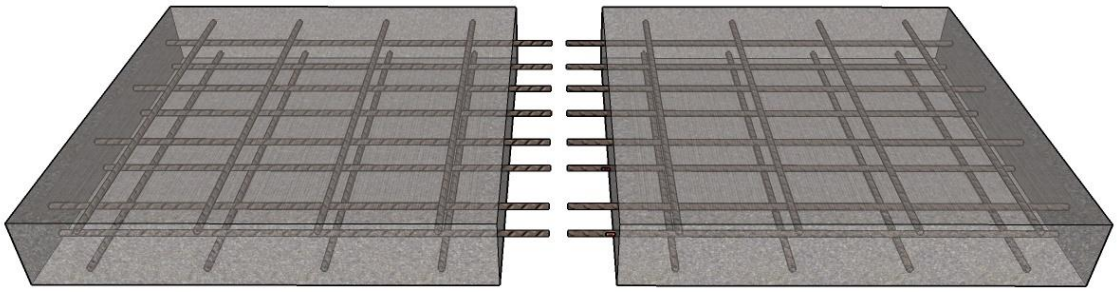

Figure 12: Positioned NSC panels

Figure 13: UHPC joint form

Figure 14: UHPC joint after curing

3.3 Slab Testing

The slabs were tested in a steel portal frame supported by 6 inches wide concrete beams and rubber pads at each end. Each specimen was loaded using a hydraulic ram and pump. From support to support, the specimens were 8 feet 6 inches in length and were loaded at 5 feet 2 inches from the west edge of the slab. Deflection measurements were taken by 7 linear variable differential transformers (LVDTs) that were placed underneath the slab in various locations (Figure 15). LVDT 1 was located within the hydraulic actuator at the load point. LVDTs 2 and 3 were placed 2 inches away from the slab edges and 5 inches away from the joint face. LVDT 5 was located 5 inches from the joint interface and 48 inches from the slab edge. LVDTs 4, 6 and 7 were placed 2 inches away from the slab edges. Two different types of strain gauges were used to measure concrete strain. Four external strain gauges were used on the edges of the slab. External strain gauges 2 and 4 were placed in the center of each end of the UHPC joint. External strain gauges 1 and 3 were placed on either side of strain gauge 2, 1 inch from

the edge of the joint. All of the external strain gauges were placed approximately 0.5 inches from the bottom of the slab. There were also 4 internal strain gauges placed on the rebar within the UHPC joint, as shown in Figures 16 and 17. Internal strain gauge 1 was placed on the bottom splice bar on the south outer edge of the joint. Internal strain gauge 2 was placed on the bottom bar protruding from the east panel on the south outer edge of the joint. Internal strain gauge 3 was placed on the bottom splice bar on the south interior. Internal strain gauge 4 was placed on the bottom bar protruding from the east panel on the south interior. The load was measured using a load cell, and the load was applied through a 10 inch by 20 inch metal plate on top of a rubber pad. All sensors were connected to a data acquisition system that collected data at 10 hertz.

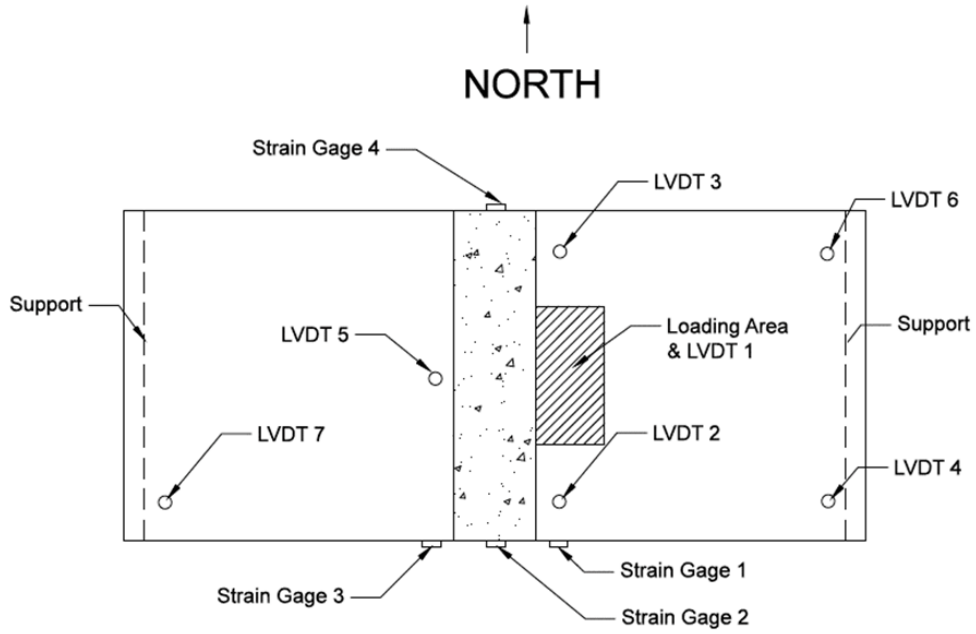

Figure 15: Instrumentation and layout for slab testing (Funderburg 2018)

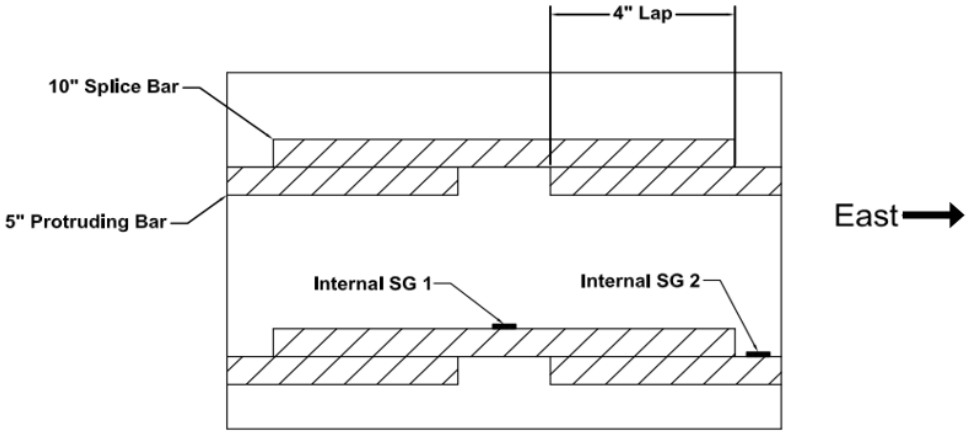

Figure 16: Cross-sectional view of UHPC joint with internal strain gauges

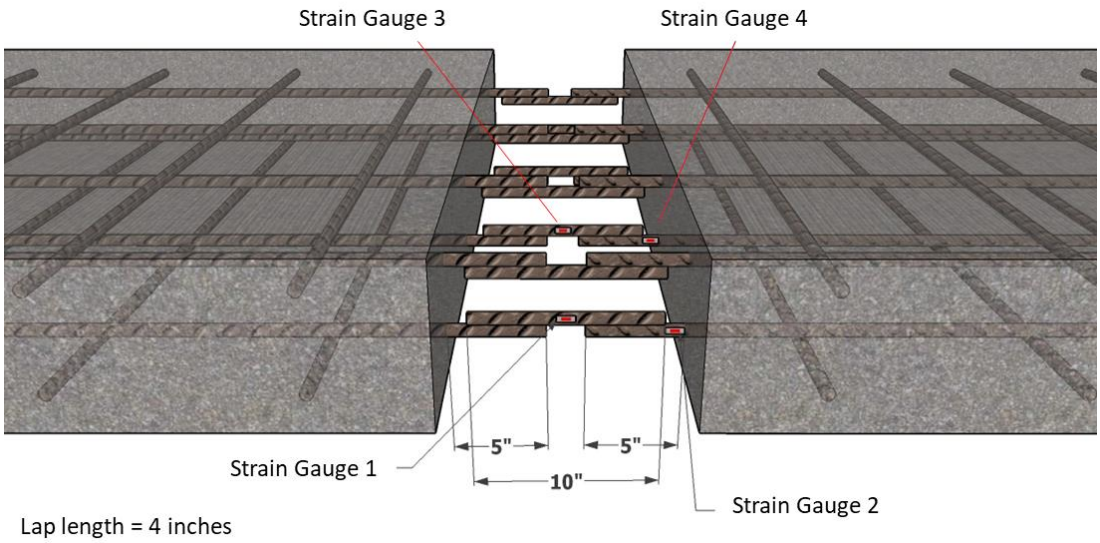

Figure 17: 3D view of UHPC joint

3.3.1 Slabs 1 and 2

Slabs 1 and 2 were initially tested using an electronically controlled servo valve MTS hydraulic ram. The MTS can produce a static load up to 22 kips. Both slabs were loaded in 1 kip increments up to the capacity of the machine. Once the capacity was reached, the slab was unloaded and the electronic system was switched out with a manually controlled load pump and a load cell with a higher capacity of 50 kips. Before the test resumed, all 7 of the LVDTs were removed from underneath the slab and LVDTs 2, 3 and 5 were replaced with wire potentiometers (wire pots). The wire pots have a longer stroke and would prevent the LVDTs from being damaged in the case that the slab deflected past the capacity of the LVDTs. Using the manual system, the slabs were loaded again in 1 kip increments until failure.

3.3.2 Slab 3

Slab 3 was tested dynamically using the same electronically controlled system as the static tests. The 3rd slab was loaded cyclically using a haversine waveform with a frequency of 1 hertz. All 7 LVDTs were placed in their original positions during this test. For the first 3 million cycles, the slab was going to be loaded to 90% of the calculated cracking moment. The calculated load for 90% of the cracking moment was 11 kips, but after physically analyzing the cracks of the statically loaded slabs, it was decided that slab 3 would be loaded to a maximum of 9 kips for the first 3 million cycles. After the first 3 million cycles, the maximum load was to be increased to 5% above the calculated cracking moment and the haversine loading would continue for 2 million more cycles or until failure. If 5 million cycles were reached, the slab would be statically tested to failure. The test setup for the slabs is shown in Figure 18.

Figure 18: Test setup for slabs

3.4 Casting and Curing of Composite MOR Specimens

Thirty-six composite MOR specimens were fabricated to analyze the effects of surface preparations and interface angles on flexural strength. The MOR specimens were fabricated with equivalent amounts of NSC and UHPC. A combination of 3 surface preparations and 4 interface angles were implemented.

3.4.1 Casting and Curing of NSC

The NSC mix design used for the composite MOR specimens was developed in the Funderburg (2018) study and is comparable to an ODOT Class AA concrete mix. The composite MOR specimens were cast with dimensions of 6 inches wide, 6 inches deep and 20 inches in length in accordance with ASTM C78 (2016). Each MOR specimen was composed of half normal concrete and half UHPC. The NSC was cast first and after 28 days of curing, the MOR specimens were cut and the surface preparations were applied. The specimens were then placed back into forms to pour the UHPC half. The specimens were cast in one of three surface preparations: wire brushed, sand blasted or exposed aggregate and one of four interface angles: 45 degrees, 60 degrees, 90 degrees or a shear key. Twelve full sized MOR specimens and 12 half-sized MOR specimens were cast using the mix design shown in Table 5. The 12 exposed aggregate MOR specimens were cast as half specimens due to the nature of the surface preparation. Table 6 shows the configurations of the composite MOR specimens NSC mix design. In addition to the MOR specimens, 4 inch by 8 inch compressive strength cylinders were cast to determine compressive strength over time. Figure 19 shows the

composite specimens after casting the NSC. All specimens were cured while covered in wet burlap and plastic tarp.

Table 5: NSC mix design

Material	Amount Per yd^3
Type 1 Portland Cement	588 lb
Rock	1841 lb
Sand	1290 lb
Water	224 lb
HRWR	3.5 fl oz./cwt
AEA	0.70 fl oz./cwt

Table 6: Composite MOR specimen configurations

Configuration	Surface Preparation	Casting Type	Total Resulting Composite Specimens
90 degrees	Sand-Blasted	2 Full specimens	4
90 degrees	Wire-Brushed	2 Full specimens	4
90 degrees	Exposed Aggregate	3 half specimens	3
60 degrees	Sand-Blasted	2 Full specimens	4
60 degrees	Wire-Brushed	2 Full specimens	4
60 degrees	Exposed Aggregate	3 half specimens	3
45 degrees	Sand-Blasted	2 Full specimens	4
45 degrees	Wire-Brushed	2 Full specimens	4
45 degrees	Exposed Aggregate	3 half specimens	3
Shear Key	Exposed Aggregate	3 half specimens	3

Figure 19: Composite MOR specimens after casting of NSC

3.4.2 Surface Preparation

Cutting Full Length Specimens

Saw cutting and surface preparation of specimens took place after curing for 28 days. All 12 full length specimens required cutting at a certain angle to make one half of a composite specimen. Using a wet saw, the specimens were cut at 45, 60 or 90 degree angles. When using the wet saw to cut specimens, one side is cut halfway through then the specimen is flipped 180 degrees and cut all the way through the specimen. Because of the nature of cutting with this saw, concrete ridges were present on some of the specimens. A small concrete grinder was used on select specimens to grind down ridges and create a visibly smooth surface before wire brushing and sand blasting surface preparations began.

Creating Exposed Aggregate Surface Preparation

All 12 exposed aggregate specimens were cast as half specimens using wooden inserts. Four interface configurations were required: 45 degree, 60 degree, 90 degree and shear key. Immediately before casting, the UHPC side of the MOR specimens had the faces of the wooden inserts coated with sugar using a spray adhesive. Sugar retards the curing of concrete so that a portion of unhardened cement could be removed to create the exposed aggregate surface preparation. After curing, the excess material was removed using a power washer. The inserts are shown in Figures 20 and 21.

Figure 20: Shear Key Insert

Figure 21: 45 degree exposed aggregate insert in MOR specimen form

Sand Blasting

The 12 specimens that had a sand blasted surface were put in a sand blasting cabinet and continuously blasted until an even surface was observed. The sand blasting cabinet used a fine sand as the blasting agent.

Wire Brushing

The 12 specimens that had a wire brushed surface were brushed evenly until the surface was visibly smooth. This surface preparation is smoother in comparison to the other two. The three types of surface preparation are shown in Figure 22.

Figure 22: Wire brushed, exposed aggregate and sand blasted surface preparations (left to right)

3.4.3 Casting and Curing of UHPC Alternative

After the NSC side of the MOR specimen were cut and the surfaces were prepared, the UHPC side of the composite specimens was cast, including 3 inch by 6 inch compressive strength cylinders. The 1 inch stainless steel fibers used in this mix are shown in Figure 23, the mix procedure was as follows:

1. Blend all dry constituents until fully combined (5-10 minutes)
2. Add water and half of HRWR over 2 minutes
3. Mix for 2 minutes
4. Add last half of HRWR over 1 minute

5. Mix for 5 minutes

6. Add fibers and continue to mix until fibers are dispersed in mixture

The J3 UHPC alternative after mixing and before casting is shown in Figure 24.

Figure 23: 1 inch stainless steel fibers

Figure 24: J3 UHPC alternative after mixing

The J3 mix was very thick and somewhat difficult to work with when casting the specimens. Once the UHPC was cast into the forms, the specimens were covered in wet burlap and plastic tarp and cured for 28 days. Figure 25 shows the composite MOR specimens after casting.

Figure 25: Composite specimens after casting

3.5 Full sized MOR Specimens

Six full size MOR specimens were cast in this study to create a baseline comparison for flexural strength of the composite MOR specimens. Three NSC MOR specimens and 3 UHPC MOR specimens were cast and tested. The NSC MOR specimens had a width of 6 inches, a depth of 6 inches and a length of 20 inches. The UHPC MOR specimens had a width of 3 inches, a depth of 3 inches and a length of 12 inches. The specimens were tested according to ASTM C78 (2016).

3.6 Testing of Composite MOR Specimens

Once the UHPC side of the MOR specimens cured for 28 days, they were tested. All of the composite MOR specimens were tested in the configuration shown in Figure 26 with the normal strength concrete on the bottom. The MOR specimens were tested as third point loading in accordance with ASTM C78 (2016). The specimens were loaded continuously and without shock on a digital Forney machine. Flexural testing was

performed, and at failure the composite MOR specimen was removed from the Forney and the length and depth of the failure interface was measured with dial calipers. If the specimen failed along the interface, measurements for both side were taken. In the case that there are two sets of measurements, the lowest flexural stress was recorded.

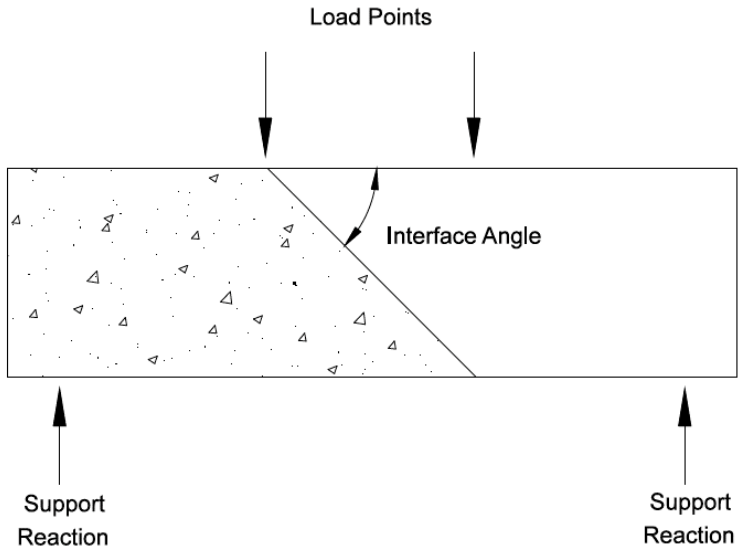

Figure 26: Relation of interface angle to loading points (Funderburg 2018)

During the demolding of the composite MOR specimens, 6 of the specimens separated at the interface before they could be tested, as shown in Figure 27. It can be seen that the UHPC had little to no bond to the NSC, which most likely caused it to separate. Four other specimens fell apart in the process of testing before any data could be collected.

Figure 27: Composite MOR that failed during demolding

3.7 Slant Shear Specimens

Four composite slant shear specimens were cast using half NSC and half UHPC. These were cast at the same time as the other composite specimens. The slant shear specimens were 6 inch by 12 inch cylinders. No surface preparation was used on these specimens as they were intended to be used as a quality control option in the application of UHPC joints. The slant shear specimens were cured in the same conditions as the composite MOR specimens and one of the specimens is shown in Figure 28.

Figure 28: Composite slant shear specimen

3.8 Slant Shear Testing

The slant shear tests were performed in accordance with ASTM C882 (2013). The specimens were tested in a Forney machine and were loaded at a rate of 35 psi/second until failure. Bond strength values were determined by dividing the maximum load by the area of the bonded surface. Figure 29 shows a slant shear specimen after testing.

Figure 29: Slant shear specimen post failure

3.9 Revised Mix Design and Recasting of Composite MOR Specimens

3.9.1 Revised Mix Design

Because of the undesirable results of the original composite MOR specimens, all 36 specimens were recast with a modified version of J3 with new fibers. Instead of using the original stainless steel fibers, Dramix® steel wire fibers were used in this mix. The revision of the mix design involved increasing the amount of high range water reducer until a mortar flow of 10 inches was reached and the new fibers could still be suspended. Test batches of 0.075 ft^3 were used. In addition to the increase of HRWR, a retarder was added to help increase the flow of the mix during placement. These two

additives created a more flowable mix, which increased the workability of the UHPC during placement. The final UHPC mix design for the composite MOR specimens is shown in Table 7.

Table 7: Modified J3 UHPC mix

Material	Amount Per yd^3
Masonry Sand	1965 lb
Type 1 Portland Cement	1180 lb
GGBFS	590 lb
Silica Fume	197 lb
Water	393 lb
HRWR	17.35 fl oz./cwt
Master Delvo Retarder	3 fl oz./cwt

3.9.2 Recasting of Composite MOR Specimens

The composite MOR specimens were re-cast with the modified mix design and Dramix® steel wire fibers (Figure 30). The modified mix was much more workable and fluid than the original mix, which can be seen in Figure 31.

Figure 30: Dramix® Steel fibers

Figure 31: Modified J3 UHPC after mixing

4 Test Results, Analysis and Comparison to Previous Study

This chapter will outline the test results and analysis of the results for all specimens in this study. First, compressive strengths for each concrete mix will be discussed followed by data for the composite MOR specimens, the slab specimens and the slant shear specimens. All data will be compared to the previous study using Ductal® (Funderburg 2018) instead of the UHPC alternative, J3.

4.1 Compressive Strength Results

4.1.1 Composite MOR NSC

The NSC mix design used for the first set of MOR specimens was equivalent to mix design 4 in the Funderburg (2018) study. This mix design was developed with in lab materials to closely match the properties of an ODOT Class AA mix. The NSC mix used for the second set of MOR specimens was batched and delivered by Dolese Bros. Co. and was also a Class AA mix. Both mix designs reached the target value of 4000 psi by 28 days (Table 8).

Table 8: Compressive strengths for MOR NSC

Age	Set 1 (psi)	Set 2 (psi)
1 - day	3050	3300
7 - day	5020	5580
28 - day	5750	4530

4.1.2 Composite MOR UHPC

All UHPC MOR specimens were made at the same time from the same mix. The UHPC alternative, J3, exceeded NSC 28 day strengths and also exceeded the target

strength of 14.8 ksi at 28 days (Table 9). The value 14.8 ksi is based off of the McDaniel (2017) study where the UHPC alternative J3 was developed.

Table 9: Compressive strengths for MOR UHPC

Age	Set 1 (psi)	Set 2 (psi)
3 - day	11,370	13,700
7 - day	14,600	14,790
28 - day	16,180	18,750

4.1.3 Full Size MOR Specimens

The full size MOR specimens used the same NSC mix design and UHPC mix design as the first set of MOR specimens (Tables 8 and 9). The compressive strengths of the full size MOR specimens reflect this very well because the 28 day strengths of the NSC and UHPC are very similar to that of the composite MOR strengths (Table 10). The NSC compressive strength reached the target value of 4000 psi at 28 days.

Table 10: Compressive strengths for full sized MOR specimens

Age	NSC (psi)	UHPC (psi)
3 - day	3830	11,370
7 - day	4250	15,810
28 - day	5670	16,030

4.1.4 Slab NSC

All slab specimens were poured at the same time using the same mix. Dolese Bros Co. batched and delivered this Class AA mix. The compressive strength reached the target value of 4000 psi at 28 days (Table 11). These compressive strengths are comparable to the compressive strengths for the MOR specimens.

Table 11: Compressive strength for slab NSC

Specimen	1 - day (psi)	7 - day (psi)	28 - day (psi)
All Slabs	1950	5420	6000

4.1.5 Slab UHPC Alternative

All UHPC joints were poured at the same time using the same mix. The UHPC alternative, J3, was cast in the joints. The compressive strength results for the UHPC joints were slightly higher than that of the MOR specimens at 3 and 7 days possibly due to the 36 hours of heat curing (Table 12). After 36 hours of heat curing, the joints cured in ambient temperatures for the remainder of the 28 days. The 28 day strength reached the target value of 14.8 ksi.

Table 12: Compressive strength for slab UHPC

Specimen	12 - hour (psi)	36 - hour (psi)	3 - day (psi)	7 - day (psi)	28 - day (psi)
All Joints	10,880	16,820	17,070	17,160	16,180

4.2 Composite MOR and Full Size MOR Test Results

The composite MOR specimens were tested once the UHPC had cured for 28 days. The maximum tensile stress at failure was determined from an equation in ASTM C78 (2016). The first set of composite MOR specimen results will be compared to the full size NSC MOR specimens. The modified composite MOR specimen results will be compared to the calculated flexural tension strength value from ACI 318 since corresponding full size MOR specimens were not fabricated for the modified composite specimens.

4.2.1 Composite MOR Specimens

Tables 13-16 show the test results for the first set of composite MOR specimens. The data is organized in relation to interface angle and surface preparation. The designation WB corresponds to wire brushed, SB corresponds to sand blasted, EA corresponds to exposed aggregate and SK corresponds to shear key. As stated in the previous chapter, 10 of the 36 specimens separated during demolding. The other 26 specimens failed at the interface when tested (Figure 32). This failure type implies that the UHPC did not properly bond to the NSC. For this test, failure in the base concrete is desired in order to exhibit monolithic behavior between the UHPC and NSC.

Figure 32: Interface failure (9-EA-90)

Table 13: 90-Degree composite MOR specimen results

90 Degree Specimens	Failure Type	Peak Load (lb)	Flexural Stress (psi)	Average Flexural Stress (psi)	Std. Deviation (psi)
1-WB-90	Interface	0	0	0	0
2-WB-90	Interface	0	0		
3-WB-90	Interface	0	0		
4-WB-90	Interface	0	0		
5-SB-90	Interface	3925	305	205	68
6-SB-90	Interface	2635	210		
7-SB-90	Interface	2385	190		
8-SB-90	Interface	1445	115		
9-EA-90	Interface	920	70	72	10
10-EA-90	Interface	1100	85		
11-EA-90	Interface	800	60		

Table 14: 60-Degree composite MOR specimen results

60 Degree Specimens	Failure Type	Peak Load (lb)	Flexural Stress (psi)	Average Flexural Stress (psi)	Std. Deviation (psi)
1-WB-60	Interface	0	0	0	0
2-WB-60	Interface	0	0		
3-WB-60	Interface	0	0		
4-WB-60	Interface	0	0		
5-SB-60	Interface	4055	315	159	142
6-SB-60	Interface	435	35		
7-SB-60	Interface	3810	285		
8-SB-60	Interface	0	0		
9-EA-60	Interface	2250	180	158	24
10-EA-60	Interface	1560	125		
11-EA-60	Interface	2175	170		

Table 15: 45-Degree composite MOR specimen results

45 Degree Specimens	Failure Type	Peak Load (lb)	Flexural Stress (psi)	Average Flexural Stress (psi)	Std. Deviation (psi)
1-WB-45	Interface	0	0	46	31
2-WB-45	Interface	520	40		
3-WB-45	Interface	1085	85		
4-WB-45	Interface	795	60		
5-SB-45	Interface	1030	80	265	118
6-SB-45	Interface	3760	290		
7-SB-45	Interface	5215	410		
8-SB-45	Interface	3600	280		
9-EA-45	Interface	1920	150	87	55
10-EA-45	Interface	610	15		
11-EA-45	Interface	1165	95		

Table 16: Shear Key composite MOR specimen results

Shear Key Specimens	Failure Type	Peak Load (lb)	Flexural Stress (psi)	Average Flexural Stress (psi)	Std. Deviation (psi)
1-EA-SK	Interface	4265	345	418	77
2-EA-SK	Interface	6600	525		
3-EA-SK	Interface	5135	385		

Figure 33 compares the average maximum flexural stress for each type of interface angle and surface preparation. Nine of the 10 specimens that separated before testing were wire brushed specimens. The exposed aggregate surface preparation performed the best in the shear key configuration. The sand blasted surface preparation performed the best in the 45 degree configuration. There is no data for the 90 degree and 60 degree wire brushed specimens. After calculating the average flexural stress of all tested specimens in a particular surface preparation, the results for wire brushed,

sand blasted and exposed aggregate were 15 psi, 210 psi, and 184 psi respectively. This implies that the sand blasted specimens performed the best overall.

It is unclear which interface angle performed the best. The shear key configuration reached the highest flexural stress at 418 psi. After taking the average flexural stress of all specimens in a particular interface angle, the results for 90 degrees, 60 degrees and 45 degrees were 92 psi, 105 psi and 132 psi, respectively. This implies that the 45 degree surface configuration performed the best. Unfortunately none of the composite MOR specimens reached the target flexural stress of 605 psi, based off of the full sized NSC MOR specimen flexural strength, which further confirms the UHPC bonded poorly to the NSC.

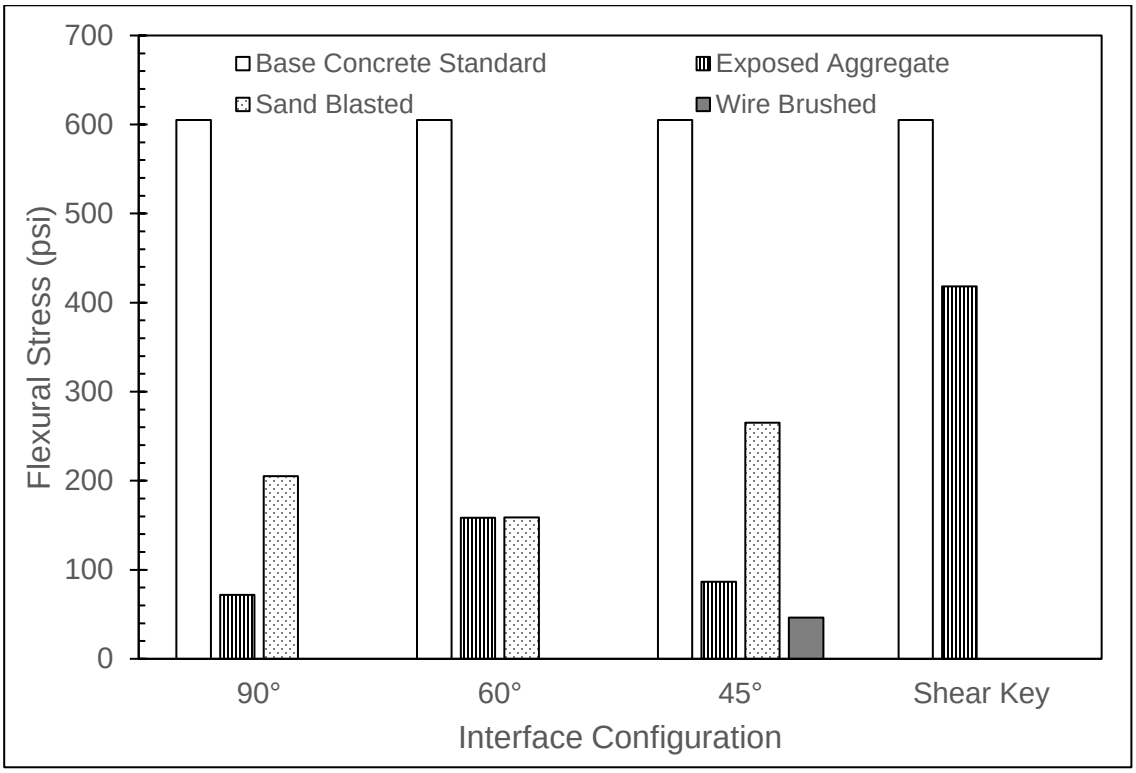

Figure 33: Average maximum flexural stress vs interface configuration

4.2.2 Modified Composite MOR Specimens

Tables 17-20 show the test results for the second set of composite MOR specimens. The data is organized in the same matter as the first set. Nine of the 36 MOR specimens failed in the base concrete while the others failed at the interface. Figure 34 shows two types of base concrete failures. The base concrete failure indicates that the NSC and UHPC acted monolithically and the bond is stronger than that of the first set of composite MOR specimens.

Figure 34: Base concrete failures (7-SB-90/3-WB-45)

Table 17: 90-Degree modified composite MOR specimen results

90 Degree Specimens	Failure Type	Peak Load (lb)	Flexural Stress (psi)	Average Flexural Stress (psi)	Std. Deviation (psi)
1-WB-90	Interface	5320	410	279	94
2-WB-90	Interface	2075	155		
3-WB-90	Interface	4165	310		
4-WB-90	Interface	3220	240		
5-SB-90	Interface	2995	220	325	119
6-SB-90	Interface	2490	195		
7-SB-90	NSC	6025	460		
8-SB-90	NSC	5390	425		
9-EA-90	Interface	1850	140	122	13
10-EA-90	Interface	1450	110		
11-EA-90	Interface	1580	115		

Table 18: 60-Degree modified composite MOR specimen results

60 Degree Specimens	Failure Type	Peak Load (lb)	Flexural Stress (psi)	Average Flexural Stress (psi)	Std. Deviation (psi)
1-WB-60	Interface	7295	555	537	16
2-WB-60	Interface	1580	120		
3-WB-60	NSC	7030	515		
4-WB-60	Interface	7300	540		
5-SB-60	Interface	5245	400	489	56
6-SB-60	NSC	6645	485		
7-SB-60	Interface	6790	520		
8-SB-60	Interface	7395	550		
9-EA-60	Interface	2285	175	192	17
10-EA-60	Interface	2800	215		
11-EA-60	Interface	2385	185		

Table 19: 45-Degree modified composite MOR specimen results

45 Degree Specimens	Failure Type	Peak Load (lb)	Flexural Stress (psi)	Average Flexural Stress (psi)	Std. Deviation (psi)
1-WB-45	NSC	6450	510	494	87
2-WB-45	Interface	6025	450		
3-WB-45	NSC	7885	625		
4-WB-45	NSC	4965	390		
5-SB-45	Interface	6470	505	527	40
6-SB-45	Interface	7640	595		
7-SB-45	NSC	6535	515		
8-SB-45	NSC	6285	495		
9-EA-45	Interface	4300	340	292	52
10-EA-45	Interface	2835	220		
11-EA-45	Interface	3965	315		

Table 20: Shear Key modified composite MOR specimen results

Shear Key Specimens	Failure Type	Peak Load (lb)	Flexural Stress (psi)	Average Flexural Stress (psi)	Std. Deviation (psi)
1-EA-SK	Interface	2145	160	193	25
2-EA-SK	Interface	2610	200		
3-EA-SK	Interface	2845	220		

Figure 35 compares the average maximum flexural stress for each type of interface angle and surface preparation. Five of the 9 specimens that failed in the base concrete were sand blasted and the other 4 were wire brushed. After taking the average flexural stress of all specimens in a particular surface preparation, the results for wire brushed, sand blasted, and exposed aggregate were 436 psi, 447 psi, and 200 psi respectively. This implies that the sand blasted specimens performed the best overall, which is consistent with the first set of MOR specimens, but the wire brushed

specimens were close behind falling within 2.5% of the sand blasted specimens. The wire brushed configuration reached the highest flexural stress of 537 psi.

After taking the average flexural stress of all specimens in a particular interface angle, the results for 90 degrees, 60 degrees and 45 degrees were 242 psi, 406 psi and 438 psi, respectively. This implies that the 45 degree surface preparation again performed the best. Ten of the composite MOR specimens reached the target flexural stress of 504 psi which is based on the calculated value of a full size NSC MOR specimen. These results are significantly better than the first set, but a majority of the specimens still failed at the interface meaning that they may not have reached the full potential of strength. Because the composite MOR specimens may not have reached the full potential of strength, they cannot be adequately compared to specimens made with Ductal® instead of J3.

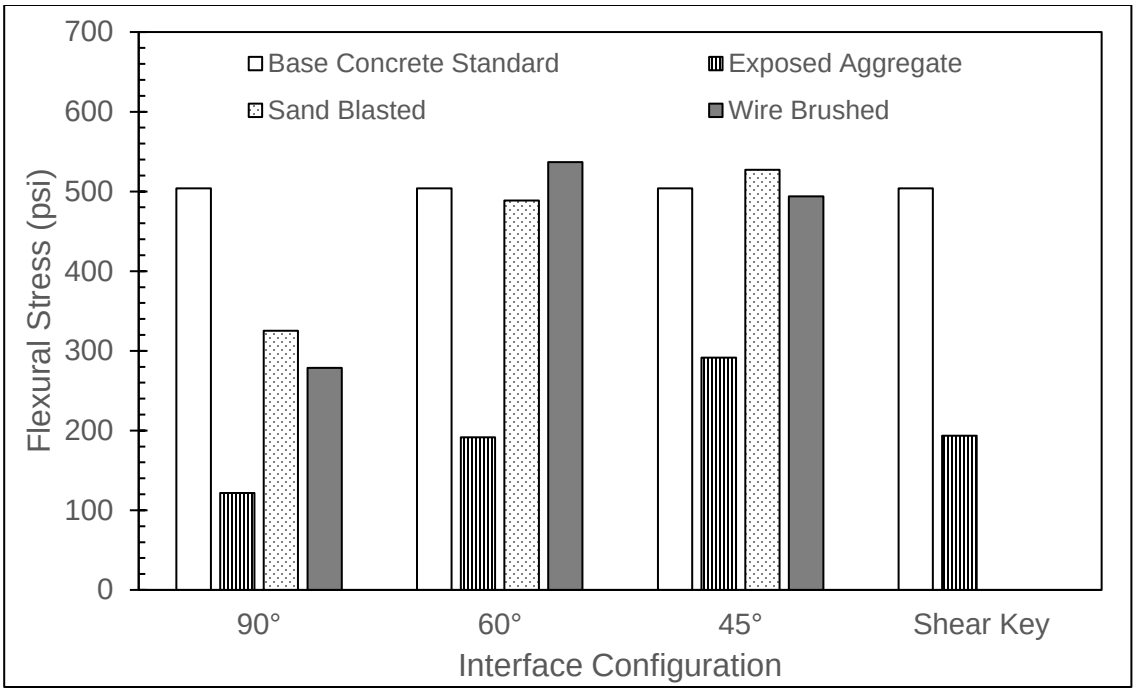

Figure 35: Average Maximum flexural stress vs. interface configuration including all values

The values for the exposed aggregate surface preparation were lower than expected. Figure 36 shows an exposed aggregate specimen after failure. A thin layer of uncured UHPC broke off on the NSC side of the composite specimen. Dragging a fingernail over the seemingly uncured concrete made an indention which confirmed that the thin layer was uncured and powdery. This happened to other exposed aggregate specimens as well. Because of the low water to cement ratio of UHPC, it has limited water to hydrate. The NSC may have absorbed the water necessary for curing the UHPC at the interface, which would weaken the bond between UHPC and NSC. The absorption potential of the exposed aggregate surface preparation is higher than the other surface preparations because it exposes more voids in the NSC. This could explain the lower than expected performance of the exposed aggregate specimens.

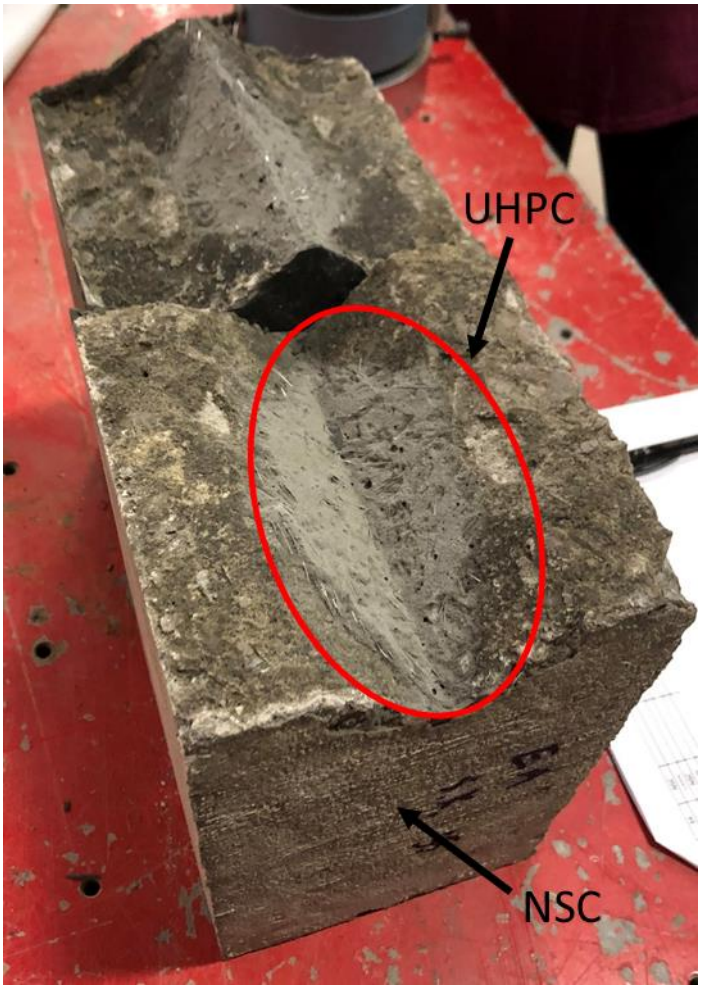

Figure 36: Interface failure on exposed aggregate, shear key specimen (2-EA-SK)

4.2.3 Full size MOR Specimens

Full size MOR specimens were fabricated in order to create a target range of flexural stress values for the composite specimens (Tables 21 and 22). The NSC MOR specimens determined the target value for the composite MOR specimens, and the UHPC MOR specimens determined a "maximum" value the composite MOR specimens could reach. For the UHPC specimens, the average flexural strength value and the standard deviation value are taken from only the second and third specimens due to the first being an outlier.

While all the composite MOR specimens stayed under the maximum value, between the two sets of composite MOR specimens, only one specimen reached the target flexural strength of 605 psi. This can be credited to the poor bond between NSC and UHPC. The angled composite MOR specimens that failed in the NSC failed similar to Figure 37 which began failing in the NSC and eventually failed due the UHPC disconnecting from the NSC. This suggests that these MOR specimens could have reached a higher flexural strength had it not been for bond issues.

Figure 37: Composite MOR base concrete failure (8-SB-45)

Table 21: NSC full size MOR specimen results

Specimen	Peak Load (lb)	Flexural Stress (psi)	Average Flexural Stress (psi)	Std. Deviation (psi)
1	8175	665	605	43
2	7500	585		
3	7010	565		

Table 22: UHPC full size MOR specimen results

Specimen	Peak Load (lb)	Flexural Stress (psi)	Average Flexural Stress (psi)	Std. Deviation (psi)
1	12055	4415	2600	195
2	7820	2795		
3	6740	2405		

4.3 Slab Test Results

Figures 38-46 show the results from testing slab 1, parts 1 and 2. Figures 47-57 show the results from testing slab 2, parts 1 and 2. The MTS system was used on the first part of slabs 1 and 2. Part 1 slab testing exhibits early cracking behavior. A manual hydraulic cylinder was used for part 2 testing. Part 2 slab testing exhibits behavior up to and including failure. Figures 58-64 show the results from slab 3 testing. The MTS system and manual pump were used to test slab 3.

4.3.1 Slab 1 Static Test Results

The maximum load reached by slab 1 during part 1 was 21.3 kips. To prevent exceeding the capacity of the MTS system, the specimen was unloaded and switched to a manual hydraulic cylinder. The first cracks appeared in the NSC at 14 kips of load. The load vs. deflection curve for this portion of testing is shown in Figure 38. After

further graphical evaluation, cracking was apparent before 14 kips and occurred closer to 10.5 kips. The point on the curve where there is an increase in deflection but no increase in load was the suspected cracking load point. After reaching 10.5 kips, the slope of the curve only decreases slightly. Once the visual cracking load of 14 kips was reached, there was a more significant reduction in slope which indicates reduced stiffness. The load corresponding to the cracking moment of a monolithic NSC slab was calculated as 12.2 kips for comparison. The graphically determined cracking load of this slab specimen is less than that of an ideal monolithic slab. This may be due to differences in tensile strength between the NSC and UHPC. When the specimen was unloaded it returned to a deflection value of 0.1 inches.

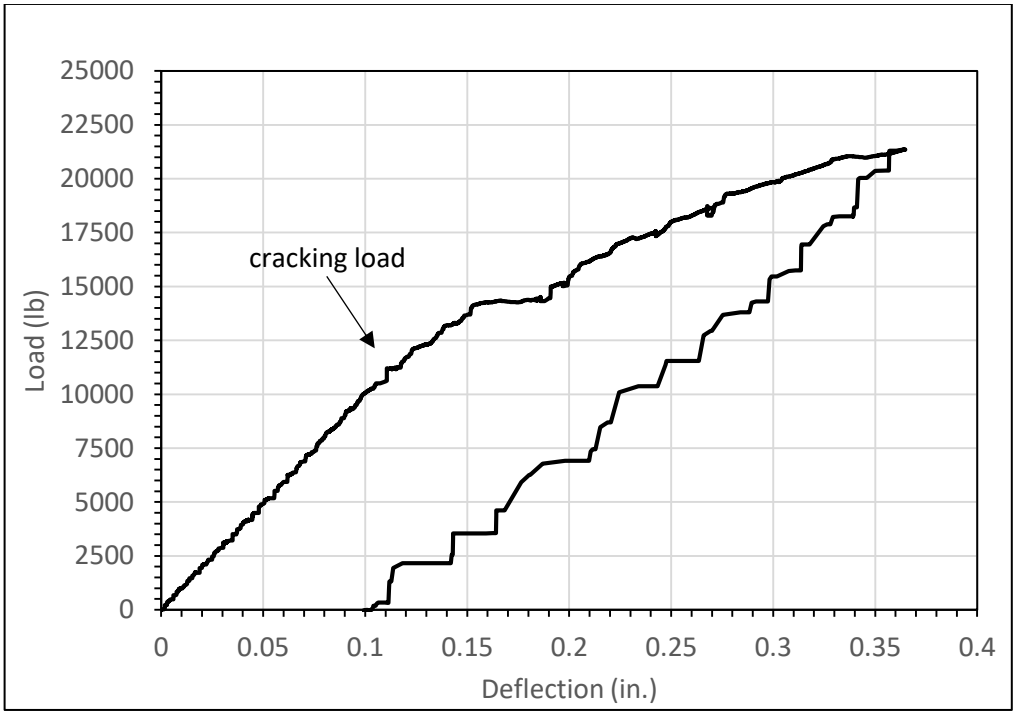

Figure 38: Load vs. Deflection curve for slab 1, part 1

Figure 39 shows the load vs. strain plot for internal strain gages 1, 3 and 4. Strain gauge 2 is not shown because of the inconsistent nature of the data. The data is

consistent with the load vs. deflection curve. All 3 strain gages seem to have an increase in strain at 14 kips (the visual cracking load of the NSC) before returning to a shallower slope throughout the rest of the curve. Strain gauge 1 and strain gauge 4 exceeded the 2000 microstrain yield point which means the 4 inch lap length is sufficient to yield the bars. The noticeably higher strains in strain gage 4 may have been due to a lack of consolidation of the UHPC around the reinforcing bar at that location or cracking nearby.

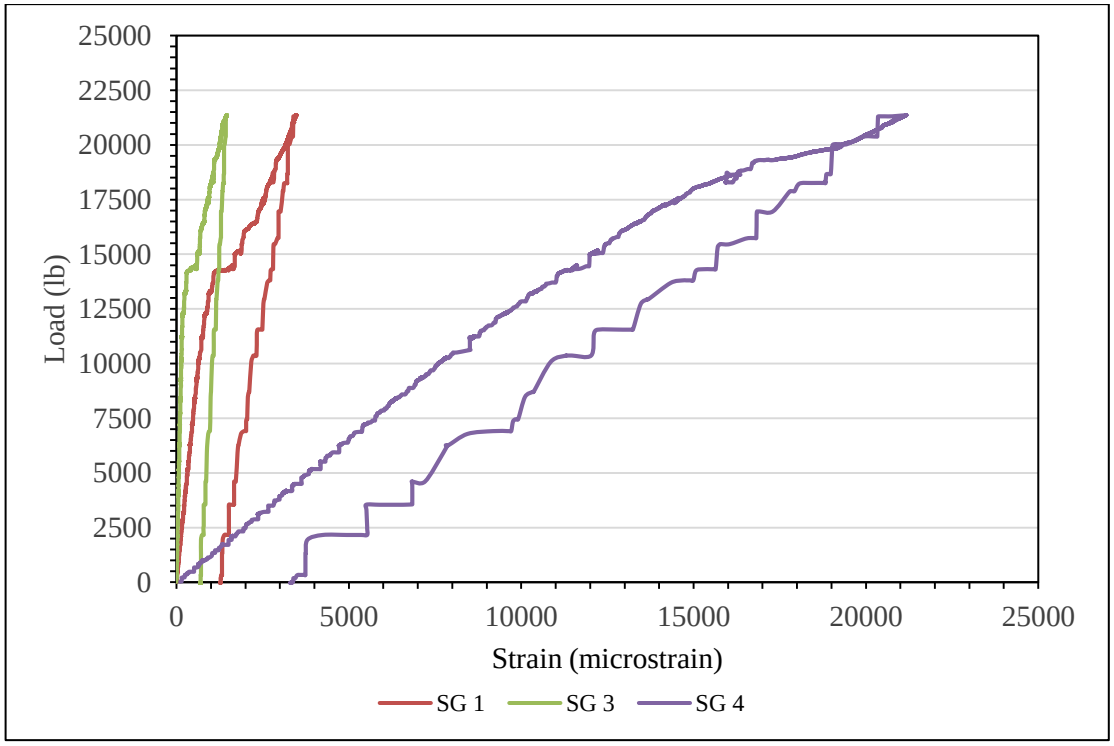

Figure 39: Load vs. Strain curve for slab 1, part 1, internal strain gauges

Figure 40 shows the load vs. strain plot for external strain gages 1 and 3. Strain gauges 2 and 4 are not shown because of the inconsistent nature of the data. Strain gauge 2 seems to have disconnected before or during testing and had little to no reading. Strain gauge 4 had an excessive amount of noise in the data and was not useful. Strain

gauge 1 also has a lot of noise but a reasonable trend can still be found. The curves for the two strain gages shown are consistent with the load deflection curve such that strain increases with the load until the slab cracks and releases tension in the strain gages. The maximum strain value reached (not including the noise) was approximately 24 microstrain. The curve for strain gage 1 seems to have a change in slope during the initial loading but the data is difficult to interpret.

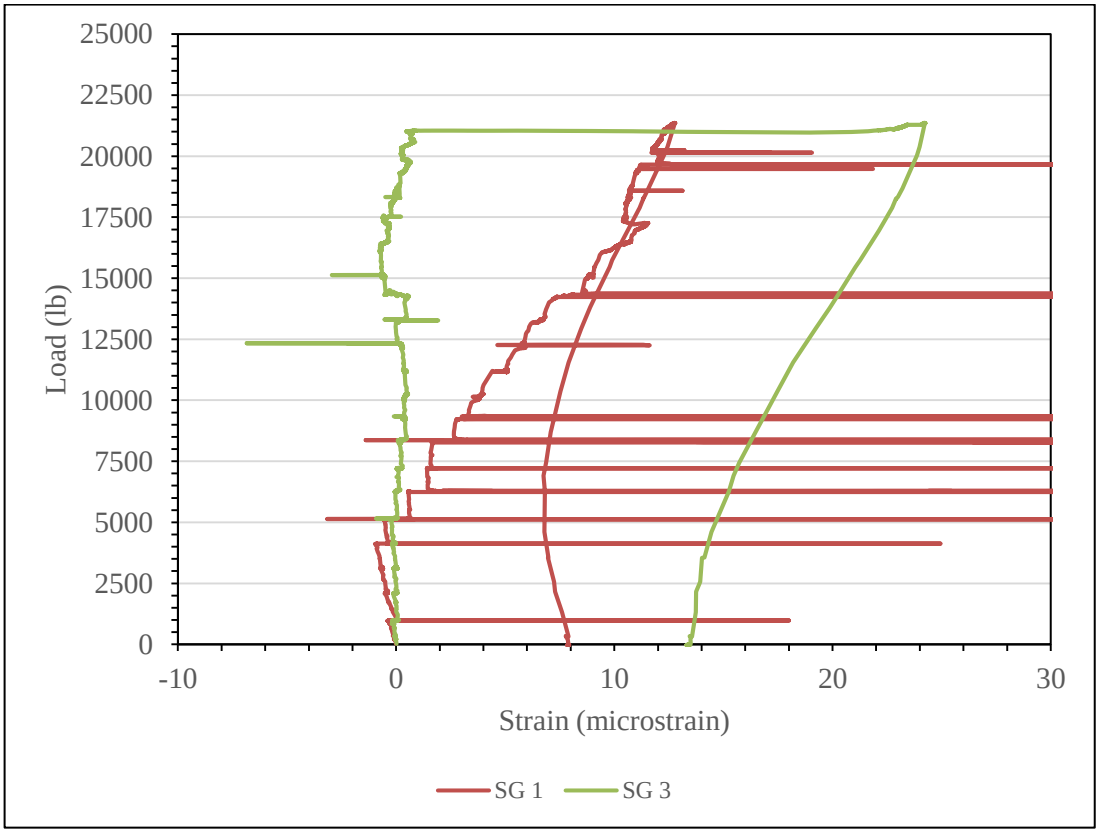

Figure 40: Load vs. Strain curve for slab 1, part 1, external strain gauges

Figure 41 shows the load vs. deflection curve plot for part 2 of testing slab 1. Because a manual pump was used for this portion of the test, the load application was more variable than the digital MTS system. As 1 kip load increments were applied, the slab was examined for cracks and within that timeframe, the load dropped slightly,

which explains the trend of the curve. Failure was determined as the slab specimen not sustaining any additional load and yielding of the reinforcing steel. Crushing was also observed across the top of the specimen in the NSC at failure. The ultimate load reached for slab 1 was 34.3 kips. Plateauing of the load vs. deflection plot is indicative of yielding in the reinforcing steel within the joint. The calculated failure load corresponding to the maximum flexural capacity of a monolithic NSC slab was 23.7 kips. The actual failure load exceeded the calculated value by 45%. The residual deflection at the end of part 1 of testing was 0.1 inches. After failure, the specimen was unloaded and returned to a value of 1.2 inches, which indicates plastic deformation. The maximum deflection during this test was 1.75 inches. Figure 42 shows the load vs. deflection curve of slab 1, parts 1 and 2, together. The unloading of part 2 is not shown here. The slope of part 2 is shallower than that of part 1. This is reasonable because the slab has already cracked once part 2 of the test had begun.

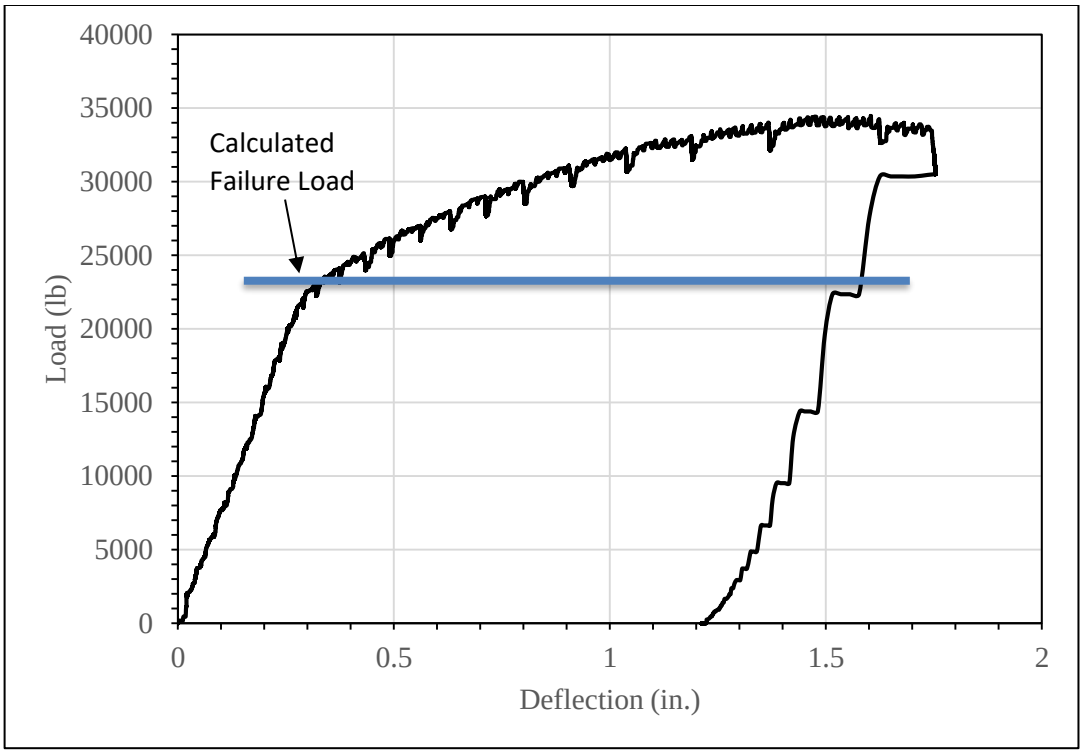

Figure 41: Load vs. Deflection curve for slab 1, part 2

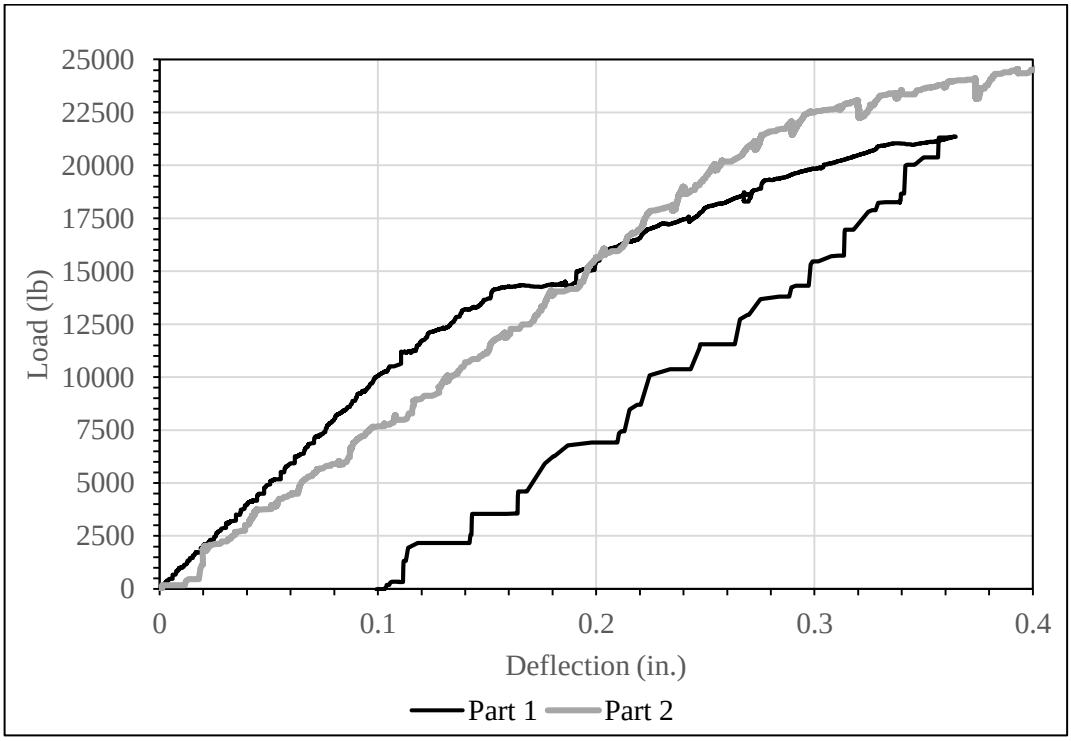

Figure 42: Load vs. Deflection curves for slab 1, parts 1 and 2

Figures 43 and 44 show cracks on the slab after failure. At failure, there were no cracks in the UHPC joint, only in the NSC. Significant cracking occurred underneath the load point. Additional cracks formed in the NSC starting at the NSC and UHPC interface. The visible separation between the NSC and UHPC interface further indicates a bond issue. All cracks moved closer to the load point as the specimen approached failure, which was expected.

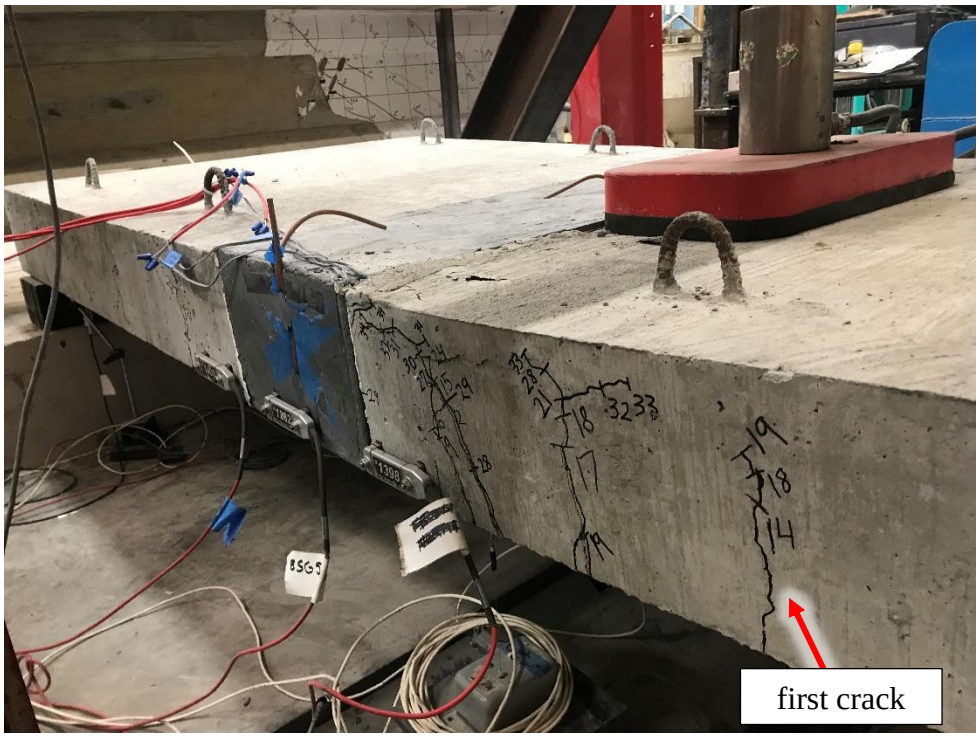

Figure 43: Cracks formed under load point for slab 1

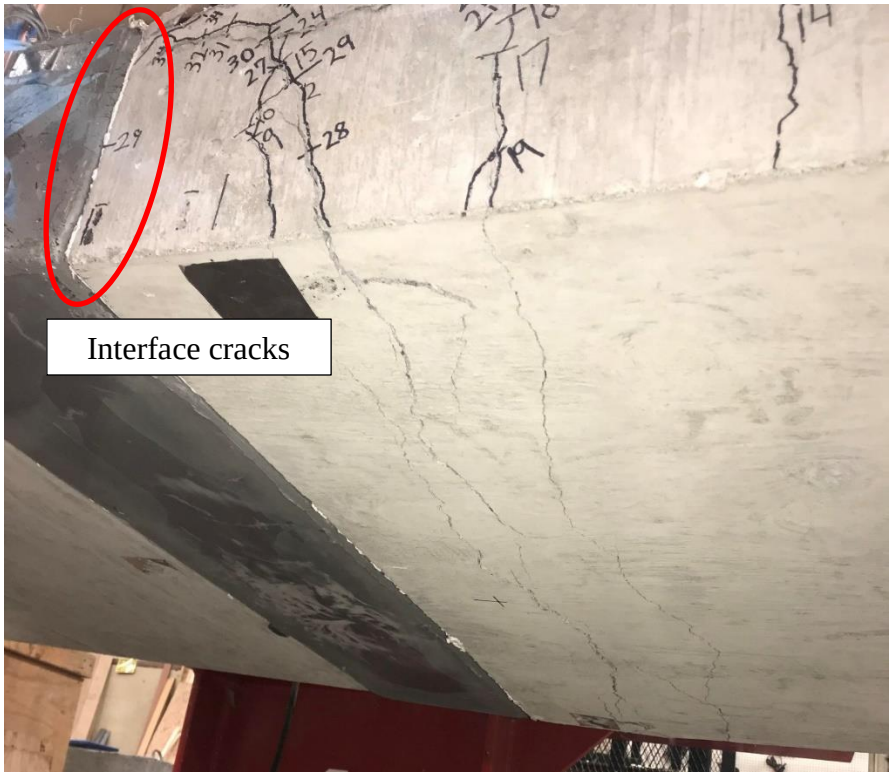

Figure 44: Cracking underneath load point for slab 1

Figure 45 shows the Funderburg (2018) study with Ductal® and the current study load vs. deflection curves of slab 1, part 1 together. Funderburg had a graphically determined cracking load of 10.9 kips and a visual cracking load of 14 kips, very similar to the values found in this study. The deflection returned to a lower value of 0.07 inches and the curve had a steeper slope throughout part 1 of this slab test.

Figure 46 shows the Funderburg (2018) study with Ductal® and the current study load vs. deflection curves of slab 1, part 2 together. Funderburg reached an ultimate load of 36.2 kips and the total deflection returned to a slightly higher value of 2.02 inches. There is only a 5% difference in the ultimate load capacity for slab 1 in these 2 studies.

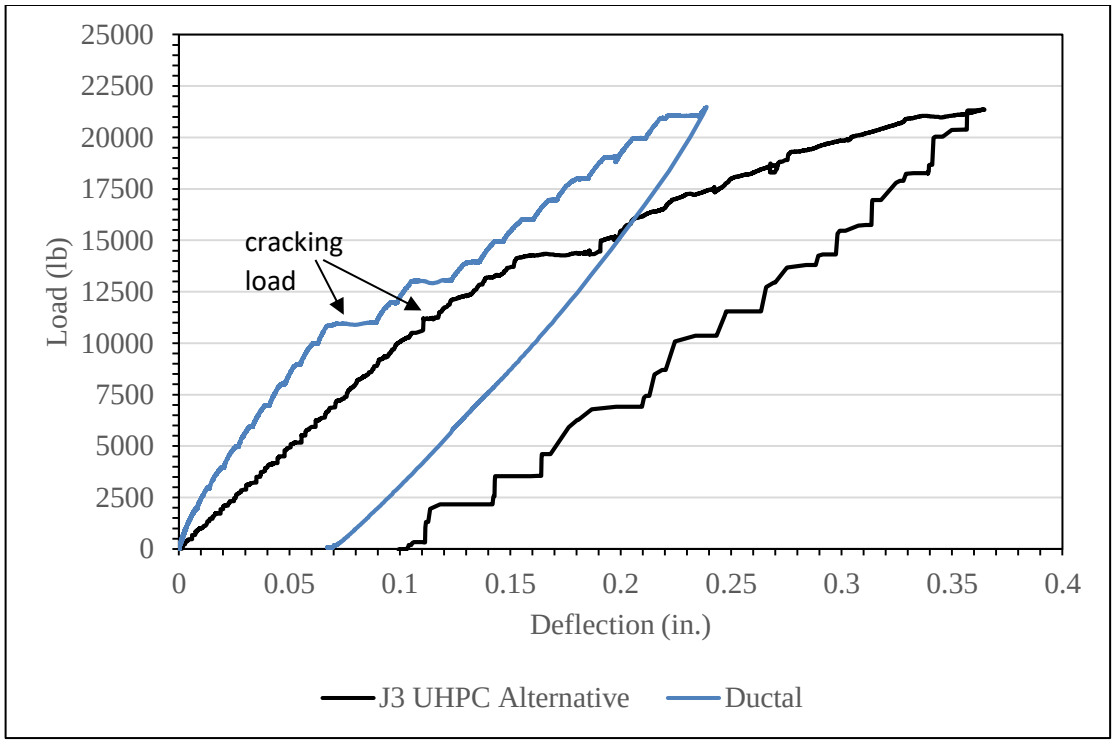

Figure 45: Load vs. Deflection curves for slab 1, part 1 compared to Ductal®

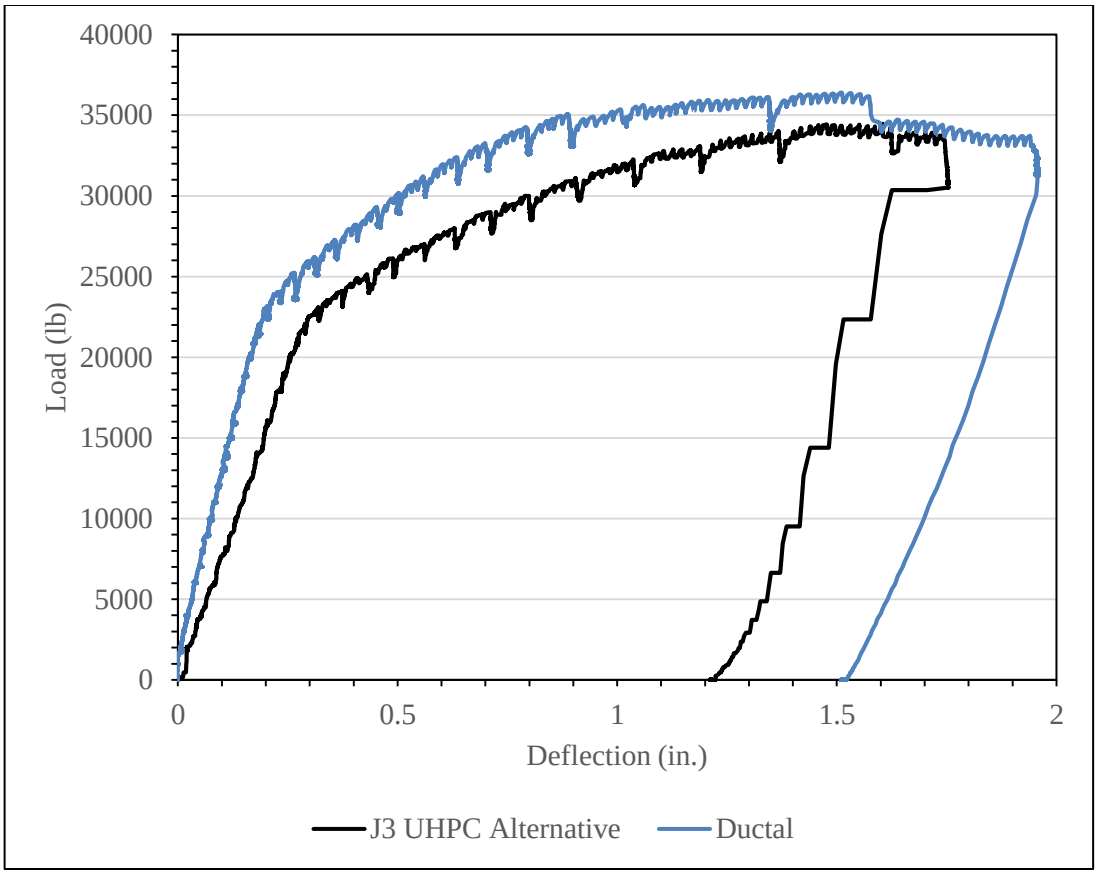

Figure 46: Load vs. Deflection curves for slab 1, part 2 compared to Ductal®

4.3.2 Slab 2 Static Test Results

The maximum load reached by slab 2 during part 1 was 21.3 kips. The intention was for slab 2 to be tested identically to slab 1. Slab 2 was mistakenly loaded constantly up to 21 kips instead of being loaded in 1 kip increments up to 21.3 kips. This caused early deformation of the slab specimen. The test was restarted, then loaded at 1 kip increments to 21.3 kips. The first visual cracks were seen at 9 kips. The graphically determined cracking load from Figure 47 was actually closer to 8.2 kips. This may not accurately represent the actual cracking load due to the initial, inaccurate loading of the slab. The point on the curve where there is an increase in deflection but no increase in load occurred much earlier in this slab test than in the first slab test. After reaching 8.2

kips, the slope of the curve stays about the same. The load corresponding to the cracking moment of a monolithic NSC slab was calculated as 12.2 kips. The graphically determined cracking load of this slab specimen is less than that of an ideal monolithic slab. This may be due to differences in tensile strength between the NSC and UHPC as well as the loading inconsistencies. When the specimen was unloaded it returned to a deflection value of 0.04 inches.

The load vs. deflection curves for slabs 1 and 2, part 1 are shown together in Figure 48. Slab 2 has a significantly shallower loading slope than slab 1. However, both slabs have a nearly identical unloading slope, so the loading differences are most likely due to the inconsistent initial loading sequence. Slab 1 and slab 2 both reached a maximum load of 21.3 kips during part 1.

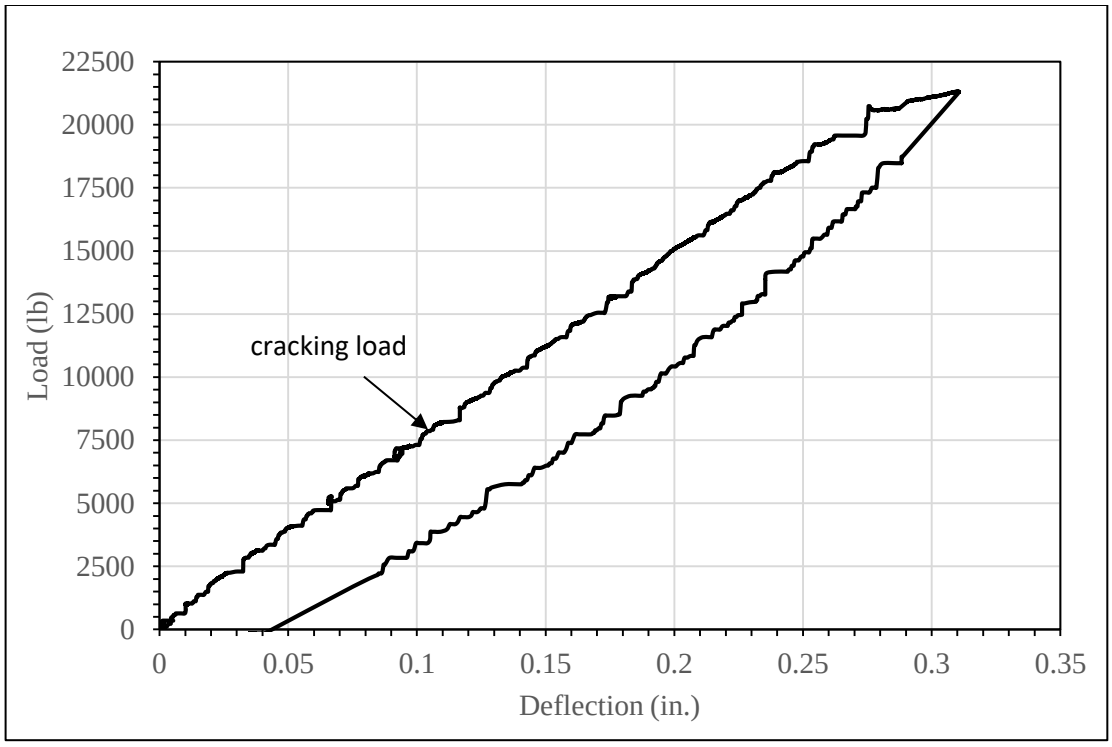

Figure 47: Load vs. Deflection curve for slab 2, part 1

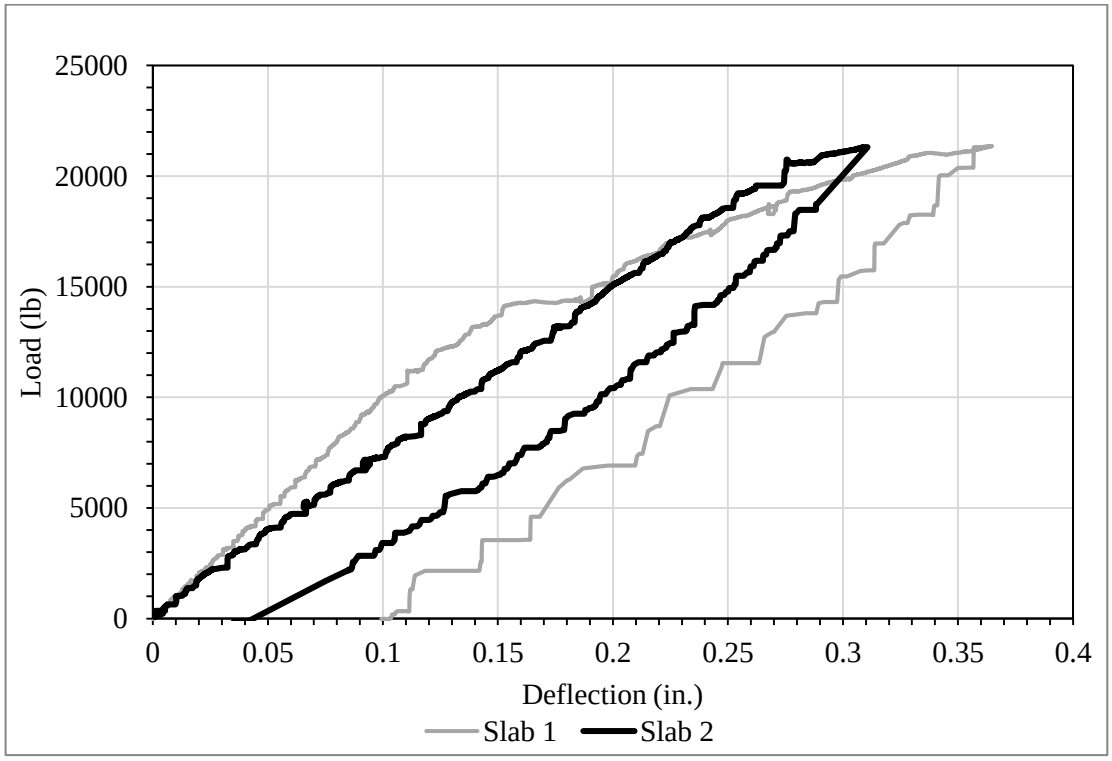

Figure 48: Load vs. Deflection curve for slabs 1 and 2, part 1

Figure 49 shows the load vs. strain plot for internal strain gages 2-4. Strain gauge 1 is not shown because it appeared to collect no data. The internal strain gage data is very unusual and is inconsistent with the load vs. deflection curve and therefore difficult to interpret. The unusual data may be due to the inconsistent loading but there may have been a problem with the strain gages themselves or problems with data recording.

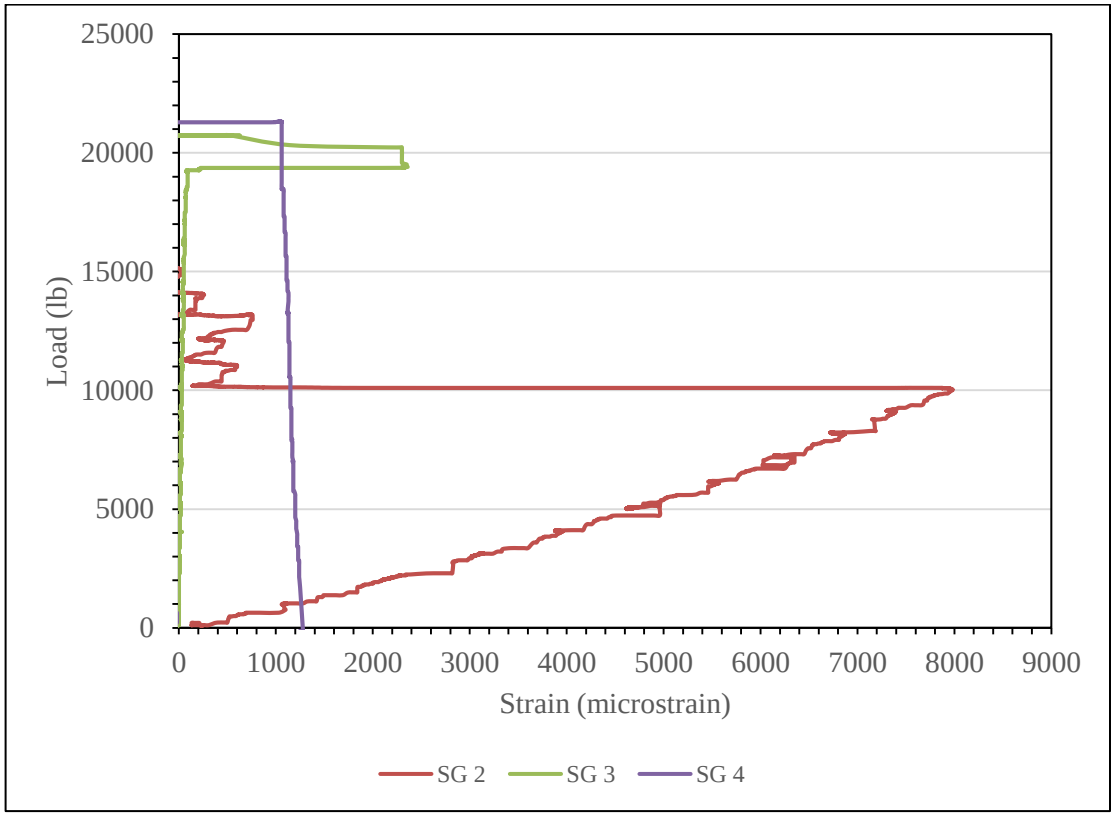

Figure 49: Load v. Strain curve for slab 2, part 1, internal strain gauges

Figure 50 shows the load vs. strain plot for external strain gages 1 and 3. External strain gauges 2 and 4 were not included in this data set because the data was not reliable. External strain gauge 2 appeared to not collect data at all with values remaining at zero. It is possible this strain gauge became disconnected from the side of

the slab before testing. Strain gauge 4 had an excessive amount of noise in the data and was not useful. Strain gauge 1 had some noise but a reasonable trend can still be found. The curves for the two strain gages shown are consistent with the load deflection curve such that strain increases with the load until the slab cracks and releases tension in the strain gages. The maximum strain value reached was approximately 22 microstrain.

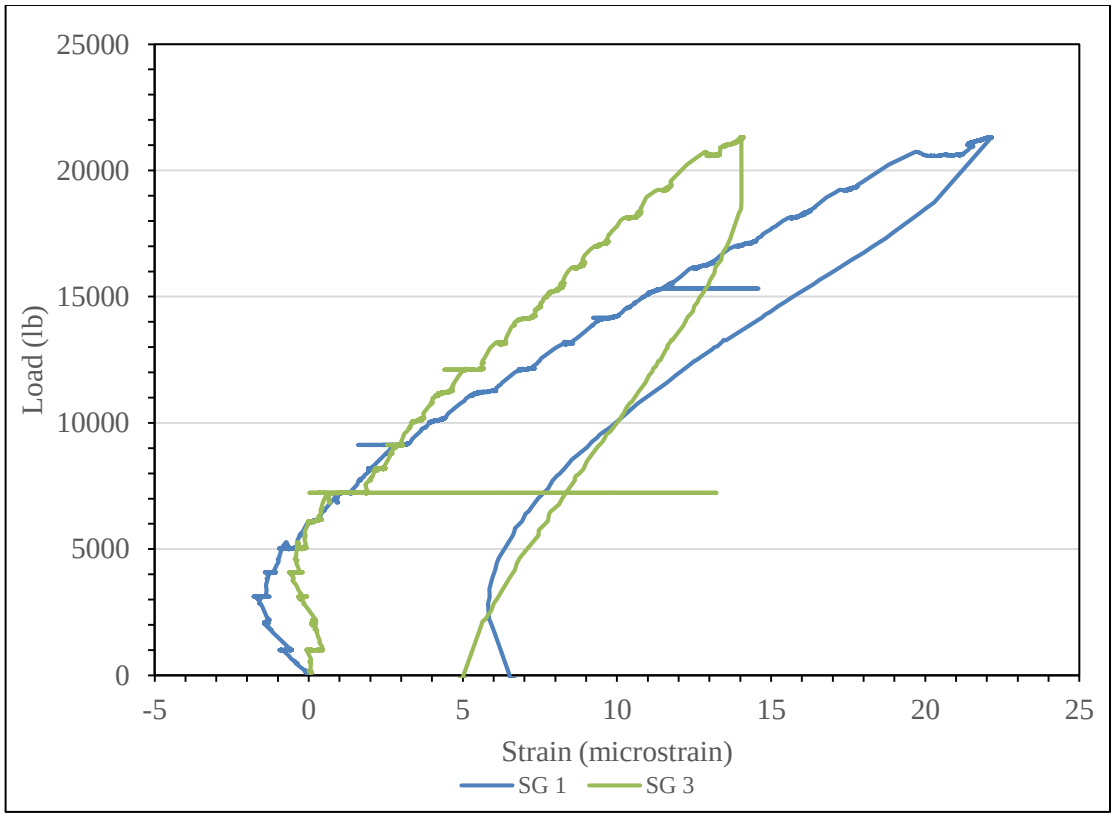

Figure 50: Load vs. Strain curve for slab 2, part 1, external strain gauges

Figure 51 shows the load vs. deflection curve plot for part 2 of testing slab 2. The load application was similar to that of the first slab, using a manual pump instead of a digital load controller. At failure, load could no longer be sustained and crushing was observed across the top of the specimen in the NSC at failure. Plateauing of the load vs. deflection plot is indicative of yielding in the reinforcing steel within the joint. The

ultimate load achieved for slab 2 was 30.3 kips. The calculated failure load corresponding to the maximum flexural capacity of a monolithic NSC slab was 23.7 kips. The actual failure load exceed the calculated value by 28%. The residual deflection at the end of part 1 of testing was 0.04 inches. After failure, the specimen was unloaded and returned to a value of 1.48 inches, which indicates plastic deformation. The maximum deflection during this test was 1.94 inches. Figure 52 shows the load vs. deflection curve of slab 2, parts 1 and 2, together. The unloading of part 2 is not shown here. The slope of part 1 and part 2 almost overlap each other, which mimics consistent loading patterns

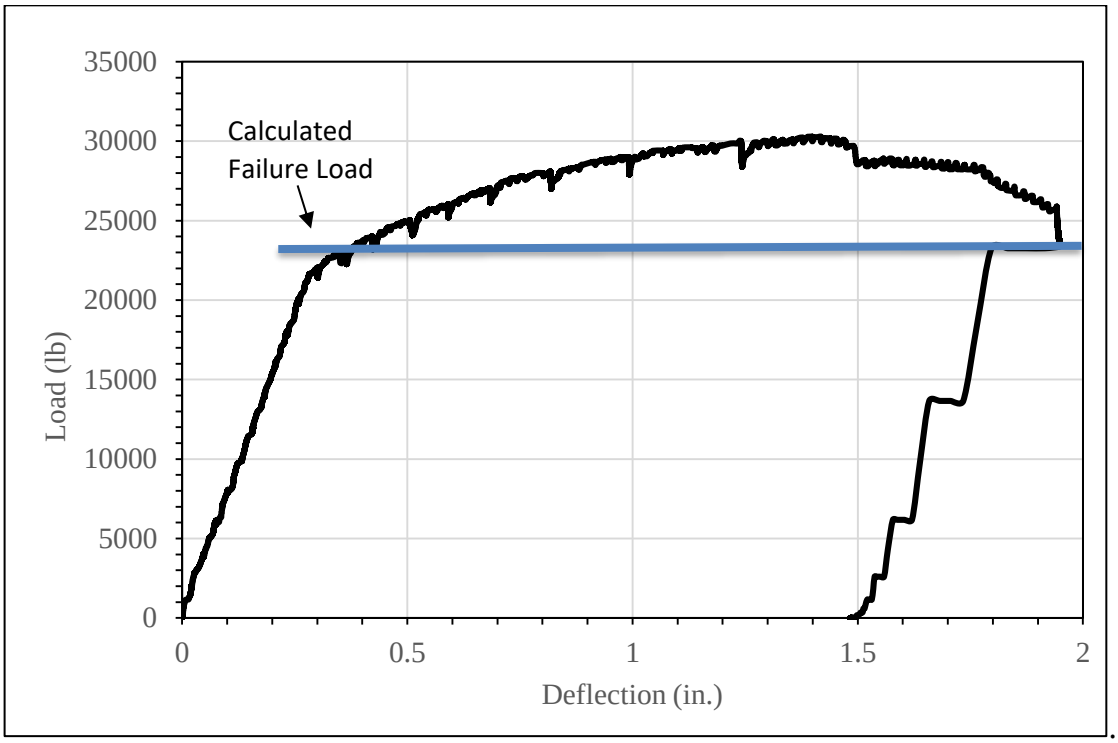

Figure 51: Load vs. Deflection curve for slab 2, part 2

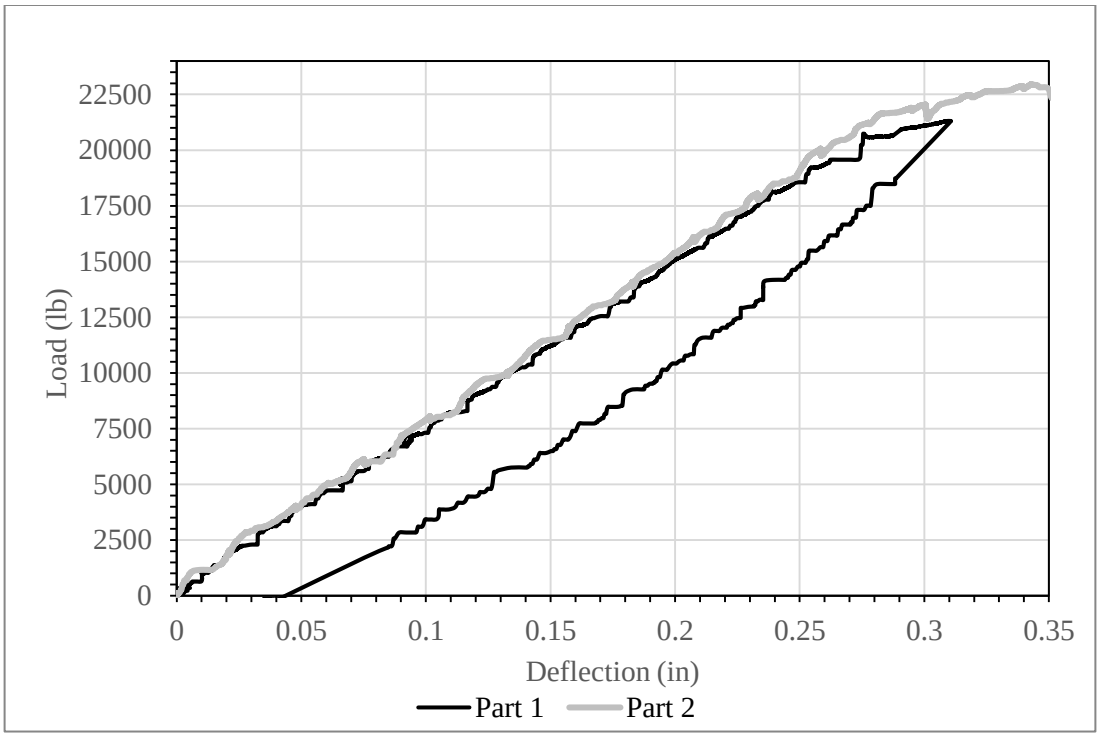

Figure 52: Load vs. Deflection curve for slab 2, parts 1 and 2

Figures 53-55 show cracks on the slab after failure. At failure, there were no cracks in the UHPC joint, only in the NSC. Significant cracking occurred underneath the load point. Additional cracks formed in the NSC starting at the NSC and UHPC interface. In Figure 55, honeycombing can be seen in the bottom corner of the UHPC joint. This consolidation issue developed due to a stiff UHPC mix, which probably caused lack of bond between the NSC and UHPC as well as the UHPC and the steel reinforcement. This could have also prevented the load from reaching a higher value.

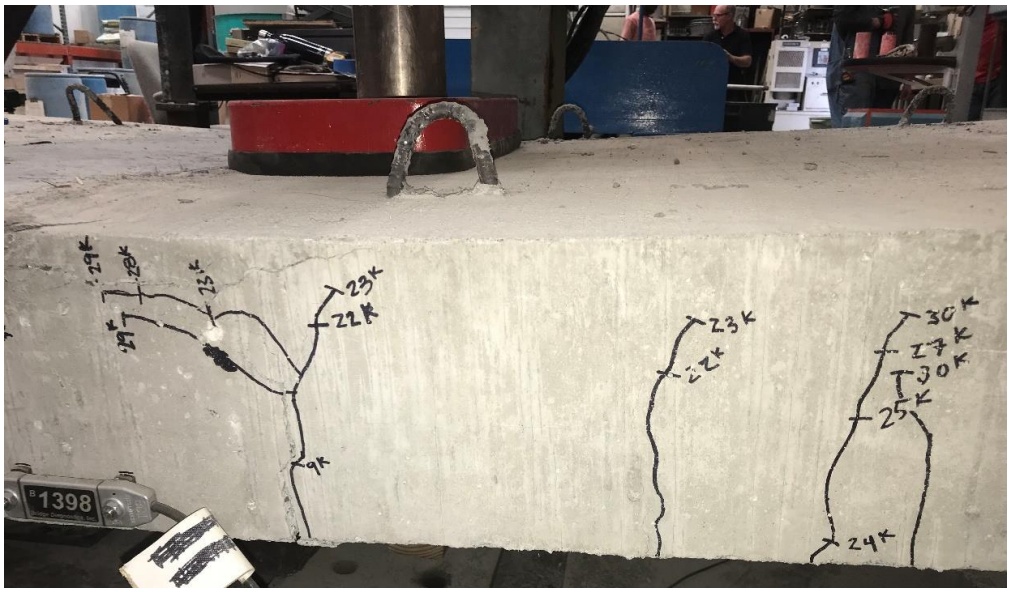

Figure 53: Cracks formed underneath load on slab 2

Figure 54: Cracks formed underneath load point on slab 2

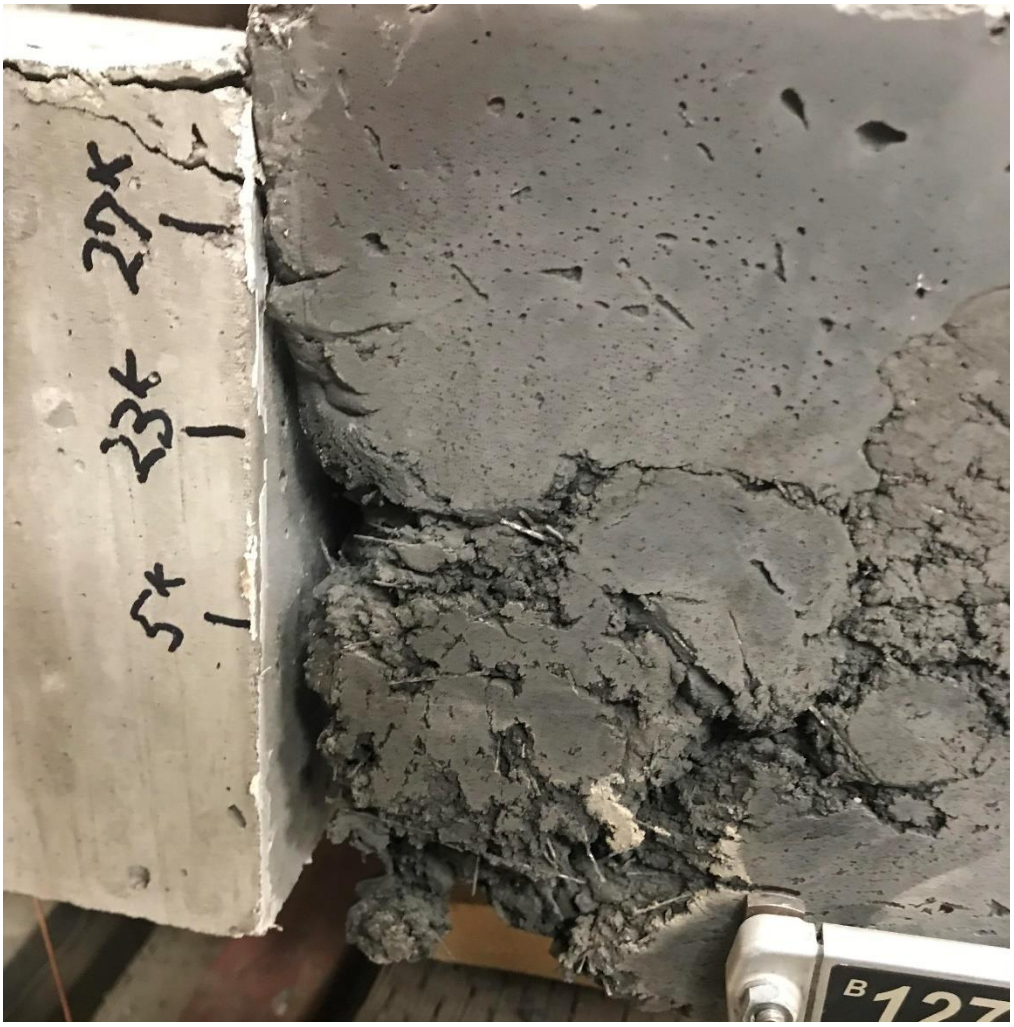

Figure 55: Cracks formed at joint interface due to honeycomb joint

Figure 56 shows the Funderburg (2018) study with Ductal® and the current study load vs. deflection curves of slab 2, part 1 together. Funderburg had a graphically determined cracking load of 13.1 kips and a visual cracking load of 14 kips. These values are higher than those found in this study. The deflection returned to a value of 0.067 inches. The Ductal® curve had a steeper slope throughout part 1 of this slab test most likely due to premature cracking from the inconsistent part 1 loading of this slab.

Figure 57 shows the Funderburg (2018) study with Ductal® and the current study load vs. deflection curves of slab 2, part 2 together. Funderburg reached an

ultimate load of 37.2 kips and the total deflection returned to 1.7 inches. There is a 23% difference in the ultimate load capacity for slab 2 in these two studies. Figure 58 shows the load vs. deflection curves for both static slabs compared to Ductal® for part 1 of testing. Figure 59 shows the load vs. deflection curves for both static slabs compared to Ductal® for part 2 of testing.

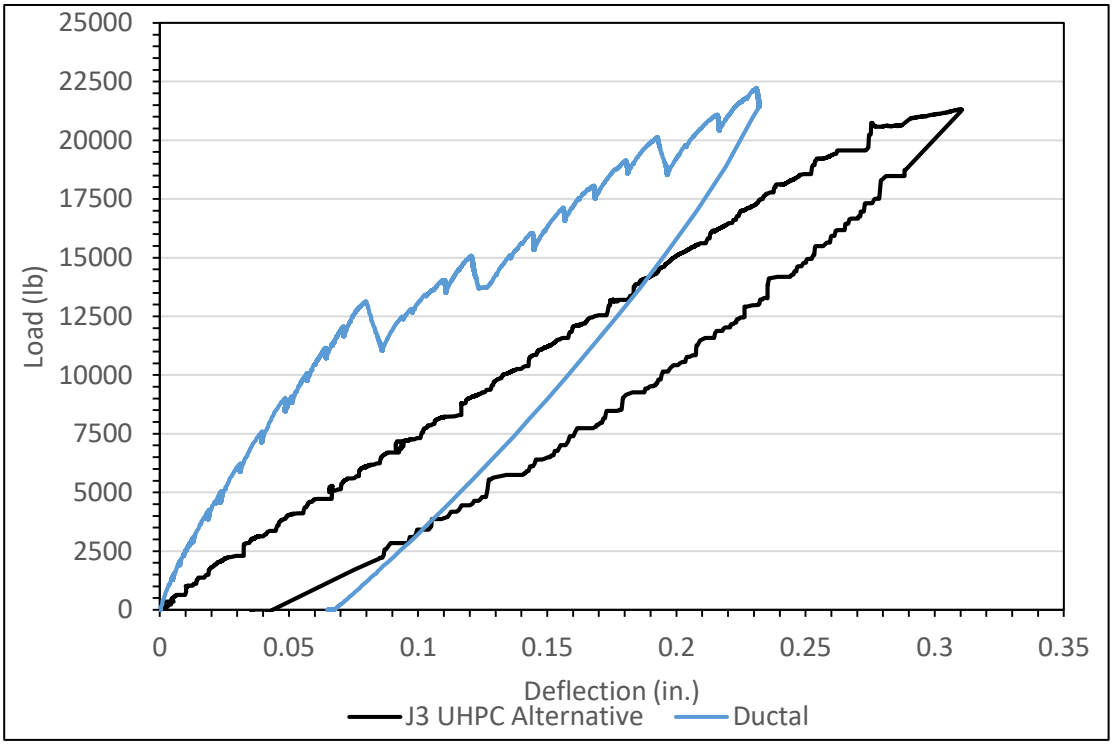

Figure 56: Load vs. Deflection curves for slab 2, part 1 compared to Ductal®

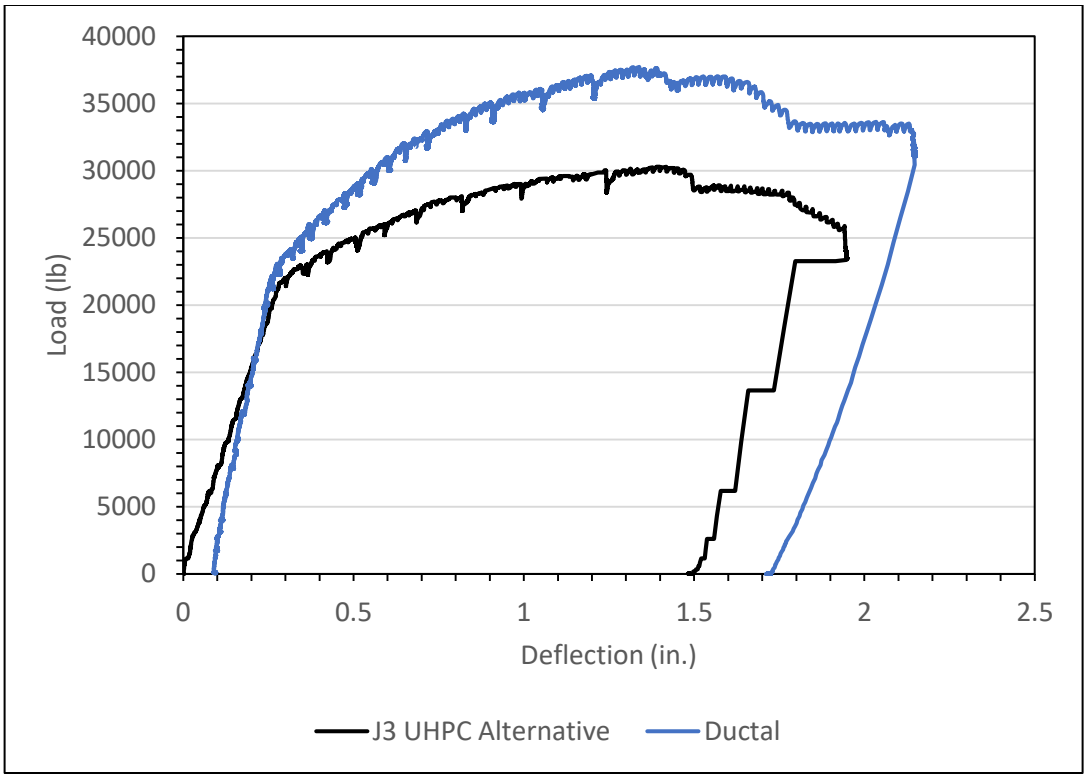

Figure 57: Load vs. Deflection curves for slab 2, part 2 compared to Ductal®

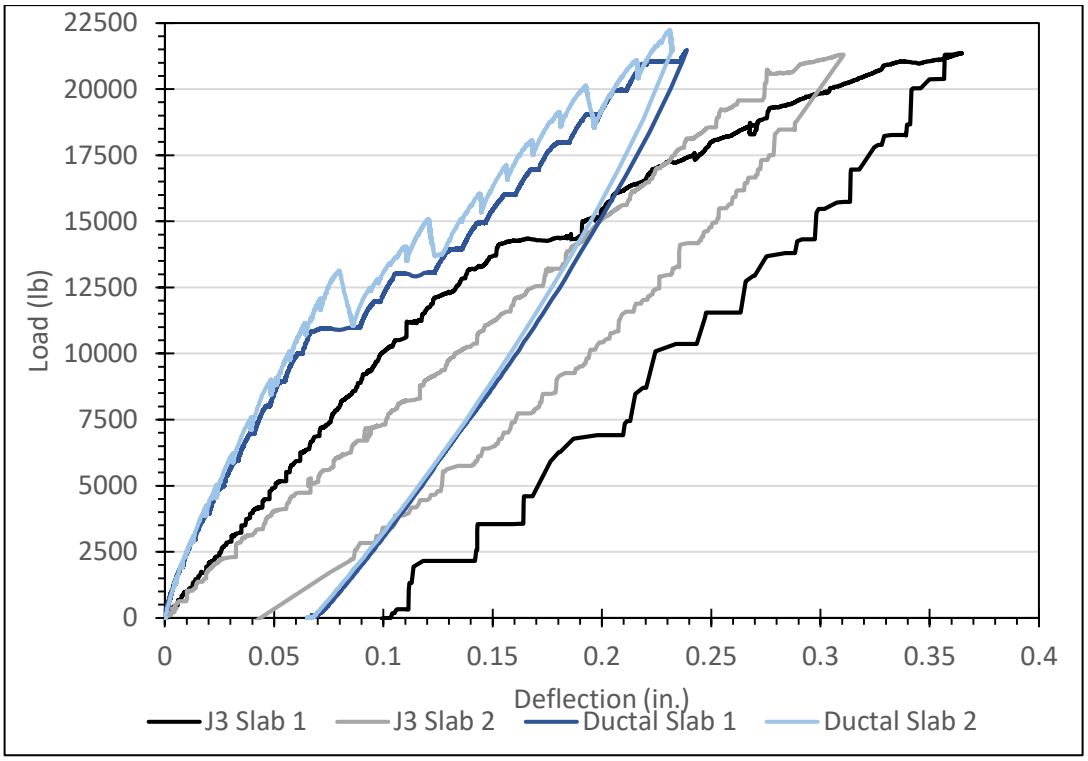

Figure 58: Load vs. Deflection curves for static slabs, part 1, J3 and Ductal®

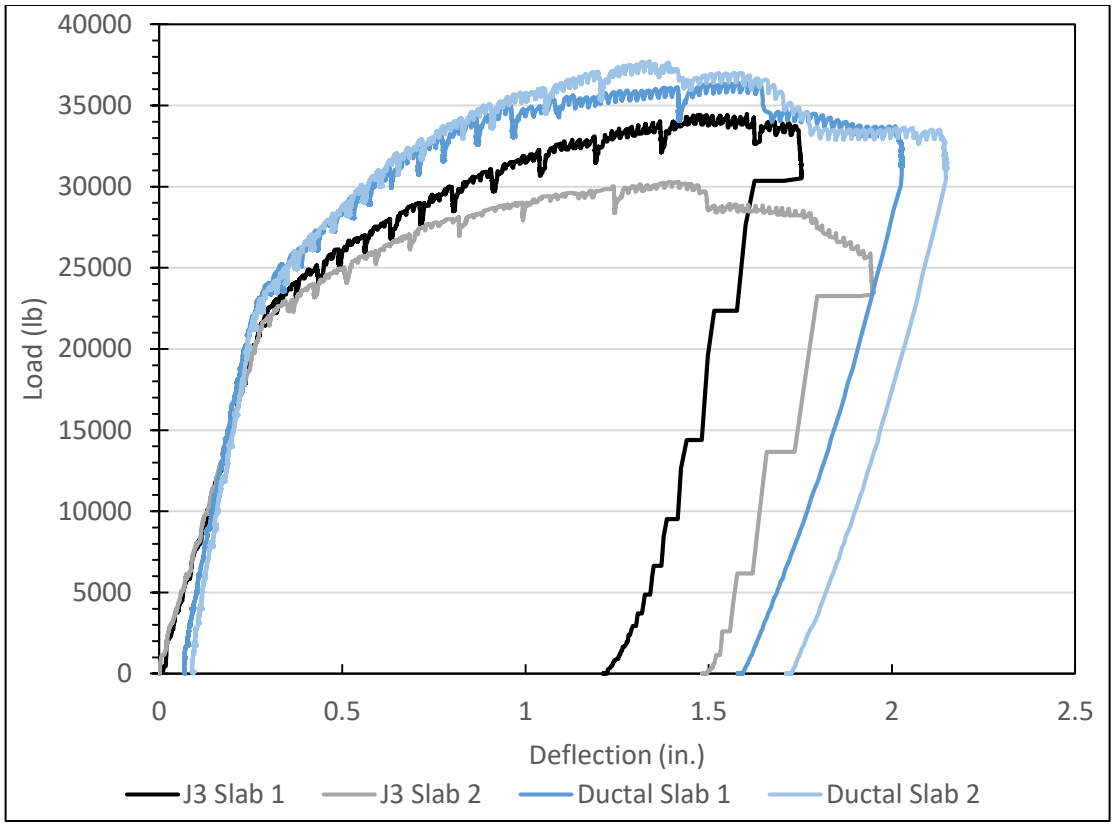

Figure 59: Load vs. Deflection curves for static slabs, part 2, J3 and Ductal®

4.3.3 Slab 3 Cyclic Test Results

Slab 3 was tested cyclically under fatigue loading. Initially, the slab was to be cyclically loaded to a maximum value lower than the cracking moment. The chosen maximum value was 90% of the cracking moment, which was 90% of 12.2 kips. Due to premature cracking of slab 3 in the Funderburg (2018) study, the lowest visually observed cracking load from slab 1 and 2, 9 kips, was used. Using the MTS system, a 1 hertz cyclic load was applied to the third slab with a maximum value of 9 kips (74% of the estimated cracking load). Figure 60 shows a typical loading cycle over 10 seconds. Figure 61 shows the load vs. deflection curve for one loading portion of a single cycle. This data from day 3 of loading is representative of the first 3 million cycles of cyclic loading (the entirety of cyclic data can be seen in Appendix A). The unloading portion

of the curve is not shown but is similar to the loading portion. The slab was preloaded to 500 pounds to prevent the load from coming up off of the slab so the curve does not start at zero. A trend line of the entire data set is shown in blue on the graph. The slope in the equation shown is the stiffness measurement of the slab. Because the first few data points of this data set are more linear, the linear trend line for the first 4 data points is also shown in orange. Figure 62 shows the load vs. deflection curve of one cycle from the Ductal® study by Funderburg (2018) and from this study. Both curves follow the same trend but the Ductal® curve is slightly steeper, therefore slightly stiffer. The stiffer Ductal® curve can also attributed to the higher modulus of elasticity (MOE) Ductal® has compared to J3. J3 has an MOE of about 5,300 ksi (McDaniel 2017) while Ductal® has a typical MOE of 7,000 ksi (Graybeal 2014). The data from day 1 and day 15 (see Appendix A) will not be included in this analysis due to abnormalities in the data. Day 1 had larger deflections credited to adjusting the MTS settings for the first day. Day 15 appeared to have a data collection error and is inconsistent with all other plots.

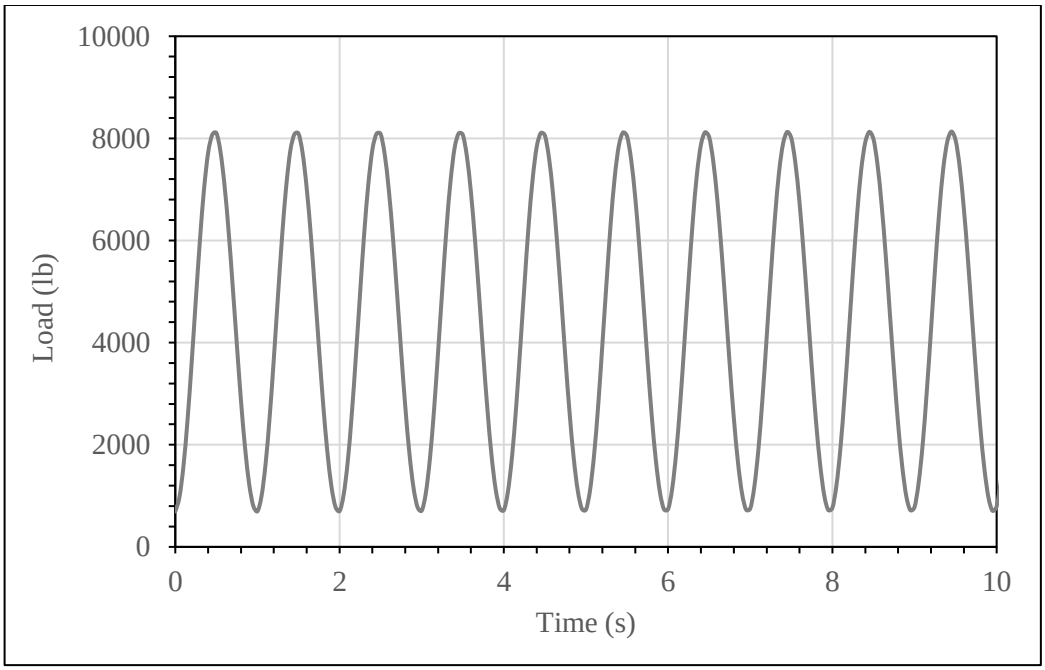

Figure 60: Typical cyclic loading over 10 seconds

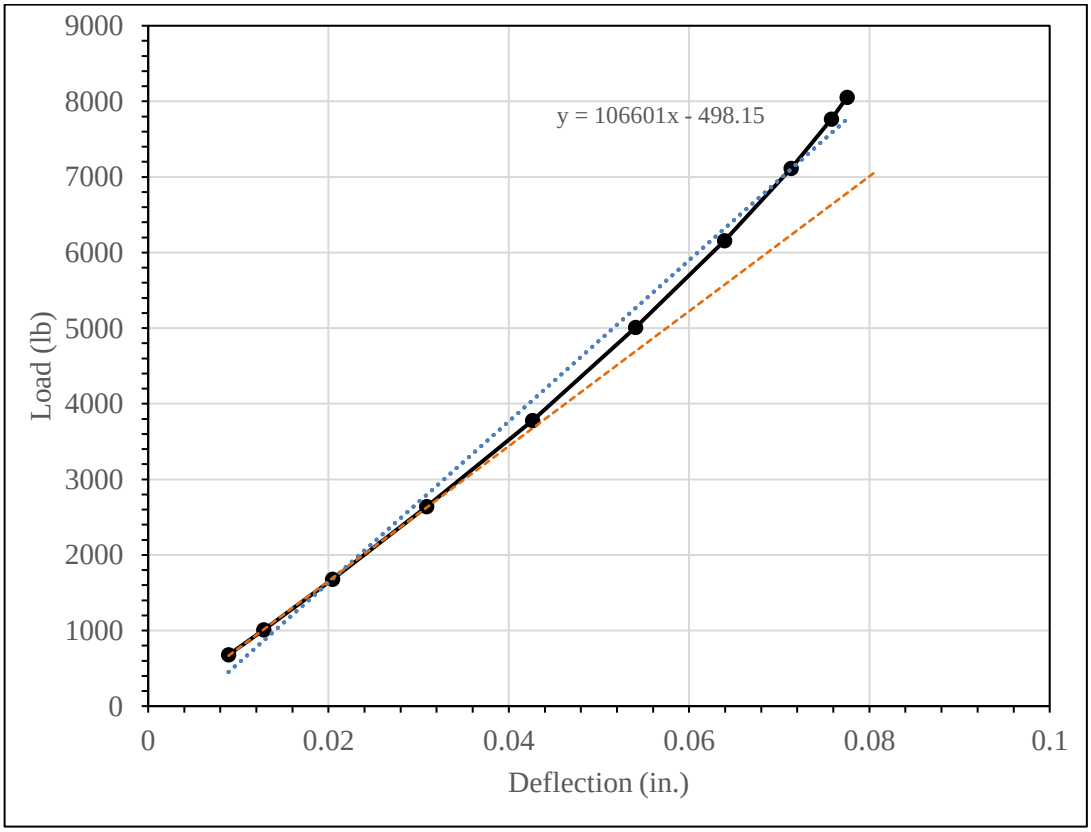

Figure 61: Load vs. Deflection for slab 3, single load cycle selected from day 3

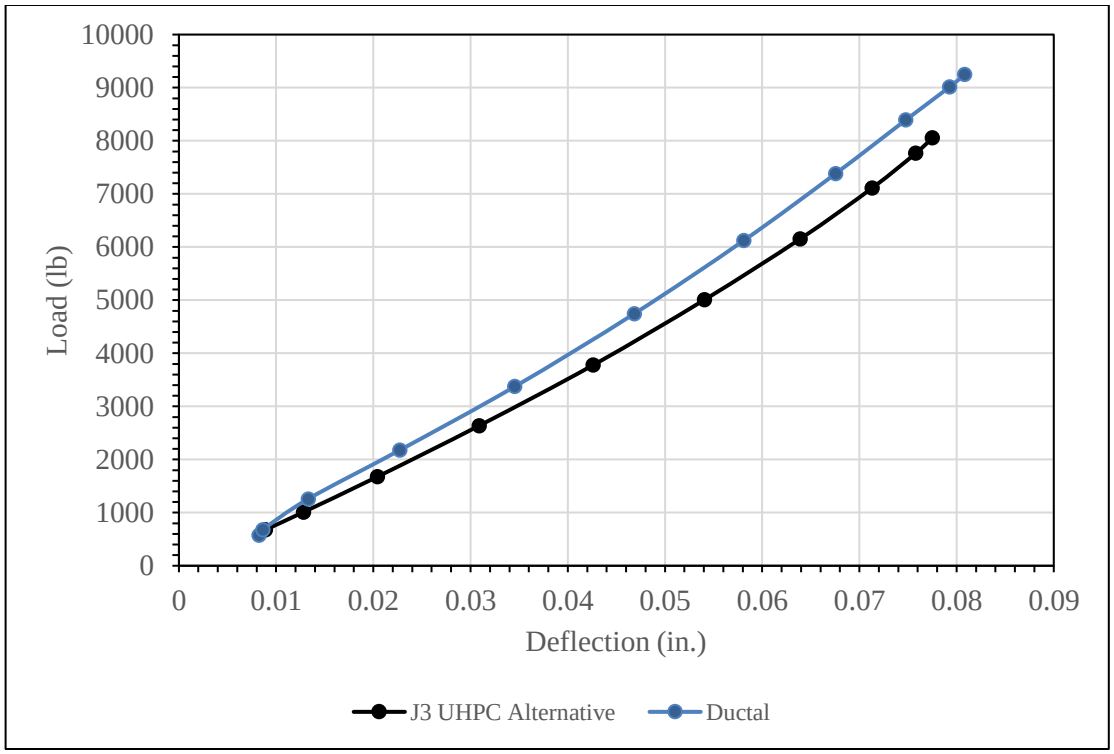

Figure 62: Load vs Deflection for slab 3, compared to Ductal®, single load cycle from day 3

Slab 3 was supposed to be loaded for 3 million cycles below the cracking moment then the load would be increased to 5% above cracking moment. Unfortunately the MTS load controller experienced multiple malfunctions and was unable to complete the testing of slab 3. The slab reached 2,225,892 cycles (25 days) below the cracking moment and did not reach 3 million cycles or failure. The data up to 2,225,892 cycles will be included in this study. The test called for continuing the cyclic test with the higher cyclic loading for 2 million more cycles or until failure then testing the slab statically until failure. This data will be included in subsequent literature.

Figure 63 shows time vs. stiffness plot for multiple days. There were approximately 88,000 cycles per day. A decrease in stiffness is observed over time. During cyclic testing at around 1,700,000 cycles (20 days), the testing machine

malfunctioned and applied a constant 16 kip load to the slab instead of applying a cyclic load ranging from 500 pounds to 9 kips. This most likely caused early cracking which would cause a rapid decrease in stiffness of the slab as seen on days 21, 23 and 25 in Figure 64. Figure 64 shows the load vs. deflection curve for multiple cycles from different days. Data for days 3-19 show very similar trends and almost overlap each other. This shows consistency in the loading until malfunction at day 20. Figure 65 shows the residual deflections throughout fatigue testing. There was a total residual deflection of 0.003 inches.

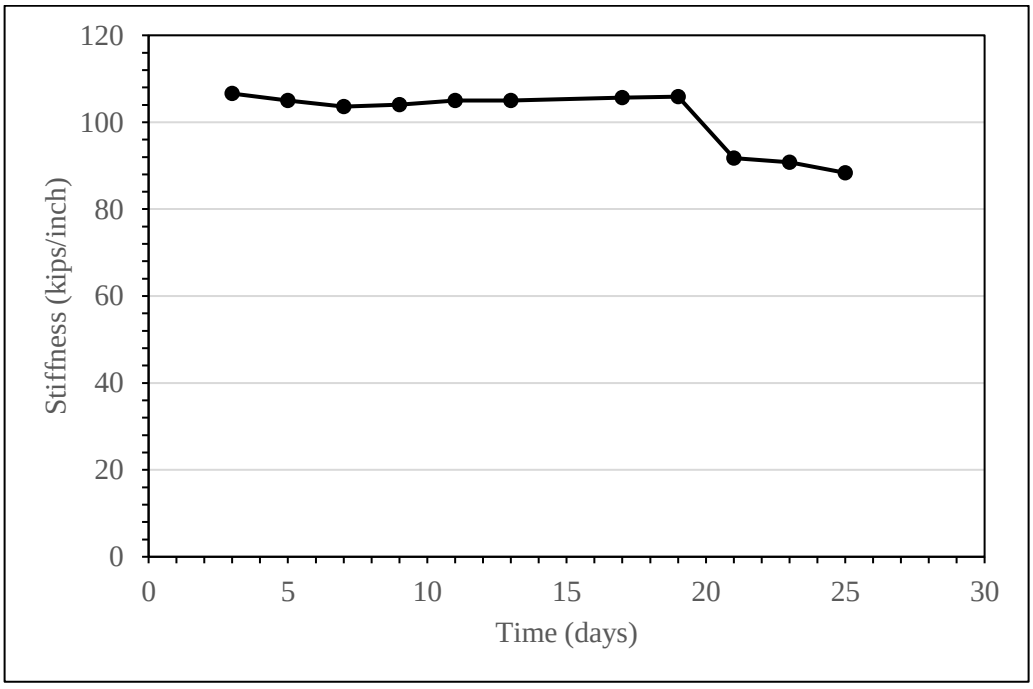

Figure 63: Slab stiffness over 25 day loading period

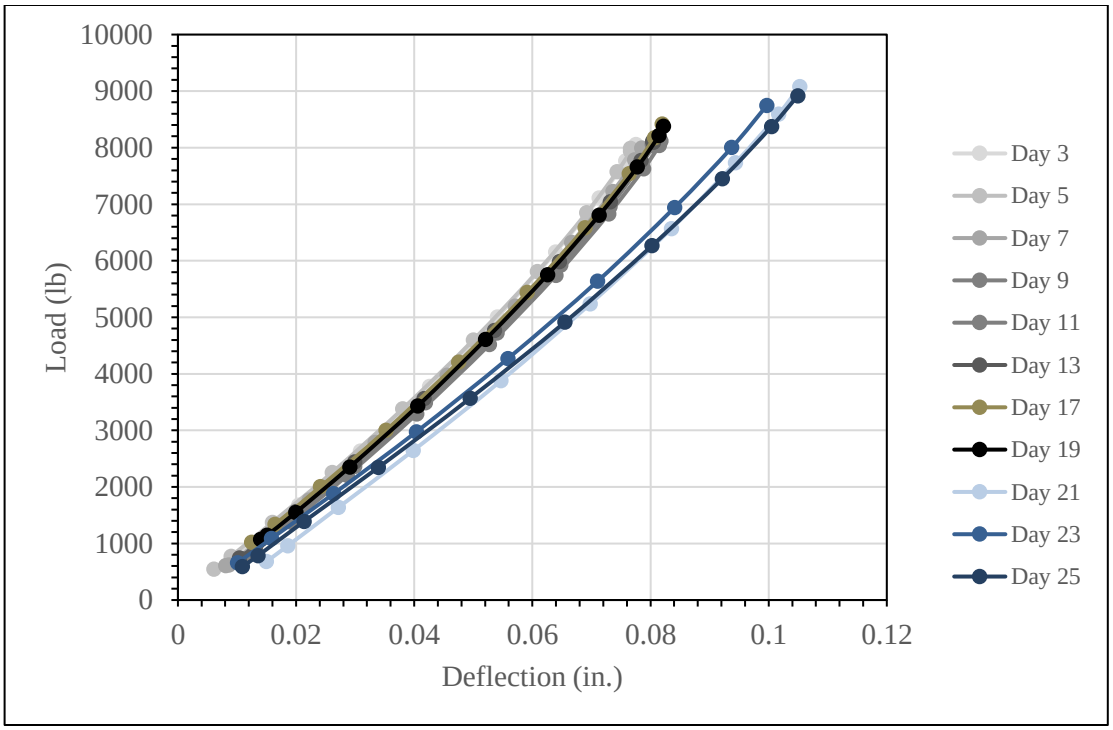

Figure 64: Comparison of load vs. deflection curves for multiple days

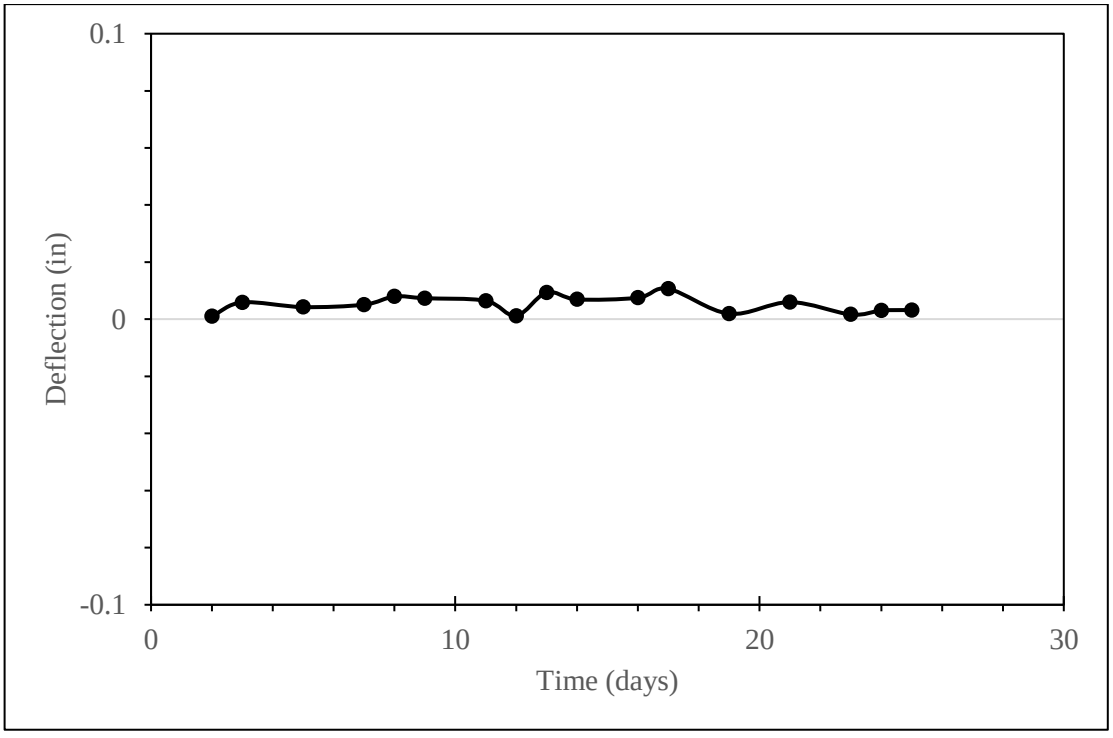

Figure 65: Residual deflections over the course of fatigue testing

4.3.4 Comparison of Slabs 1, 2 and 3

Figure 66 shows the load vs. deflection curve for the initial loading from the static test of slabs 1 and 2 and one cyclic loading from slab 3. Slab 2 has a shallower slope than slab 1 and 3 due to premature cracking during the static test. Slabs 1 and 3 have very similar slopes which demonstrates similar flexural behavior. Slabs 1 and 2 reached a much higher flexural capacity than expected which may be due to the UHPC providing additional strength a monolithic NSC slab would not have. All 3 slabs cracked only in the base concrete and then showed weaknesses at the joint interface. This is similar to the behavior seen with some of the composite MOR specimens that failed in the NSC.

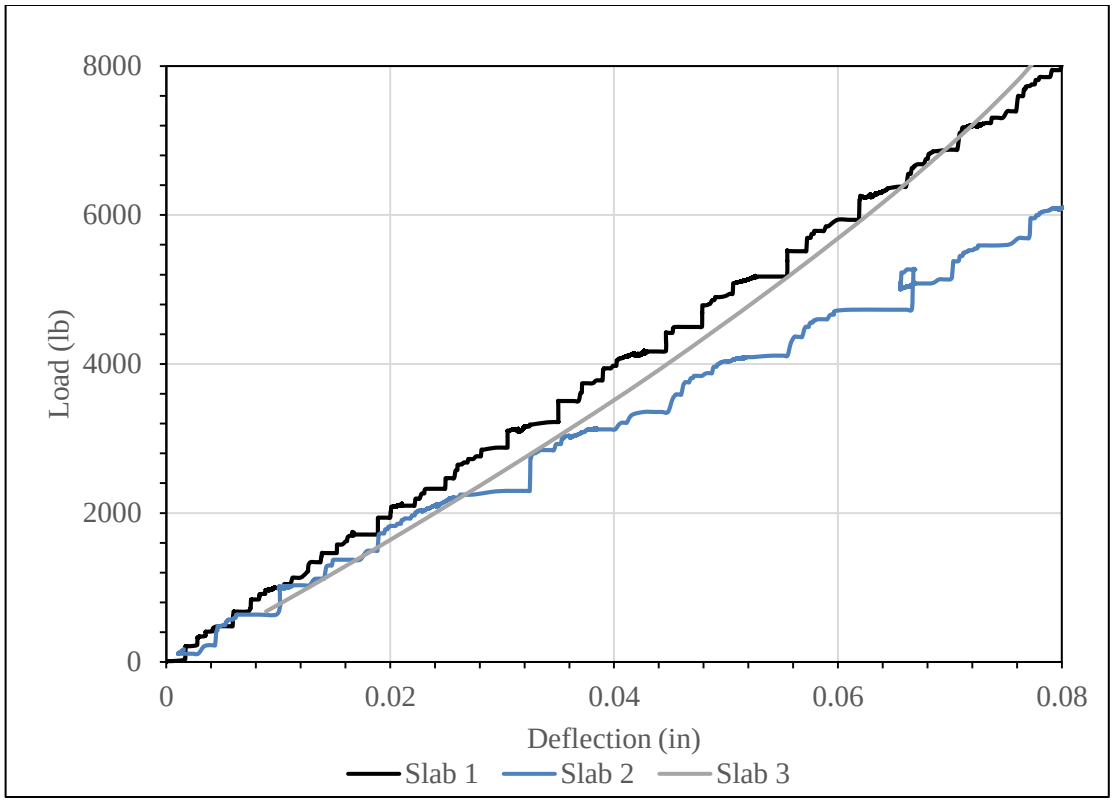

Figure 66: Load vs Deflection curve for initial portion of loading for all 3 slabs

4.4 Slant Shear Test Results

Slant shear testing was performed on 6 inch by 12 inch cylinders. After each failure, measurements were taken in accordance with ASTM C882 (2013). The bond strength was calculated by dividing the load carried by the specimen at failure by the area of the interface. The results are shown in Table 23.

Table 23: Maximum load and bond strength for slant shear specimens

Specimen	Maximum Load (lb)	Bond Strength (psi)	Corresponding Compressive Strength (psi)	NSC 28-day Compressive Strength (psi)
Cylinder 1	123,670	2280	4370	5750
Cylinder 2	110,130	2230	3900	
Cylinder 3	152,010	2870	5380	
Cylinder 4	123,290	2380	4360	
Average	127,275	2440	4503	
Std. Deviation	15,286	254	541	

All slant shear specimens failed at the interface and all bond strength values were within 18% of the average. The Funderburg (2018) study had an average bond strength of 2670 psi. There is less than a 10% difference between the average bond strength for the J3 mix compared to Ductal®.

5 Findings, Conclusions, Recommendations and Future Work

The primary goal of this study was to implement the UHPC alternative developed in the McDaniel (2017) study in specimens that were comparable to the Funderburg (2018) study. The purpose of this was to determine if the UHPC alternative is comparable to the proprietary Lafarge product, Ductal®. The following chapter summarizes the findings, conclusions and recommendations from this research study.

5.1 Findings

The following findings were observed throughout the course of this research study:

- Heat curing of UHPC increased the early age strength properties.
- The first set of composite MOR specimens had very low bond strengths with 28% of the specimens separating during de-molding.
- The second set of composite MOR specimens performed much better than the first set, with no specimens separating during demolding.
- For the first set of MOR specimens, the average flexural strength for the wire brushed, sand blasted, and exposed aggregate specimens was 15 psi, 210 psi, and 184 psi, respectively.
- For the second set of MOR specimens, the average flexural strength for the wire brushed, sand blasted, and exposed aggregate specimens was 436 psi, 447 psi, and 200 psi, respectively.

- For the first set of MOR specimens, the average flexural strength for the 45 degree, 60 degree, and 90 degree specimens was 133 psi, 106 psi, and 92 psi, respectively.
- For the second set of MOR specimens, the average flexural strength for the 45 degree, 60 degree, and 90 degree specimens was 438 psi, 406 psi, and 242 psi, respectively.
- For the first set of MOR specimens, the average flexural strength for the shear key specimens was 418 psi.
- For the second set of MOR specimens, the average flexural strength for the shear key specimens was 193 psi.
- For the second set of MOR specimens, the average flexural strength of the 60 degree and 45 degree, sand blasted and wire brushed specimens all exceeded or came within 3% of exceeding the NSC flexural strength.
- Approximately 25% of the second set of composite MOR specimens failed in the base concrete.
- The ultimate flexural load capacity of slab 1 (34.3 kips) exceeded the calculated flexural load capacity of a monolithic NSC slab of the same size (23.7 kips) by a total of 45%.
- The ultimate flexural load capacity of slab 2 (30.3 kips) exceeded the calculated flexural load capacity of a monolithic NSC slab of the same size (23.7 kips) by a total of 28%.
- The average flexural load capacity of slabs 1 and 2 (32.3 kips) came within 12% of the average flexural load capacity of slabs 1 and 2 from the Funderburg study

(36.7 kips) using Ductal®. Without including the cracked specimen (slab 2), the difference reduces to 7%.

- The flexural stiffness of slab 3 under fatigue loading decreased by approximately 0.68 kips/inch between days 1 and 19 and decreased by approximately 14 kips/inch between days 19 and 21 after a 16 kip load was wrongfully applied. Additionally, residual deflections increased over time to a maximum of 0.01 inches.
- All slabs experienced some degree of separation at the NSC-UHPC interface at ultimate load.
- The internal strain gauges on slab 1 exceeded the yield strain indicating that the reinforcing steel yielded.
- The bond strength for the slant shear specimens in this study (2440 psi) came within 9% of the bond strength found in the Funderburg study (2670 psi) using Ductal®.

5.2 Conclusions

Based on the results of the testing detailed in this study, the following conclusions are presented:

- Heat curing of UHPC is required to achieve the early age strength advantages of the material.
- Sufficient workability is required to achieve high bond strengths between UHPC and NSC.

- The use of a thinner/lighter steel fiber allowed for increased flowability of the modified J3 mix.
- The modified J3 mix showed significantly improved flowability without compromising compressive strength and noticeably improved bond strength with the normal strength concrete substrate.
- Sand blasting is the best surface preparation for composite MOR specimens like those in this study although it is suspected that exposed aggregate could perform just as well. These surface preparations would likely perform best in the field.
- The 45 degree interface angle is the best interface configuration for composite MOR specimens like those in this study. This interface angle would likely perform best in the field.
- Using the modified J3 mix produced favorable results especially for the 60 degree and 45 degree, sand blasted and wire brushed specimens. These specimens had a flexural strength that exceeded or almost exceeded the base concrete flexural strength, showing that the bond between UHPC and NSC is stronger than the NSC alone.
- Slab 1 far exceeded the calculated failure load, which may indicate that the UHPC joint provided additional strength to the slab.
- After being prematurely cracked, slab 2 still exceeded the calculated failure load showing that the additional strength gained from the UHPC joint can offset possible strength loss from cracking.

- The flexural strength of the slabs in this study are comparable to those in the Funderburg study, and had slab 2 not been prematurely cracked, the difference in ultimate flexural strengths would be much less.
- Once a higher load was applied, the overall flexural stiffness of slab 3 decreased proportionally and the residual deflection increased slightly.
- The NSC-UHPC interface on the slabs could potentially be a weak point but failure was mainly due to cracking and crushing of the NSC on the first two slabs, much like in the Funderburg study. Because the third slab was not tested to failure, those results will have to be included at a later time.
- UHPC mix, J3, provided sufficient bond strength with a 4 inch lap length to yield the #5 reinforcing bars in the slab joint.
- Slant shear testing displayed that the bond strength of the UHPC to the NSC was comparable to the Funderburg study although the correlation between slant shear bond strength and flexural bond strength is still unclear.
- The UHPC alternative, J3, is an adequate substitute for the proprietary product, Ductal® in terms of strength and performance as a repair material in some applications.

5.3 Recommendations and Future Work

The following recommendations are presented based on the research conducted in this study and those preceding it:

- After repair of the MTS controller, the remainder of cyclic and static testing on slab 3 should be completed in order to accurately characterize and compare with the other 2 slabs in this study and slabs in the Funderburg study.
- The UHPC alternative, J3, should be further modified to make it more workable and improve its bond to NSC. Once the mix is modified and bond is improved between the UHPC alternative and NSC, more specimens that will assess the bond of the material should be fabricated and tested.
- Studies should be performed to assess bond strength and performance of UHPC repair joints and composite MOR joints for specimens with a dampened surface to determine the effects of moisture on the bond. This test should be done with both Ductal® and J3.
- UHPC alternative, J3, is a promising repair material for bridge joints and can possibly be used in place of Ductal® in some applications. Additional research should be conducted to assess the best mix design and the best practices including heat curing, bond performance, and other behavioral qualities.

References

Aghdasi, Parham, Heid, Ashley E., Chao, Shin-Ho, "Developing Ultra-High-Performance Fiber-Reinforced Concrete for Large-Scale Structural Applications," ACI Materials Journal, Vol. 133, No. 5, Sep.-Oct. 2016, pp. 559-570.

ASTM. (2013). "Standard Test Method for Bond Strength of Epoxy-Resin Systems used with Concrete by Slant Shear," C882-13, West Conshohocken, PA.

ASTM. (2016). "Standard Test Method For Flexural Strength of Concrete (Using Simple Beam with Third-Point Loading)," C78-16, West Conshohocken, PA.

ASTM. (2017). "Standard Test Method For Splitting Tensile Strength of Cylindrical Concrete Specimens," C496 -17, West Conshohocken, PA.

ASTM. (2017). "Standard Test Method for Compressive Strength of Cylindrical Concrete Specimens," C39-17, West Conshohocken, PA.

Bierwagen, D. et al., "Ultra-High Performance Concrete Waffle Slab Bridge Deck for Wapello County, Iowa," HPC Bridge Views, Issue No. 65, January/February 2011.

Bornstedt, G. "Connecting Precast Concrete Bridge Deck Panels with Ultra High Performance Concrete (UHPC)," Western Bridge Engineer's Seminar, Phoenix, AZ, September 25–28, 2011. Abstract only.

British Standard. (1999). "Products and systems for the protection and repair of concrete structures. Test methods. Determination of slant shear strength." BS EN 12615:1999, British Standards Institution, 12.

Buitelaar, P. (2004). "Ultra High Performance Concrete: Development and application during 25 years." Plenary Session international Symposium on UHPC.

Carbonell Munoz, M. A., 2012, “Compatibility Of Ultra High Performance Concrete As Repair Material: Bond Characterization With Concrete Under Different Loading Scenarios”

Carbonell Munoz, M. A., Harris, D. K., Ahlborn, T. M., and Froster, D. C., “Bond Performance between Ultrahigh-Performance Concrete and Normal-Strength Concrete,” ASCE Journal of Materials in Civil Engineering, Vol. 26, No.8, Aug 2014.

Climaco, J. C. T. S., and Regan, P. E. (2001). "Evaluation of bond strength between old and new concrete in structural repairs." Mag. Concr. Res., 53(6), pp. 377-390.

Diab, A. M., Eldin, M. R. T., and Elmoaty, A. E. M. A., “Slant Shear Bond Strength Between Self Compacting Concrete and Old Concrete,” Construction and Building Materials 130, 12 November 2016, pp.73-82.

Floyd, R.W., and Volz, J. S., “ODOT Research Project Proposal: Evaluation of Ultra-High Performance Concrete for Use in Bridge Connections and Repair,” The Board of Regents of the University of Oklahoma, Jul 2016.

Funderburg, Chandler, 2018, “Evaluation Of Surface Preparation And Bond Angle Combinations For Bridge Joint Replacement Using Ultra-High Performance Concrete”

Graybeal, B. (2010) “Behavior of Field-Cast Ultra-High Performance Concrete Bridge Deck Connections Under Cyclic and Static Structural Loading,” FHWA-HRT-11-023, Federal Highway Administration, McLean, VA.

Graybeal, B., “Tech Note | Ultra-High Performance Concrete,” FHWA-HRT-11-038, March 2011, Federal Highway Administration, McLean, VA.

Graybeal, B., “Ultra-High Performance Concrete: A State-of-the-Art Report for the Bridge Community,” FHWA-HRT-13-060, June 2013, Federal Highway Administration, McLean, VA.

Graybeal, B., “Design and Construction of Field-Cast UHPC Connections,” FHWA-HRT-14-084, 2014, Federal Highway Administration, McLean, VA.

Halit Yazıcı, Hüseyin Yiğiter, Anıl Ş. Karabulut, Bülent Baradan,”Utilization of fly ash and ground granulated blast furnace slag as an alternative silica source in reactive powder concrete”, Fuel, Volume 87, Issue 12, 2008, Pages 2401-2407, ISSN 0016-2361, https://doi.org/10.1016/j.fuel.2008.03.005.

Ibrahim, Ahmed, El-Chabib, Hassan, Eisa, Ahmed, “Ultrastrength Flowable Concrete Made with High Volumes of Supplementary Cementitious Materials,” Journal of Materials in Civil Engineering, Dec. 2013, pp. 1830-1839.

Júlio, Eduardo N.B.S, Branco, Fernando A.B, Silva, Vítor D, “Concrete-to-concrete bond strength. Influence of the roughness of the substrate surface”, Construction and Building Materials, Vol. 18, No. 9, November 2004, 0950-0618.

Keierleber, B. et al., “FHWA, Iowa Optimize Pi Girder,” ASPIRE, Winter 2010, pp. 24–26. Available at http://www.aspirebridge.org [Cited November 28, 2017].

McDaniel, Amy, “Development Of Non-Proprietary Ultra-High-Performance Concrete Mix Design”, 2017

Mi Zhou, Wei Lu, Jianwei Song, George C. Lee, “Application of Ultra-High Performance Concrete in bridge engineering”, Construction and Building Materials, Volume 186, 2018, Pages 1256-1267, ISSN 0950-0618.

Momayez, A., Ehsani, M. R., Ramezanianpour, A. A., and Rajaie, H., “Comparison of Methods for Evaluating Bond Strength Between Concrete Substrate and Repair Materials”, Cement and Concrete Research, Vol. 35, No. 4, April 2005, pp. 748-757.

Moore, B., “Little Cedar Creek Bridge—Big Innovation,” ASPIRE, Spring 2012, p. 27. Available at http://www.aspirebridge.org [Cited November 28, 2017].

Oklahoma Department of Transportation, “ODOT Standard Specifications,” Transportation Commission, 2009, pp. 551.

Ozyildirim, H.C. and Volgyi, J.F.J., “Virginia’s Developments in the Use of Concrete in Bridges,” ASPIRE, Winter 2008, pp. 50–52. Available at http://www.aspirebridge.org [Cited November 28, 2017].

N. Randl, T. Steiner, S. Ofner, E. Baumgartner, T. Mészöly, “Development of UHPC mixtures from an ecological point of view”, Construction and Building Materials, Volume 67, Part C, 2014, Pages 373-378, ISSN 0950-0618, https://doi.org/10.1016/j.conbuildmat.2013.12.102.

Royce, M.C., “Concrete Bridges in New York State,” ASPIRE, Fall 2011, pp. 46–48. Available at http://www.aspirebridge.org. [Cited November 28, 2017].

Shutt, C.A., “UHPC Joint Provides New Solutions,” ASPIRE, Fall 2009, pp. 28–30. Available at http://www.aspirebridge.org [Cited November 28, 2017].

Tayeh, B. A., Abu Bakar, B. H., Mehat Johari, M. A., and Voo, Y. L., "Evaluation of bond strength between normal concrete substrate and ultra-high performance fiber concrete as a repair material", Procedia Engineering 54, 2013, pp. 554-563.

Yang, S.I., Millard, S.G., Soutsos, M. N., Barnett, S.J., Le, T.T., "Influence of Aggregate and Curing Regime on the Mechanical Properties of Ultra-High Performance Fiber Reinforced Concrete (UHPFRC)," Construction and Building Materials, Vol. 23, Mar. 2009, pp. 291-298.

Yoo, Doo-Yeol, Yoon, Young-Soo, "Structural performance of ultra-high-performance concrete beams with different steel fibers", Engineering Structures, Volume 102, Nov. 2015, Pages 409–423.

Yu, R., Spiesz, P, Brouwers H.J.H., "Mix design and properties assessment of Ultra-High Performance Fibre Reinforced Concrete (UHPFRC)", Cement and Concrete Research, Volume 56, 2014, Pages 29-39, ISSN 0008-8846.

Yu, R., Spiesz, P., Brouwers, H.J.H., "Development of an Eco-Friendly Ultra-High Performance Concrete (UHPC) with Efficient Cement and Mineral Admixtures Uses," Cement and Concrete Composites, Oct. 2015, pp. 383-394.

Yu Su, Jun Li, Chengqing Wu, Pengtao Wu, Zhong-Xian Li, "Effects of steel fibres on dynamic strength of UHPC", Construction and Building Materials, Volume 114, 2016, Pages 708-718, ISSN 0950-0618.

Appendix A: Figures

Figure 67: Slab joint during heat curing

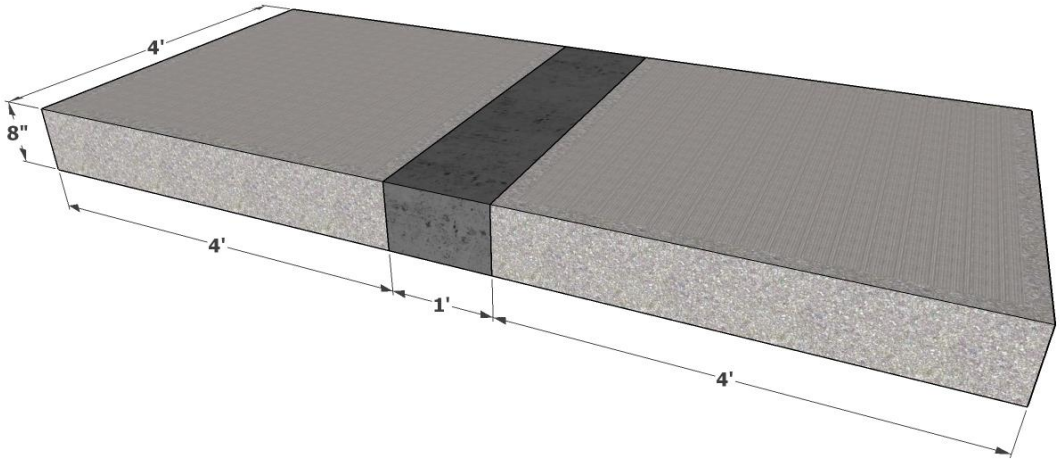

Figure 68: Rendering of slab with UHPC joint

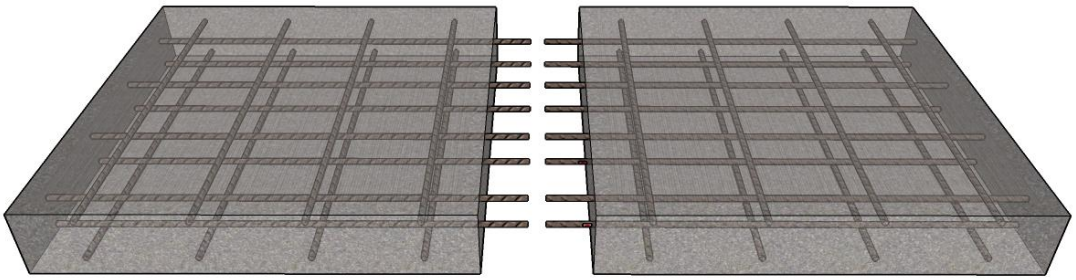

Figure 69: Rendering of slab rebar layout

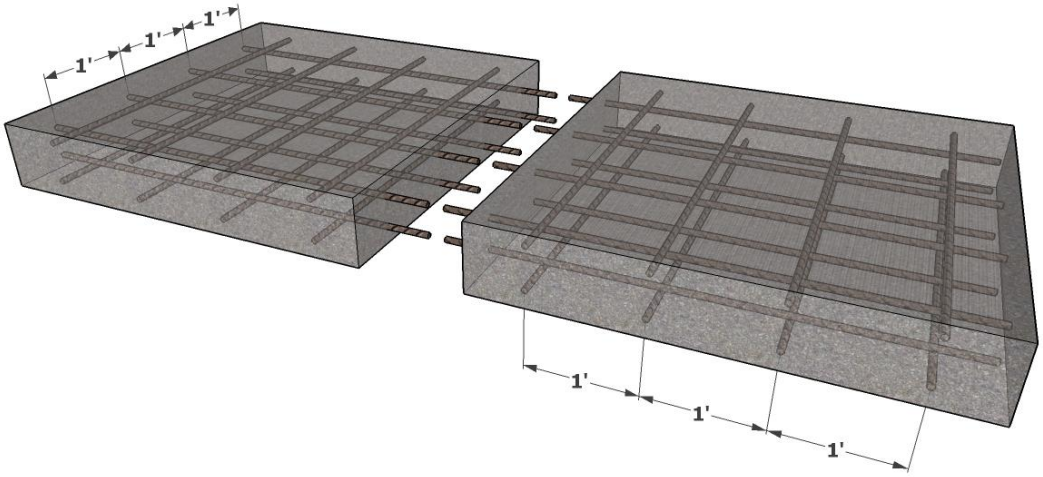

Figure 70: Rendering of slab rebar layout and dimensions

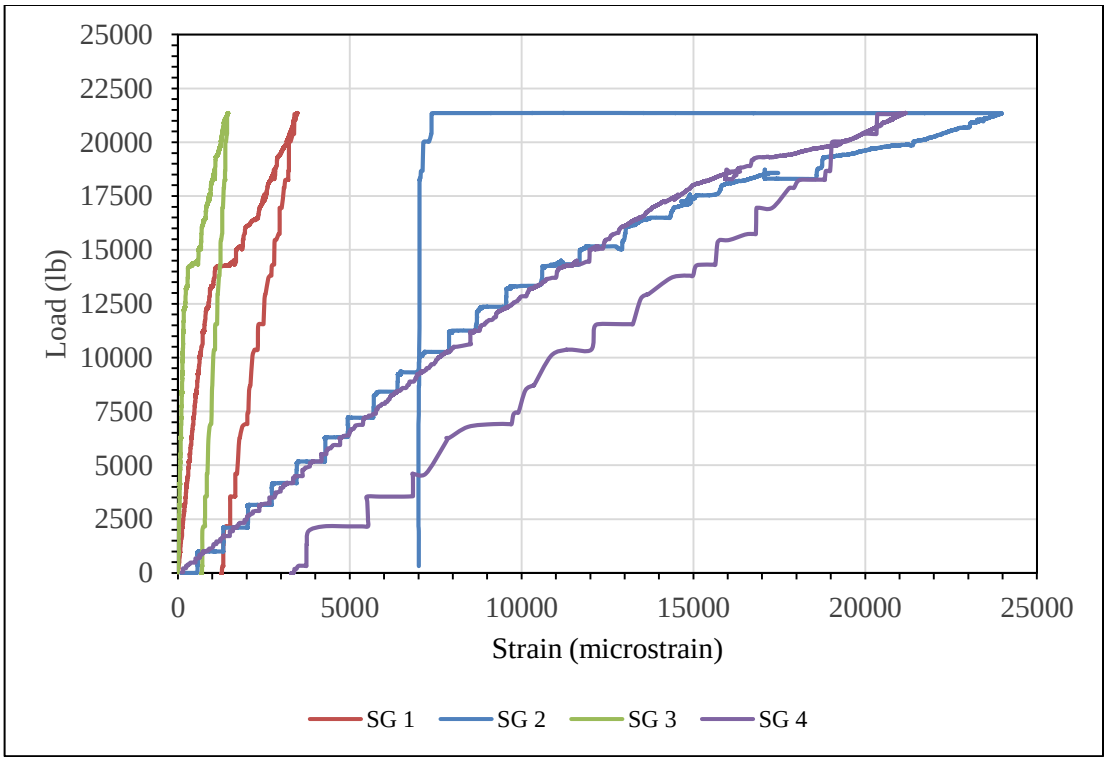

Figure 71: Load vs. Strain curve for slab 1, part 1, all internal strain gauges

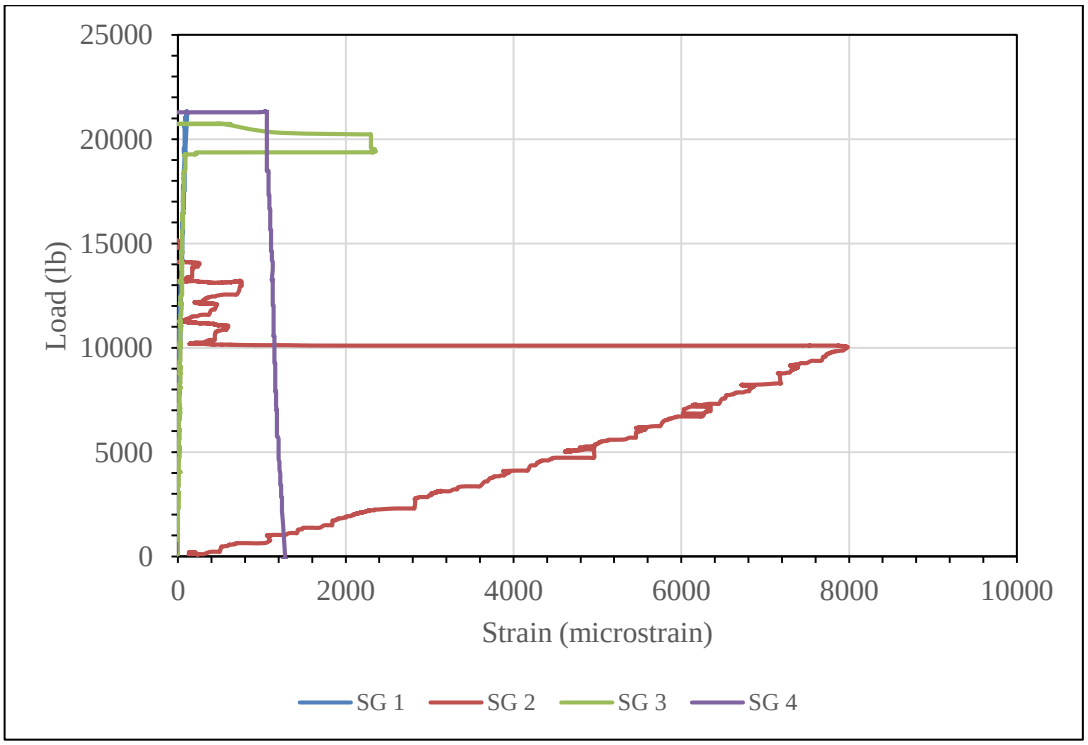

Figure 72: Load vs. Strain curve for slab 2, part 1, all internal strain gauges

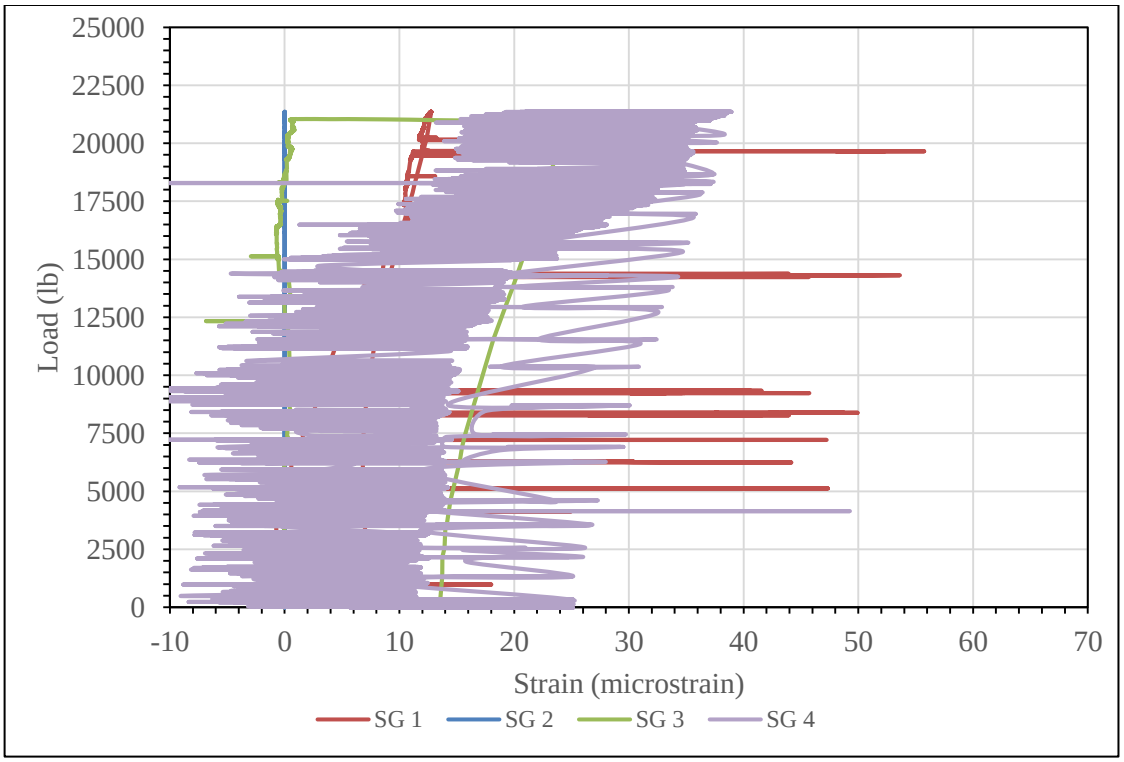

Figure 73: Load vs. Strain curve for slab 1, part 1, all external strain gauges

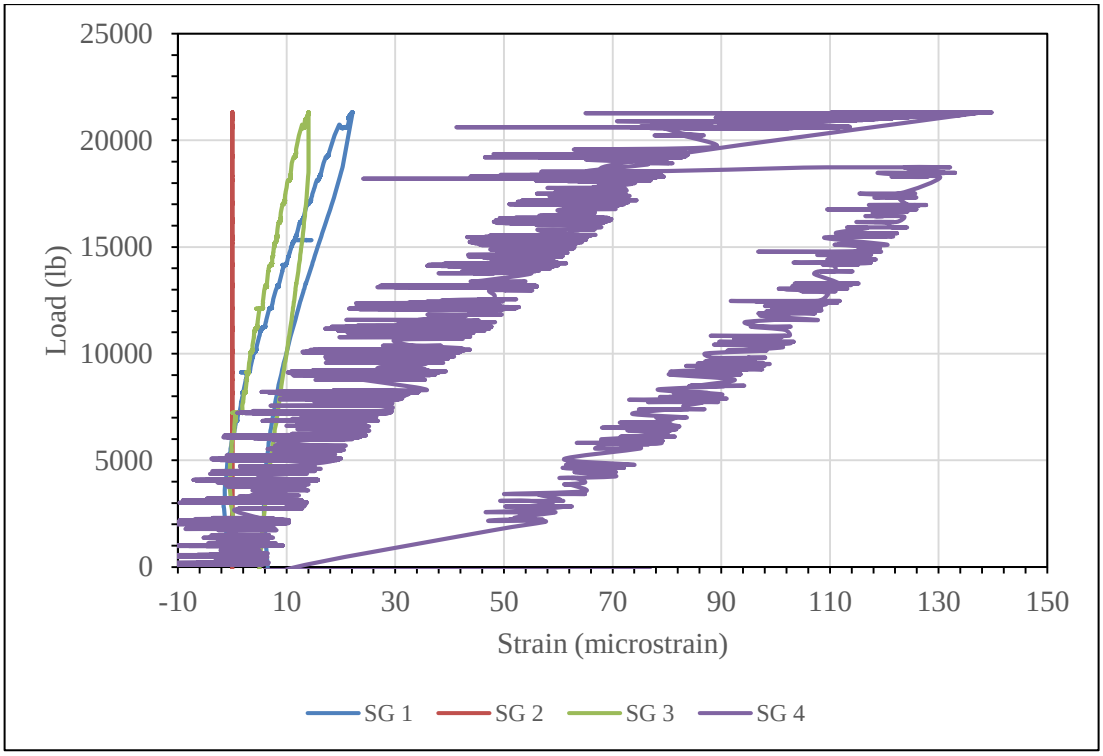

Figure 74: Load vs. Strain curve for slab 2, part 1, all external strain gauges

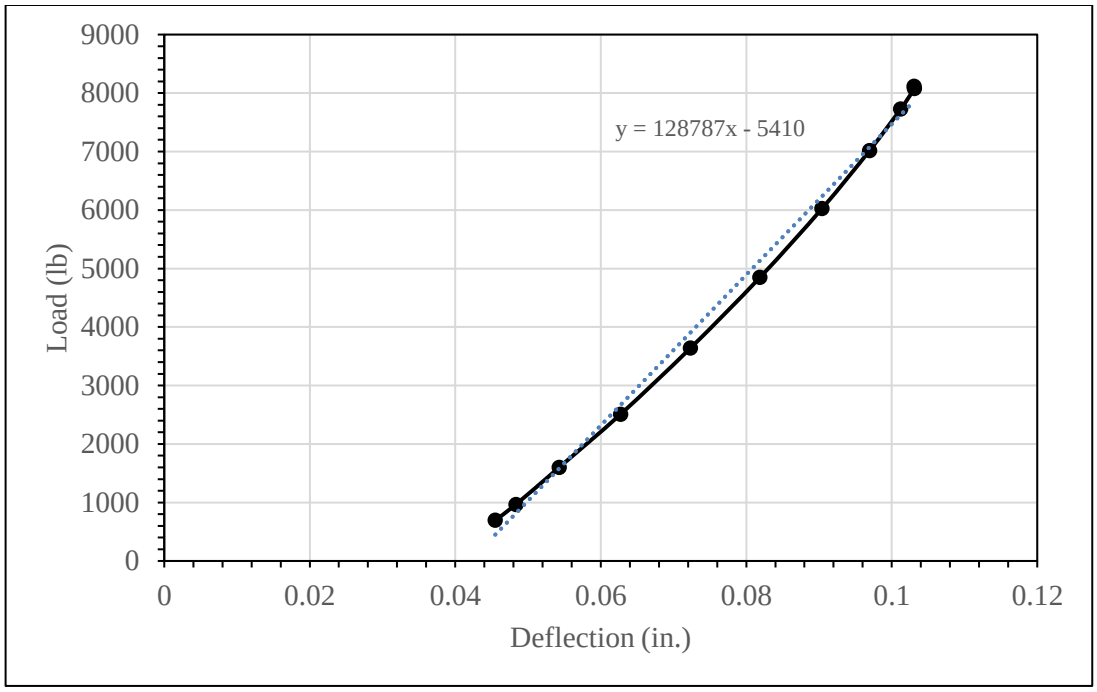

Figure 75: Load vs. Deflection for slab 3, single load cycle selected from day 1

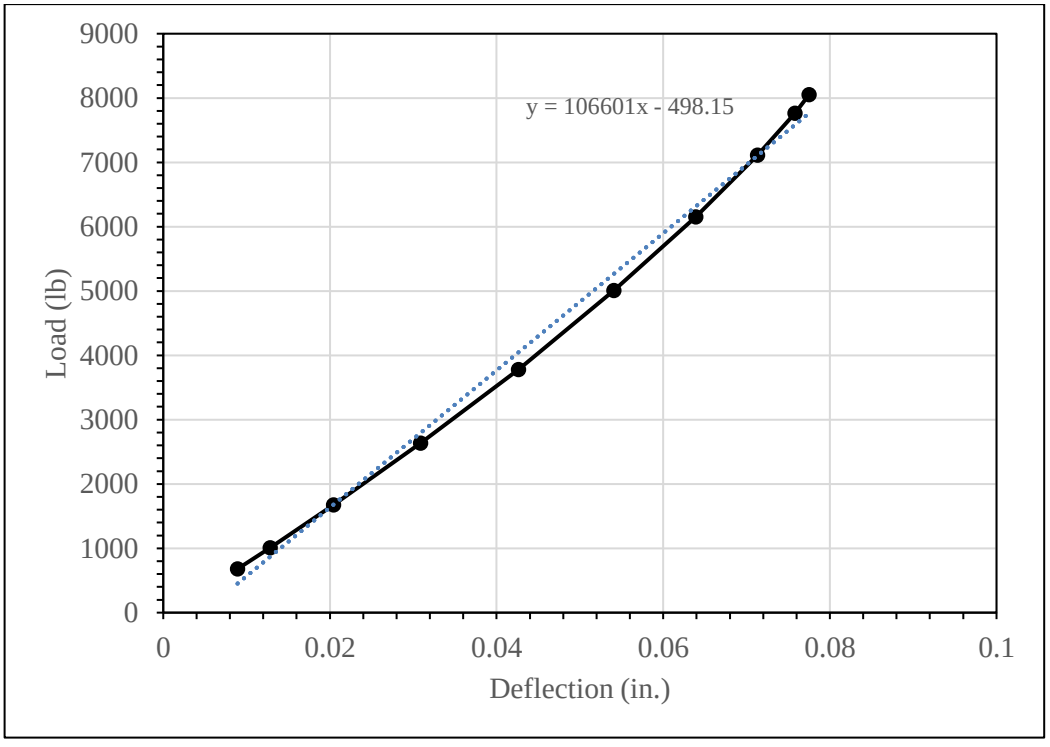

Figure 76: Load vs. Deflection for slab 3, single load cycle selected from day 3

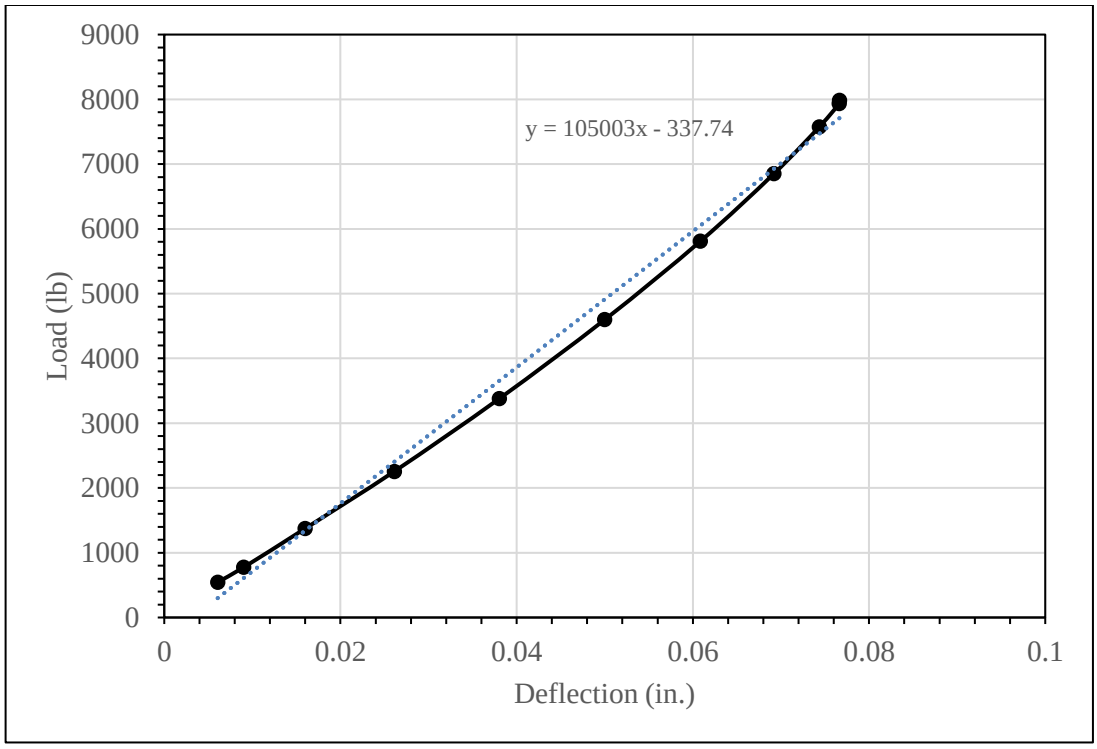

Figure 77: Load vs. Deflection for slab 3, single load cycle selected from day 5

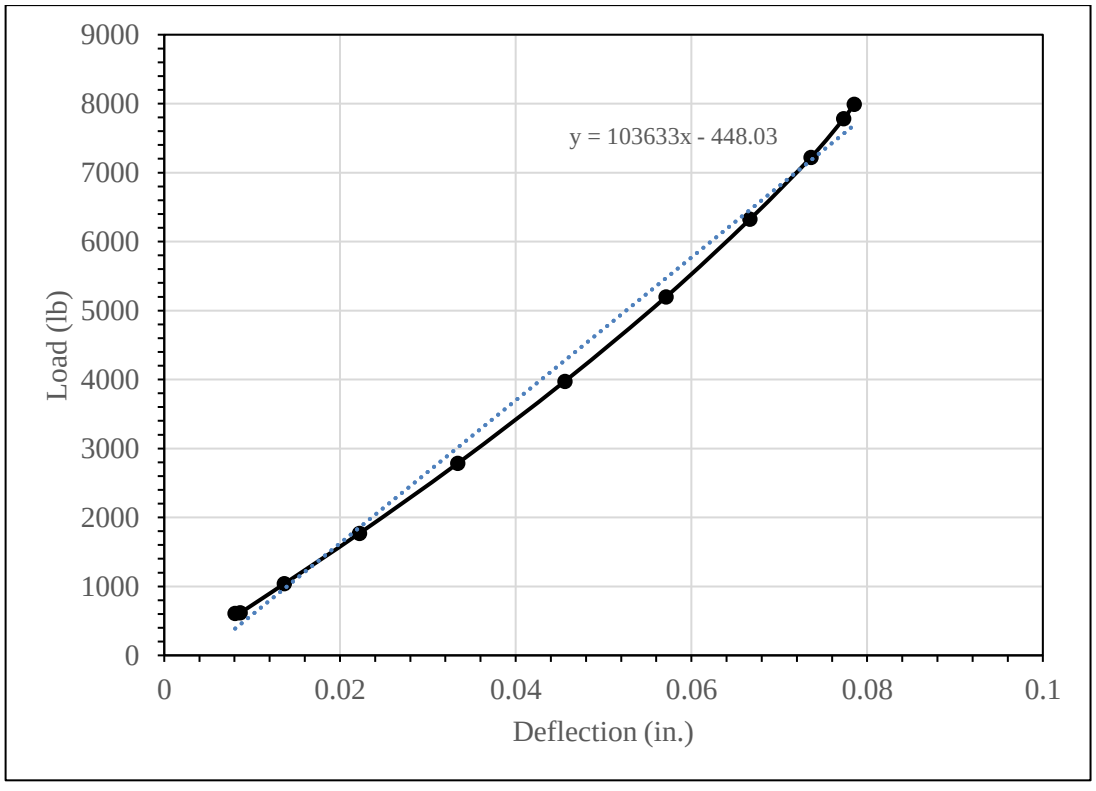

Figure 78: Load vs. Deflection for slab 3, single load cycle selected from day 7

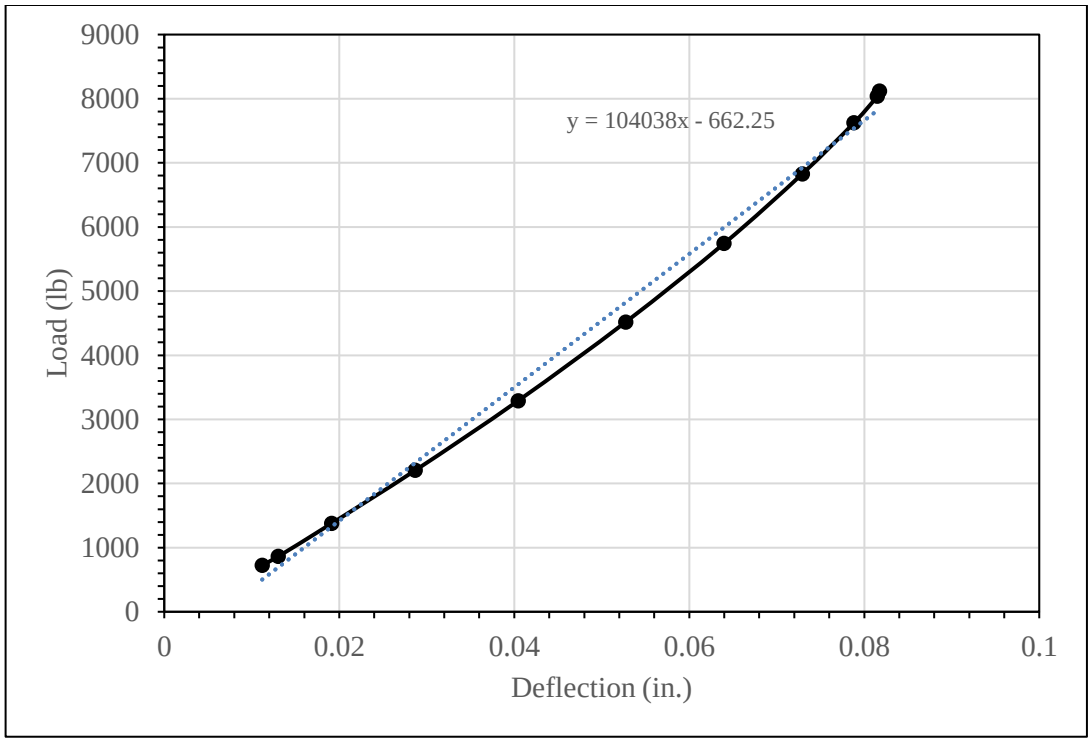

Figure 79: Load vs. Deflection for slab 3, single load cycle selected from day 9

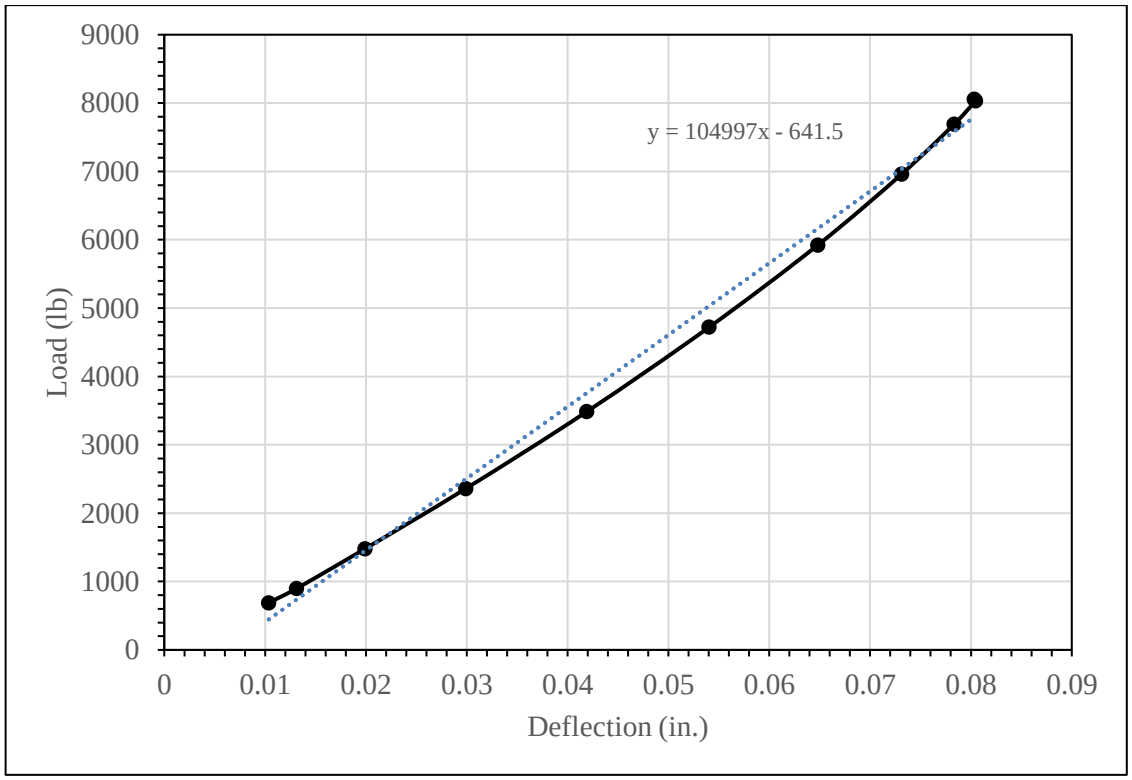

Figure 80: Load vs. Deflection for slab 3, single load cycle selected from day 11

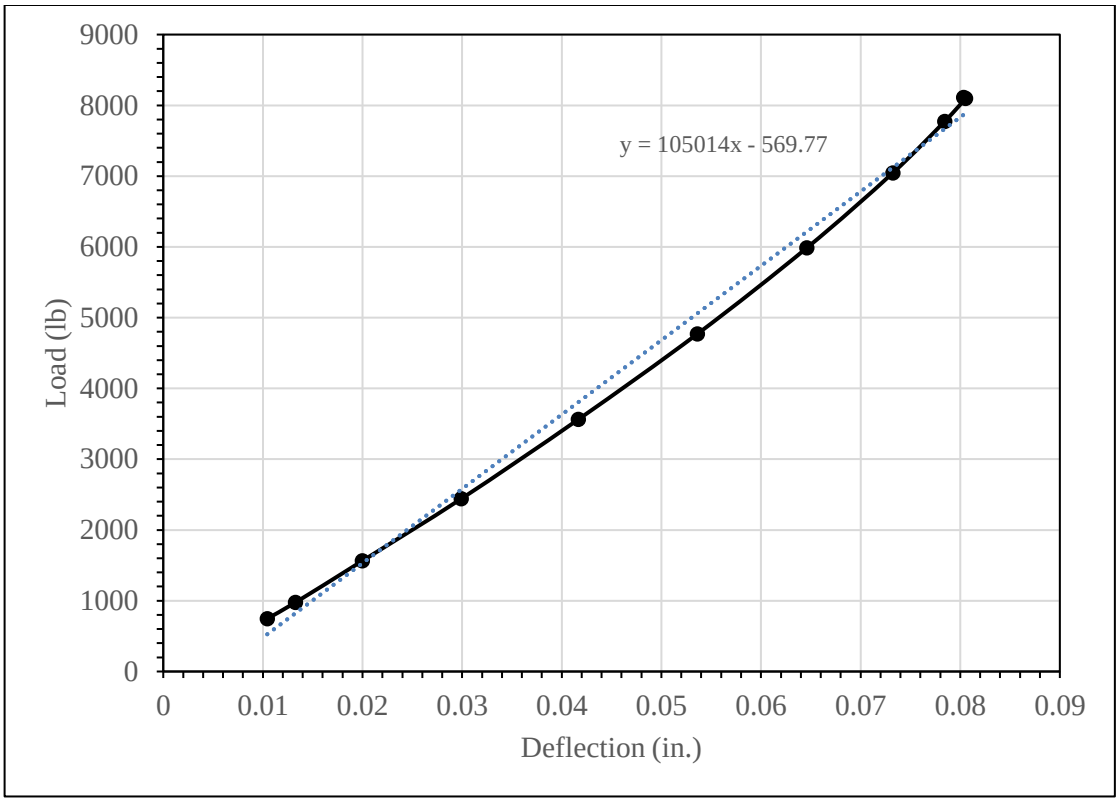

Figure 81: Load vs. Deflection for slab 3, single load cycle selected from day 13

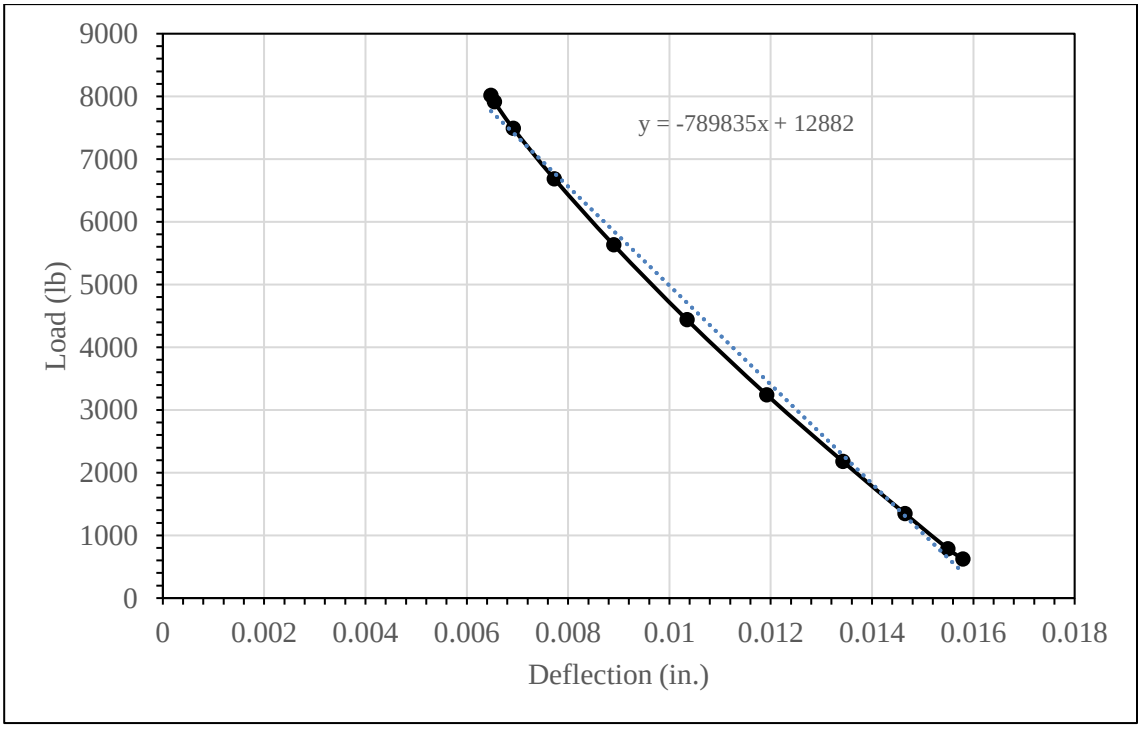

Figure 82: Load vs. Deflection for slab 3, single load cycle selected from day 15

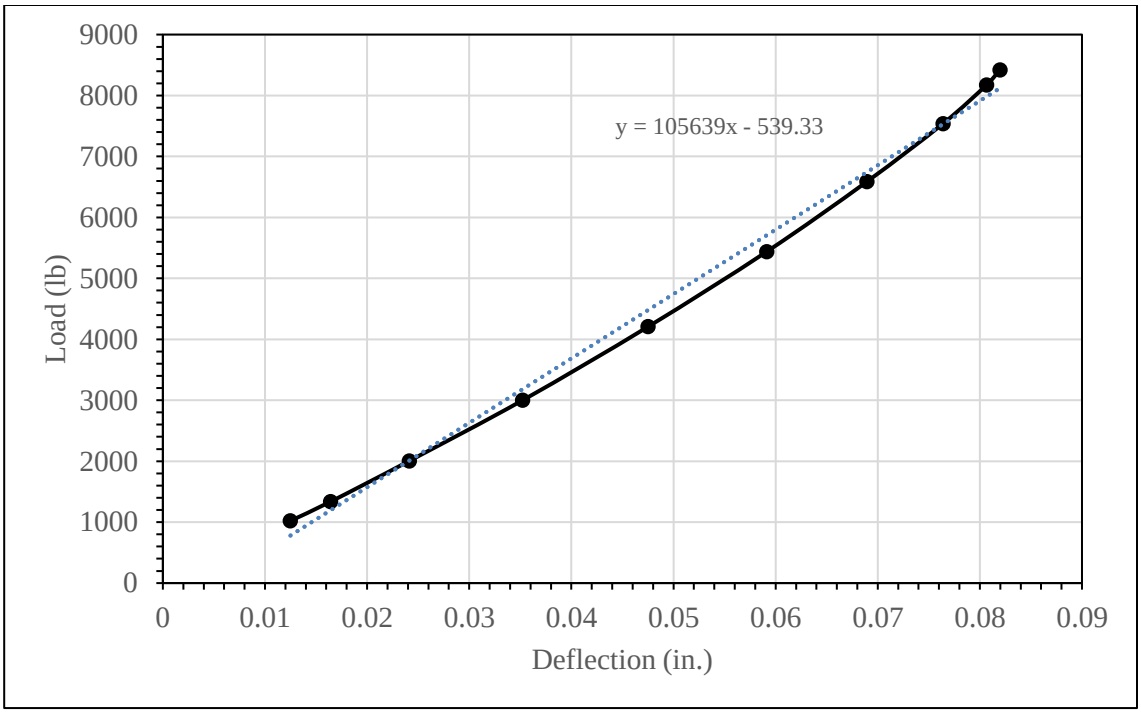

Figure 83: Load vs. Deflection for slab 3, single load cycle selected from day 17

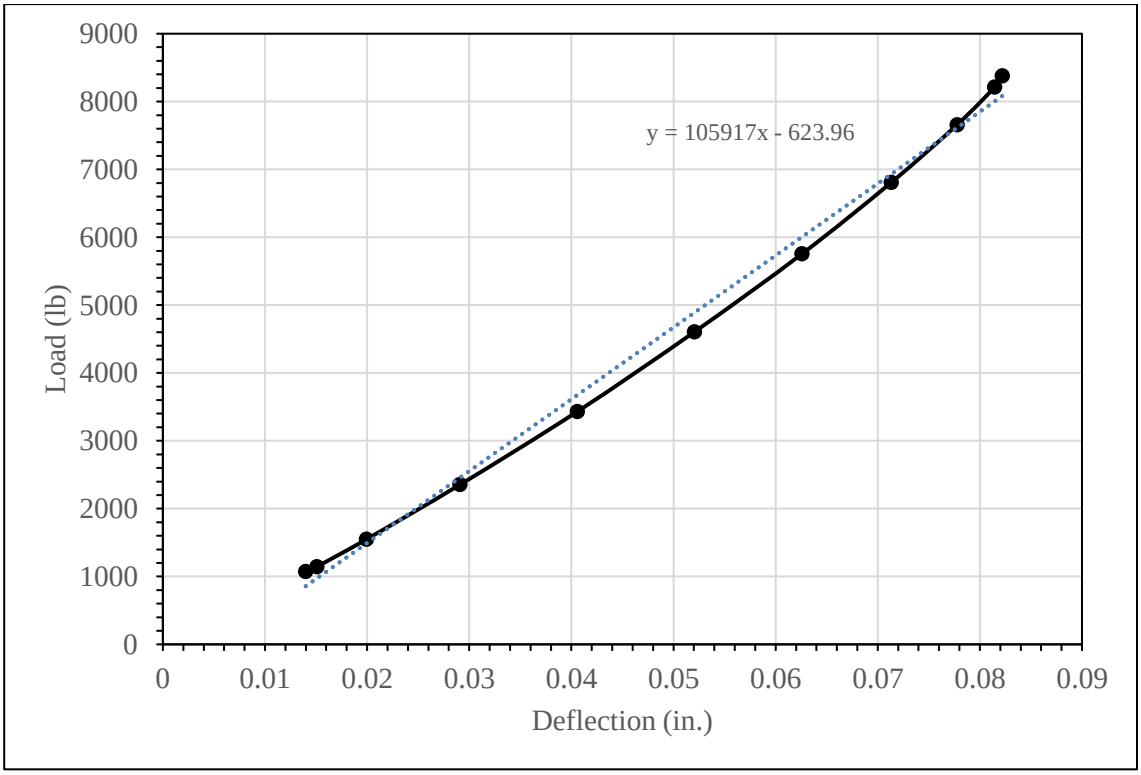

Figure 84: Load vs. Deflection for slab 3, single load cycle selected from day 19

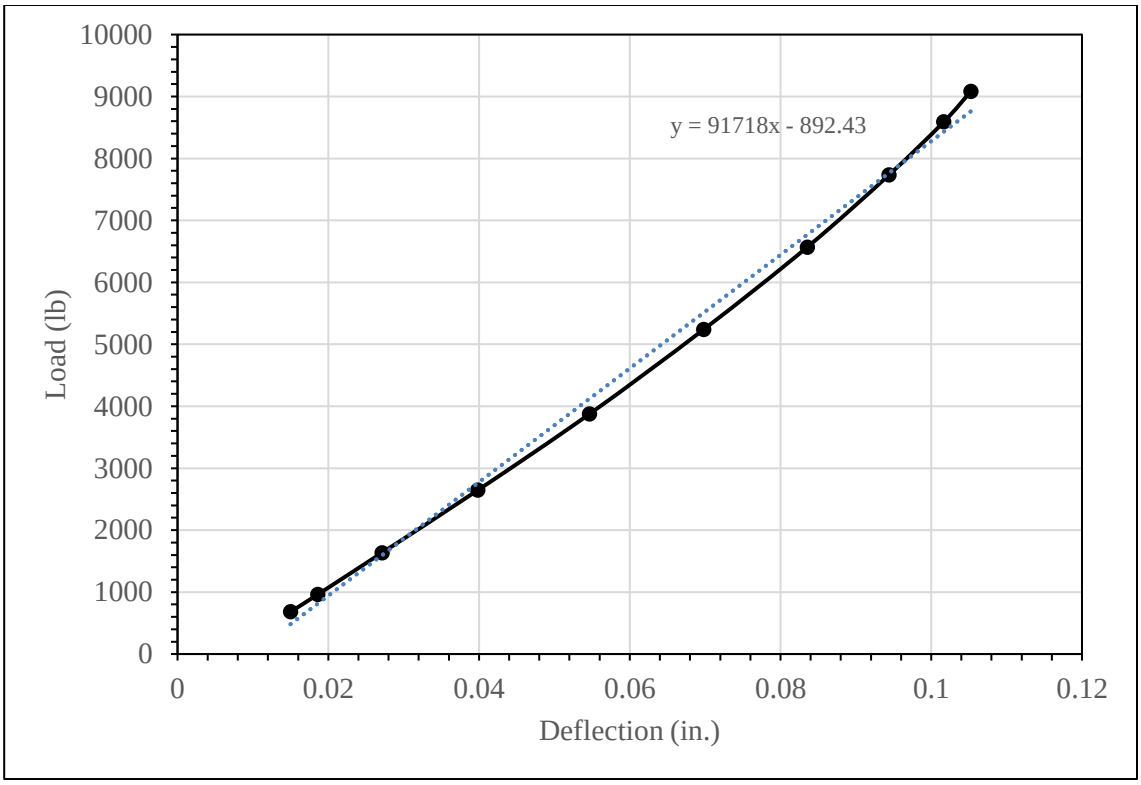

Figure 85: Load vs. Deflection for slab 3, single load cycle selected from day 21

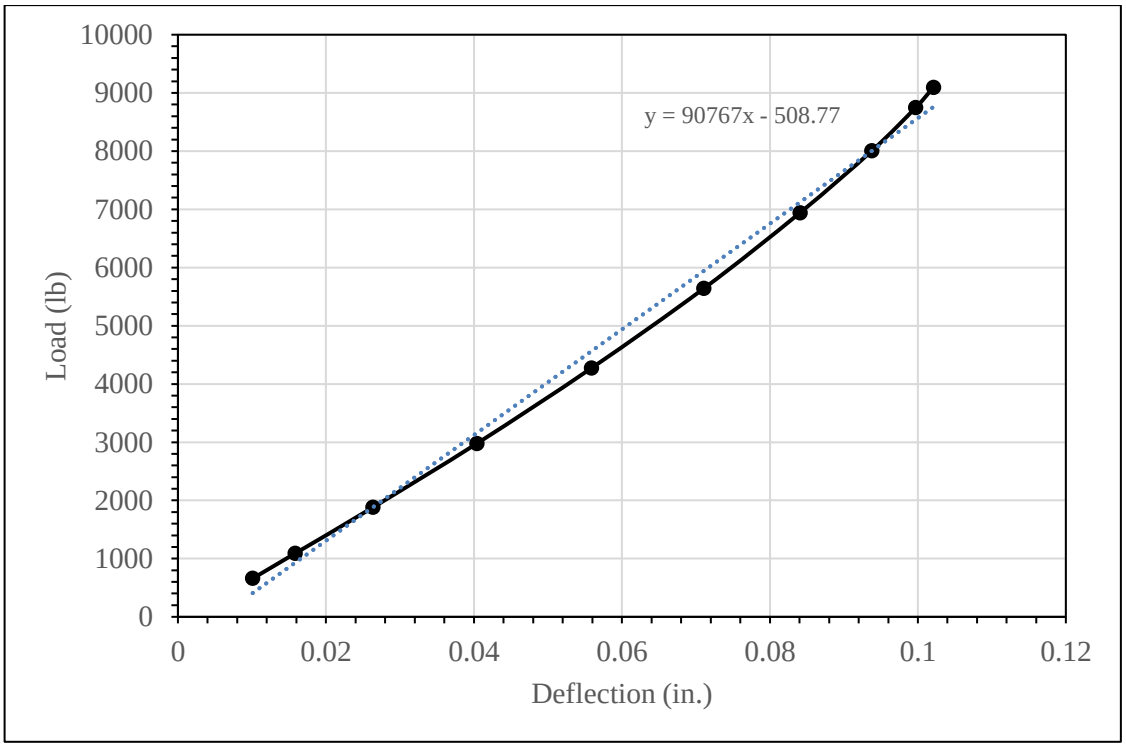

Figure 86: Load vs. Deflection for slab 3, single load cycle selected from day 23

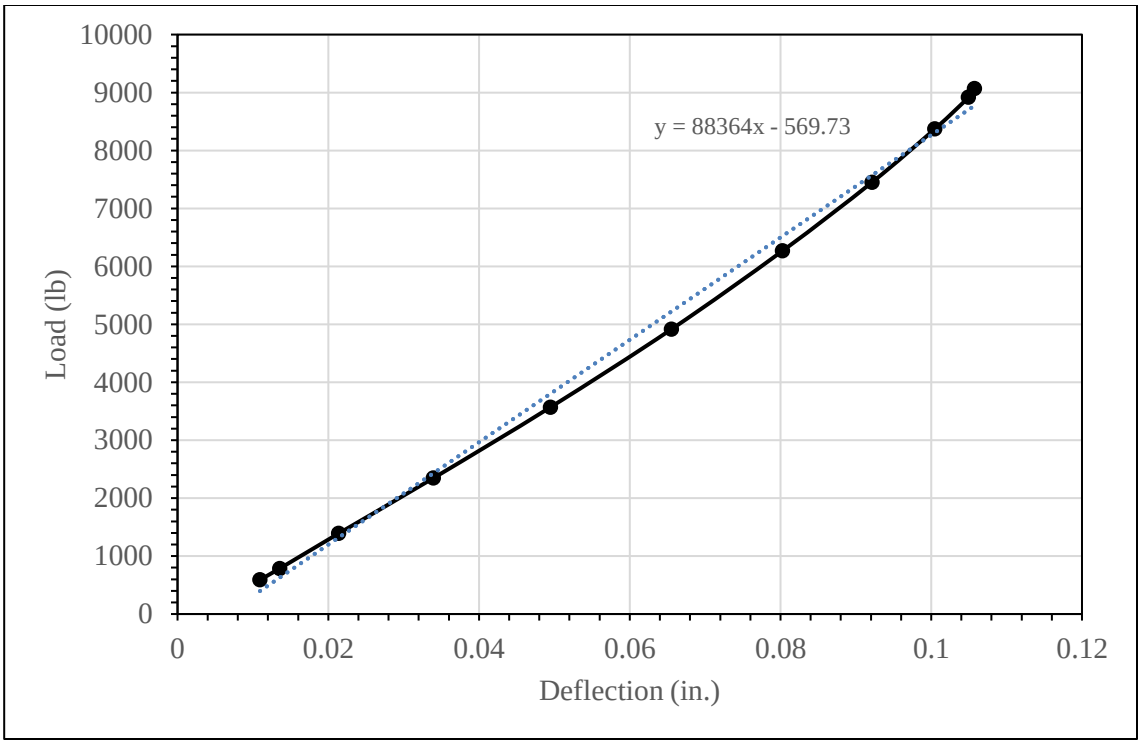

Figure 87: Load vs. Deflection for slab 3, single load cycle selected from day 25

Appendix B: Calculations

Maximum Tensile Stress at Failure

$$R = \frac{PL}{bd^2} \quad \text{(ASTM C78)}$$

where

R = MOR, psi

P = maximum observed load, lb

L = span length of the specimen from support to support, in.

b = width of the specimen at location of failure, in.

d = depth of specimen at location of failure, in.

$$fr = 7.5\sqrt{f'c} \quad \text{(ACI 318)}$$

where

fr = flexural tension strength, psi

f'c = compressive strength of NSC, psi

Cracking Moment and Corresponding Load

$$M_{cr} = \frac{f_r I_s}{y_t}$$

Where

$f_r = 7.5\sqrt{f'c} = 7.5\sqrt{5500\ psi} = 556.2\ psi$

$I_s = \frac{bh^3}{12} = \frac{(48\ in.)(8\ in.)^3}{12} = 2{,}048\ in.^4$

$y_t = 4\ in.$

So,

$$M_{cr} = \frac{f_r I_s}{y_t} = \frac{(580.9\ psi)(2{,}048\ in.^4)}{4\ in.} = 297{,}445\ lb \cdot in. = 24.8\ kip \cdot ft$$

To find the corresponding point load for a non-symmetric simple span of length L = A + B:

$$P = \frac{ML}{AB} = \frac{(24.8\ kip \cdot ft)(8.5\ ft)}{(5.167\ ft)(3.333\ ft)} = 12.24\ kips$$

Note that

M_{cr} = cracking moment, lb-in.

f_r = modulus of rupture of concrete, psi

I_s = moment of inertia of gross section of slab about centroidal axis, in.^{4}

b = width of compression face of member, in.

h = overall depth of member, in.

y_t = distance from the centroid of the cross section to the tension face, in.

f'_c = compressive strength of concrete, psi

Flexural Capacity and Corresponding Load

Assuming both layers of steel are in tension during loading,

$$M_n = A_{s1} f_y \left(d_1 - \frac{c}{2}\right) + A_{s2} f_y \left(d_2 - \frac{c}{2}\right)$$

Where

$A_{s1} = A_{s2} = 4(0.31\ in.^2) = 1.24\ in.^2$

$f_y = 60\ ksi$

$d_1 = 6.063\ in.$

$d_2 = 2.44\ in.$

$$a = \frac{2A_s f_y}{0.85 f'_c b} = \frac{2(1.24\ in.^2)(60\ ksi)}{0.85(6\ ksi)(48\ in.)} = 0.61\ in.$$

$$c = \frac{a}{\beta_1} = \frac{0.61\ in.}{0.80} = 0.76\ in.$$

Checking the assumption that the steel yields:

$$\varepsilon_{s1} = \frac{0.003}{c}(d_1 - c) = \frac{0.003}{0.76}(6.063 - 0.76) = 0.021 > 0.00205$$

$$\varepsilon_{s2} = \frac{0.003}{c}(d_2 - c) = \frac{0.003}{0.76}(2.44 - 0.76) = 0.007 > 0.00205$$

So,

$$M_n = (1.24\ in.^2)(60\ ksi)\left[\left(6.063\ in. - \frac{0.76\ in.}{2}\right) + \left(2.44\ in. - \frac{0.76\ in.}{2}\right)\right]$$

$$= 576.1\ kip \cdot in. = 48.0\ kip \cdot ft$$

To find the corresponding point load for a non-symmetric simple span of length L = A + B:

$$P = \frac{ML}{AB} = \frac{(48.0\ kip \cdot ft)(8.5\ ft)}{(5.167\ ft)(3.333\ ft)} = 23.69\ kips$$

Note that

M_n = nominal flexural strength at section, lb-in.

A_{s1} = area of the bottom layer of longitudinal tension reinforcement, in.^{2}

A_{s2} = area of the top layer of longitudinal tension reinforcement, in.^{2}

f_y = specified yield strength of reinforcement, ksi

d_1 = distance from extreme compression fiber to centroid of bottom layer of longitudinal tension reinforcement, in.

d_2 = distance from extreme compression fiber to centroid of top layer of longitudinal tension reinforcement, in.

a = depth of equivalent rectangular stress block, in.

c = distance from extreme compression fiber to neutral axis, in.

ε_{s1} = value of net tensile strain in the bottom layer of longitudinal tension reinforcement, unitless

ε_{s2} = value of net tensile strain in the top layer of longitudinal tension reinforcement, unitless